TECHNISCHE UNIVERSITÄT WIEN
VIENNA UNIVERSITY OF TECHNOLOGY

Diplomarbeit

Feedforward-Verstärker für GSM2+

ausgeführt zum Zwecke der Erlangung des akademischen Grades eines Diplom-Ingenieurs
unter der Leitung von

O.Univ.Prof. Dipl.-Ing. Dr.techn. Gottfried Magerl
und
Univ.Ass. Dipl.-Ing. Holger Arthaber

INSTITUT FÜR ELEKTRISCHE MESS- UND SCHALTUNGSTECHNIK
INST. NR. 354

eingereicht an der

TECHNISCHEN UNIVERSITÄT WIEN
FAKULTÄT FÜR ELEKTROTECHNICK UND INFORMATIONSTECHNIK

von

Michael E. Gadringer
Matr.Nr. 9627145
Aigen 13
A-4910 Tumeltsham

Wien, 29. Oktober 2002

Diploma Thesis

Feedforward amplifier for GSM2+

performed at the

Institute for Electrical Measurement and Circuit Design

Technical University of Vienna

supervised by

O.Univ.Prof. Dipl.-Ing. Dr.techn. Gottfried Magerl

and

Univ.Ass. Dipl.-Ing. Holger Arthaber

by

Michael E. Gadringer

Matr.Nr. 9627145

Aigen 13

A-4910 Tumeltsham

Vienna October 29, 2002

Kurzfassung

Ziel dieser Diplomarbeit ist die Untersuchung der Frage, in wie weit das Feedforward-Linearisierungskonzept zur Erhöhung der Ausgangsleistung eines bestehenden Verstärkers für GSM2+ (**G**lobal **S**ystem for **M**obile communication) Basisstationen verwendet werden kann. Dabei sollen trotz erhöhter Ausgangsleistung die Bestimmungen des GSM2+ Standard erfüllt werden. Ein adaptives Regelungssystem soll den Feedforward-Verstärker robust gegen Störungen machen.

Das gesamte Projekt wurde in Kooperation zwischen der SIEMENS AG WIEN und dem INSTITUT FÜR ELEKTRISCHE MESS- UND SCHALTUNGSTECHNIK, ARBEITSGRUPPE MIKROWELLENTECHNIK, TECHNISCHE UNIVERSITÄT WIEN durchgeführt.Die Firma SIEMENS AG WIEN stellte den Verstärker und Teile der Messausrüstung zur Verfügung und half bei der Lösung der aufgetretenen Probleme. Der Aufbau und die Messung des Verstärkers wurden an der TECHNISCHEN UNIVERSITÄT WIEN durchgeführt.

Die Grundlage für den Feedforward-Verstärker bildete ein kommerziell verfügbarer Leistungsverstärker der Firma SIEMENS. Dieser Verstärker kann bis zu 34 W Ausgangsleistung innerhalb des PCS-Frequenzbandes (**P**ersonal **C**ommunication **S**ystem) liefern. Bis zu dieser Ausgangsleistung werden die Vorgaben des GSM2+ Standards eingehalten. Eine weitere bestimmende Komponente des Feedforward-Verstärkers bildet der Vektor-Abschwächer. Dieser Abschwächer kann über zwei Stromschleifen sowohl in Betrag und Phase eingestellt werden. Der verwendete Vektor-Abschwächer wurde als Hybrid-HF-Schaltung zugekauft.

Basierend auf diesen Komponenten wurde das Feedforward-Linearisierungskonzept realisiert. Nach erfolgreicher Inbetriebnahme des Feedforward-Verstärkers und der Implementierung der adaptiven Regelung wurden die Eigenschaften dieses Verstärkers gemessen und die Messergebnisse mit dem Verstärker in ursprünglichen Zustand verglichen. Es konnte eine Erhöhung der Ausgangsleistung bei einem Zweiton-Eingangssignal um 18 dB bei einen Intermodulationsabstand von 50 dB erzielt werden. Bei dem Betrieb mit einem GSM2+-Signal ließ sich keine Erhöhung der Ausgangsleistung unter Einhaltung des Standards erreichen. Durch Modifikationen an der gewählten Struktur sollten sich speziell die Schwachpunkte im Bereich der spektralen Masken vermeiden lassen.

Diese Diplomarbeit gliedert sich in eine Einführung in die Theorie des Feedforward-Linearisierungskonzeptes, die Messung und Beschreibung der aktiven Komponenten des Verstärkers, die Realisierung des Feedforward-Verstärkers und die Messung dieses adaptiv geregelten Verstärkers. Am Ende wird ein Vergleich der Eigenschaften des Verstärkers im ursprünglichen Zustand und des adaptiv geregelten Feedforward-Verstärkers geboten.

Abstract

This diploma thesis discusses the construction and performance of an adaptive feedforward linearized SCPA (**S**ingle **C**arrier **P**ower **A**mplifier) for GSM Phase 2+. The goal is to increase the output power of the amplifier under the constrain of fulfilling main parts of the GSM Phase 2+ specification. The adaptive controlling system is used to make the feedforward linearization technique robust against changes of device behavior and environment conditions.

The whole project was done in cooperation between SIEMENS AG VIENNA and the INSTITUTE OF ELECTRICAL MEASUREMENT AND CIRCUIT DESIGN, MICROWAVE ENGINEERING GROUP, VIENNA UNIVERSITY OF TECHNOLOGY. Most measurements where done at the VIENNA UNIVERSITY OF TECHNOLOGY. SIEMENS AG VIENNA supplied the equipment and helped to solve the problems which occurred during the project.

The determining devices of this feedforward amplifier are the main power amplifier and the vector attenuator. The main power amplifier is a commercially available power amplifier built by SIEMENS which is able to deliver 34 W RF-output power in PCS-band while fulfilling the GSM Phase 2+ specification. The vector attenuator is a hybrid-MIC (**M**icrowave **I**ntegrated **C**ircuit) produced by MICRO PRECISION TECHNOLOGY. This device is able to adjust magnitude and phase of the attenuation controlled by two current loops.

Based on these components the feedforward amplifier was realized. After the successful startup of this amplifier the characteristics of the adaptive controlled feedforward amplifier were measured. The comparison with the original amplifier showed a significant improvement of the linearity performance for a two-tone input signal. The operation according to the GSM2+ standard reveals some weak points of the concept. A change in the design of the feedforward structure should improve the performance of this amplifier and should increase the output power of this structure.

This diploma thesis includes a general introduction into the theory of feedforward amplifier, the characterization of the main components, the setup of a feedforward amplifier and the enhancement of this amplifier by two adaptive loop controllers. In the end of this thesis the performance of the adaptively controlled feedforward amplifier is compared to the performance of the main power amplifier.

Acknowledgement

I would like to thank the members of the Microwave Engineering Group at the Institute for Electrical Measurement and Circuit Design, Vienna University of Technology. I am grateful to O.Univ.Prof. Dipl.-Ing. Dr.techn. Gottfried Magerl and my advisor Univ.Ass. Dipl.-Ing. Holger Arthaber and Univ.Ass. Dipl.-Ing. Markus Mayer and Dipl.-Ing. Dieter Smely for their support with practical experience and their participation in inspiring discussions.

I am indebted to Dipl.-Ing. Christian Bauer, Ing. Dieter Serringer and Dipl.-Ing. Walter Steiner of Siemens AG Vienna for their support and their patient assistance that made it easy for me to work on the project.

I wish to extend my thanks to my fellow students Thomas Dietmaier, Robert Jelinek and Holger Wolfmayr for the great cooperation during our time at the university.

Contents

List of Figures

Abbreviations

ACPR	**A**djacent **C**hannel **P**ower **R**atio
BTS	**B**ase **T**ransceiver **S**tation
CDF	**C**umulative **D**ensity **F**unction
CF	**C**rest **F**actor
CP	**C**ancellation **P**erformance
CPG	**Cop**lanar **G**round (waveguide)
DC	**D**irectional **C**oupler
DUT	**D**evice **U**nder **T**est
EA	**E**rror **A**mplifier
EDGE	**E**nhanced **D**ata Rates For **G**SM **E**volution
EPWRSTPV1	**E**dge **P**ower**st**age **P**CS-band **V1**
ETSI	**E**uropean **T**elecommunication **S**tandards **I**nstitute
EVM	**E**rror **V**ector **M**agnitude
FFA	**F**eed**f**orward **A**mplifier
GMSK	**G**aussian **M**inimum **S**hift **K**eying
GPIB	**G**eneral **P**urpose **I**ndustry **B**us
GPRS	**G**eneral **P**acket **R**adio **S**ervice
GSM	**G**lobal **S**ystem For **M**obile Communication
HSCSD	**H**igh **S**peed **C**iruit **S**witched **D**ata
IMD	**Inter**modulation **D**istance
IMP	**Inter**modulation **P**roduct
MA	**M**ain **A**mplifier
MIC	**M**icrowave **I**ntegrated **C**ircuit
MPT	**M**icro **P**recision **T**echnologie Inc.
NPR	**N**oise **P**ower **R**atio
PAE	**P**ower **A**dded **E**fficiency
PAR	**P**eak To **A**verage **R**atio
PCB	**P**rinted **C**ircuit **B**oard
PCS	**P**ersonal **C**ommunication **S**ystem
PDF	**P**ropability **D**ensity **F**unction
PS	**P**owersplitter
PSK	**P**hase **S**hift **K**eying
PWRSTMPV2	**P**ower**st**age **M**icroBTS **P**CS-band **V2**
RF	**R**adio **F**requency
SCPA	**S**ingle **C**arrier **P**ower **A**mplifier
SMA	**Sub**miniature A
SMD	**S**urface **M**ounted **D**evice
TMDA	**T**ime **D**ivision **M**ultiple **A**ccess
UMTS	**U**niversal **M**obile **T**elecommunication **S**ystem
VA	**V**ector **A**ttenuator
VSA	**V**ector **S**ignal **A**nalyzer

Symbols

B	signal bandwidth
E_s	energy per modulated symbol
T_s	symbol duration
$\Re\{\cdot\}$	real part of a complex number of function
$\Im\{\cdot\}$	imaginary part of a complex number of function
f	frequency
$\mathrm{f_c}$	carrier frequency
s_i	actual symbol
$\widetilde{s}(t)$	complex baseband signal
$\Phi(f)$	phase of a signal or system
α	amplitude mismatch in a cancellation loop
τ	delay of a system or signal (first order approximation)
τ_g	group delay
η	efficiency
$e^{j\phi}$	phase mismatch in a cancellation loop
φ_c	phase of the unmodulated carrier
ω	angular frequency
ω_c	angular frequency of the carrier
$\left(\vec{a}, \vec{b}\right)$	scalar product of the two vectors $\vec{a}$ and $\vec{b}$

Chapter 1

GSM2+ basics

1.1 Introduction

The continuously increasing wireless market has put a tremendous pressure on the service providers to increase the availability and the number of services. The demand for high service availability implies a high coverage and capacity. Fulfilling these conditions leads to a rise in the number of base stations and a increasing number of carriers for each station [Tec99]. Due to the fact of growing complexity of the services, higher data-rates at the communication link between the mobile station and the base station are needed. The third generation mobile communication system UMTS (**U**niversal **M**obile **T**elecommunication **S**ystem) is able to handle the demand for high data-rate communication links and high service flexibility, but the erection of a completely new communication network takes quite a long time. A much faster solution is to extend the standard for the existing second generation mobile communication system GSM. The implementation of higher data-rate communication links in the existing GSM-standard is called GSM Phase 2+, 2.5G or EDGE (**E**nhanced **D**ata Rates For **G**SM **E**volution) [ETS01a]. This chapter will give an introduction to the specification for the GSM2+ standard [ETS00, ETS01b] concerning a base station RF (**R**adio **F**requency)-amplifier.

1.2 GSM2+

Within the scope of the GSM2+ standard two modulation formats are defined [ETS01b]:

- Differential encoded GMSK (**G**aussian **M**inimum **S**hift **K**eying)
  - Symbol rate: 270.8 ksymb/s, bit rate: 270.8 kbit/s
  - Gaussian shaped symbol filter with BT = 0.3
- 8PSK (**P**hase **S**hift **K**eying)
  - Symbol rate: 270.8 ksymb/s, bit rate: 812.5 kbit/s
  - Linearized GMSK pulse filter

GMSK is the classical modulation format of the GSM-standard. It supports data rates up to 14.4 kbit/s. The main aim of GSM2+ was to increase the maximum data-rate to 69.2 kbit/s maintaining the same burst structure. Data-rates up to 553.6 kbit/s are possible, when all 8 slots of the TDMA (**T**ime **D**ivision **M**ultiple **A**ccess) frame are used[1] [KPD01]. GSM2+ 8PSK modulation were used to measure the amplifiers within this thesis.

1.2.1 GSM2+ 8PSK Symbol mapping

As shown above GSM2+ 8PSK operates with a three time higher bit rate than the original specification. The increase of the bit rate under the constrain of a constant symbol rate is achieved by mapping groups of three bits onto one symbol. The actual symbol s_i is calculated as defined in [ETS01b, chap. 3.2]

$$s_i = e^{j\frac{2\pi l}{8}} \tag{1.1}$$

where the symbol parameter l is given by table 1.1. Figure 1.1 shows the symbol constellation.

input bit sequence (d_i, d_{i+1}, d_{i+2})	symbol parameter l
(1,1,1)	0
(0,1,1)	1
(0,1,0)	2
(0,0,0)	3
(0,0,1)	4
(1,0,1)	5
(1,0,0)	6
(1,1,0)	7

Table 1.1: Mapping between bits and the symbol parameter l

In this configuration a sequence of two orthogonal symbols (e.a. (1,1,1) $\rightarrow$ (0,0,1)) will force the signal trace to pass through the origin. This will lead to an aggravate specification for the RF-amplifier transmitting the modulated signal. To reduce this problem, an additional counterclockwise rotation between the symbols with $\frac{3\pi}{8}$ is defined:

$$s_i' = s_i \cdot e^{j\frac{i3\pi}{8}} \tag{1.2}$$

This symbol rotation prevents the signal trace from passing through the origin. The minimum distance $d_{s_{min}}$ between the signal trace and the origin can be calculated as shown in figure 1.2 using simple triangulation. The maximum distance $d_{s_{max}}$ is set to unity.

[1] Transmitting more than one TDMA slot forces the use of HSCSD (**H**igh **S**peed **C**ircuit **S**witched **D**ata) or GPRS (**G**eneral **P**acket **R**adio **S**ervice) software interfaces.

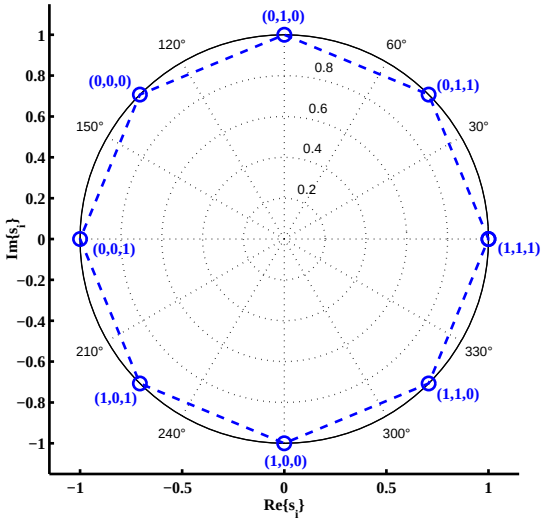

Figure 1.1: Constellation of the 8PSK symbols

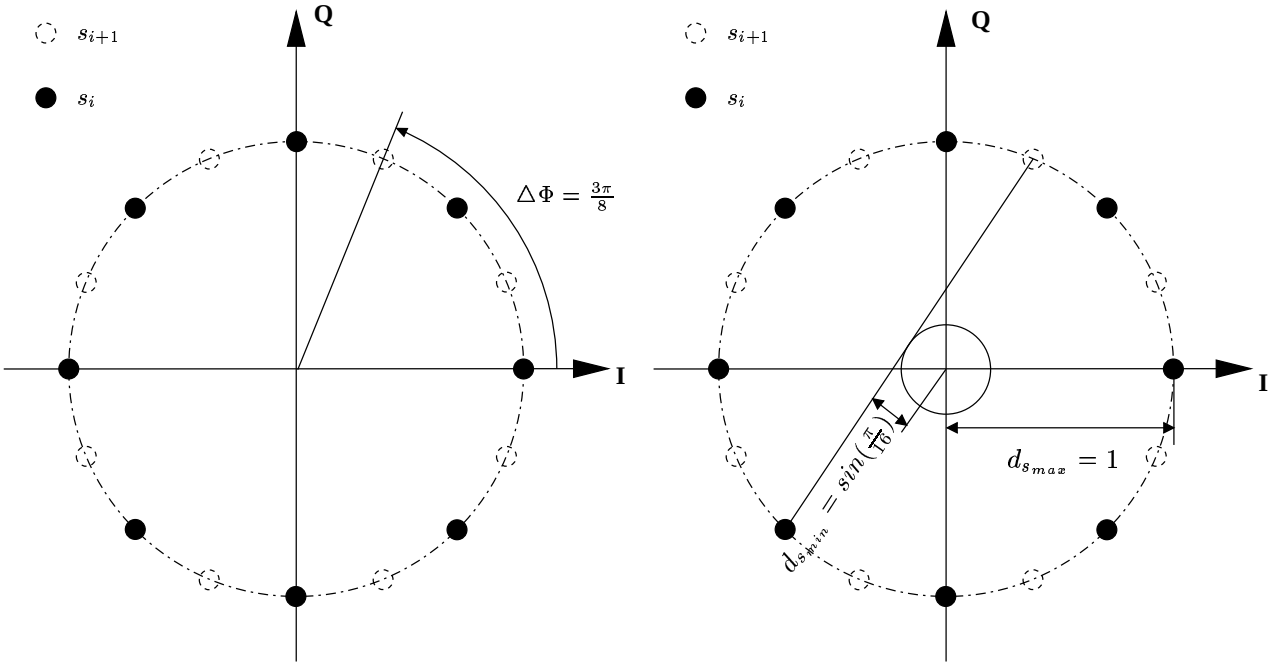

Figure 1.2: Symbol rotation and minimum distance between the signal trace and the origin

1.2.2 GSM2+ 8PSK pulse shaping

In the time domain the symbols s_i' are represented by Dirac pulses exciting a linear pulse shaping filter. This filter is a linearized GMSK pulse, i.e. the main component in a Laurent decomposition

[Lau86] of the GMSK modulation. The impulse response is defined according to [ETS01b]:

$$c_o(t) = \begin{cases} \prod_{i=0}^{3} S(t+iT) & , for\ 0 \le t \le 5T \\ 0 & , else \end{cases} \tag{1.3}$$

$$S(t) = \begin{cases} \sin(\pi \int_0^t g(\tau)d\tau) & , for\ 0 \le t \le 4T \\ \sin(\frac{\pi}{2} - \pi \int_0^{t-4T} g(\tau)d\tau) & , for\ 4T < t \le 8T \\ 0 & , else \end{cases} \tag{1.4}$$

where

$$g(t) = \frac{1}{2T}\left(Q\left(2\pi \cdot 0.3\frac{t-5T/2}{T\sqrt{ln(2)}}\right) - Q\left(2\pi \cdot 0.3\frac{t-3T/2}{T\sqrt{ln(2)}}\right)\right) \tag{1.5}$$

and

$$Q(t) = \frac{1}{\sqrt{2\pi}} \int_t^{\infty} e^{-\frac{\tau^2}{2}} d\tau \tag{1.6}$$

Figure 1.3 shows the shape of the linearized GMSK pulse (e.a. the impulse response of the filter described in equation 1.3). The filter described in equation 1.3 is then used to limit the

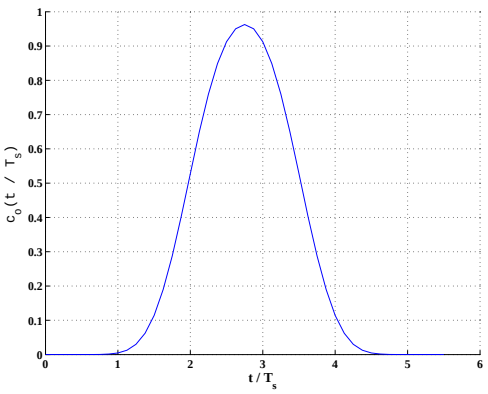

Figure 1.3: Shape of a linearized GMSK pulse

bandwidth of the weighted Dirac pulses signal:

$$\widetilde{y}(t) = \sum_i s_i' \cdot c_o(t - iT + 2T) \tag{1.7}$$

Finally the trace of an according to equation 1.7 filtered random bit sequence is shown in figure 1.4.

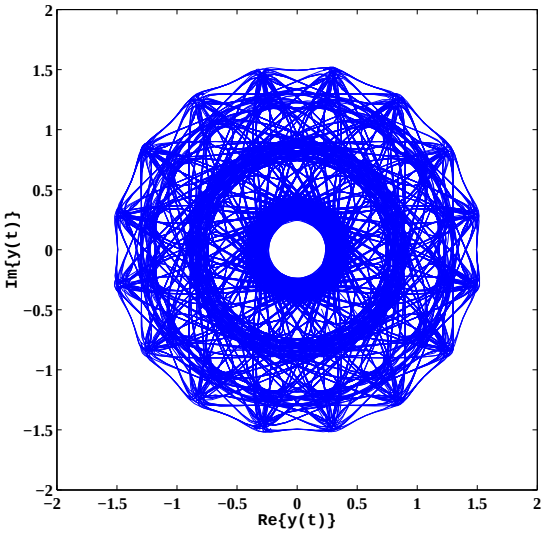

Figure 1.4: Trace of a 8PSK filtered PN bit sequence

1.2.3 GSM2+ Modulation accuracy

The GSM2+ standard [ETS00, chap. 4.6] defines an Error Vector Magnitude (EVM) as a figure of merit for the modulation accuracy. Figure 1.5 shows the calculation of the error vector within the signal space. The phase and amplitude error shown in figure 1.5 can be calculated as presented

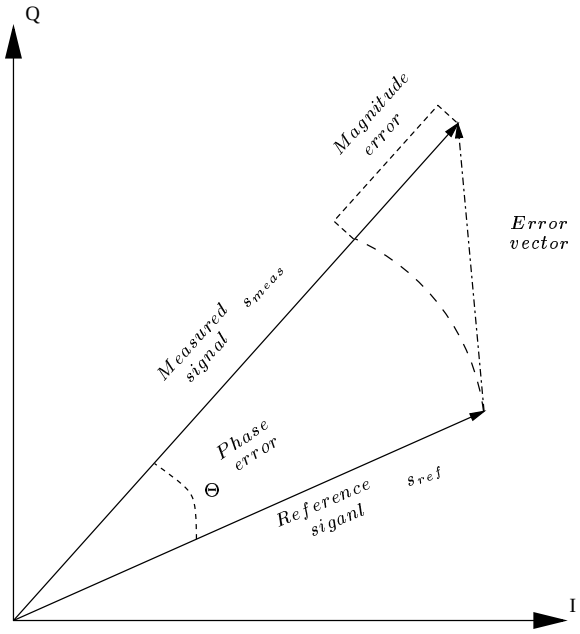

Figure 1.5: EVM calculation

in [KPD01]:

$$\begin{aligned} &\text{magnitude error} = |s_{meas}| - |s_{ref}| \\ &\text{phase error} = \arg\{s_{meas}\} - \arg\{s_{ref}\} \end{aligned} \tag{1.8}$$

Using equation 1.9 the magnitude of the error vector for the k$^{\text{th}}$-symbol can be calculated.

$$\text{EVM}[k] = |s_{meas}[k] - s_{ref}[k]| \tag{1.9}$$

To calculate the EVM as defined in the standard [ETS00] equation 1.10 can be used:

$$\text{EVM}_{\text{rms}}(\%) = \sqrt{\frac{\sum_{k=1}^{N} \text{EVM}[k]^2}{\sum_{k=1}^{N} |s_{ref}[k]|^2}} \cdot 100\% \tag{1.10}$$

According to the standard [ETS00] the EVM_{rms} must be lower than 7 % for the BTS (**B**ase **T**ransceiver **S**tation). Additionally to the EVM_{rms} following indicators are also defined in the standard [ETS00]:

- Peak EVM:

  The peak EVM is the peak EVM error deviation with a burst averaged over 200 burst. The peak EVM has to be lower than 22 % for a BTS.

- 95:th percentile:

  The 95:th percentile is the point where 95 % of the individual EVM values are below 11 %. Only 5 % of the symbols are allowed to have a EVM exceeding the 95:th percentile point. Again this should be achieved over 200 bursts.

- Origin offset suppression (I/Q offset suppression):

  According to the GSM2+ standard [ETS00, chap 4.6.2] the amplifier output signal should be demodulated and passed through a raised-cosine filter. After the filtering the signal can be written as:

  $$\text{Z}(k) = \text{S}(k) + \text{EVM}(k) + \text{C}_\text{o} \tag{1.11}$$

  where $Z(k)$ names the demodulated, filter and sampled amplifier signal, $\text{S}(k)$ represents the ideal transmitter signal, observed through the receive filter, $\text{EVM}(k) = \text{Z}(k) - \text{S}(k) - \text{C}_\text{o}$ identifies the error vector and C_o specifies the constant origin offset. The origin offset suppression is then defined as:

  $$\text{Origin offset suppression} = -10\log_{10}\left(\frac{|C_o|^2}{\frac{1}{N}\sum_{k=1}^{N}|S(k)|^2}\right) \tag{1.12}$$

  The measured origin offset suppression must exceed 35 dB for a BTS.

1.2.4 GSM2+ spectrum mask

The term spectrum mask is used to specify the RF spectrum due to modulation and wide band noise. The spectrum mask is defined as the maximum allowed relative output level (dB) for a given offset from the carrier frequency. The output power has to be measured according to table 1.2.

(f-f_c) < 1800 kHz	zero frequency scan, filter and video bandwidth of 30 kHz
(f-f_c) = 1800 kHz	zero frequency scan, filter and video bandwidth of 100 kHz
(f-f_c) >1800 kHz	swept measurement, filter and video bandwidth of 100 kHz

Table 1.2: Measurement setting for the spectrum mask

Table 1.3 shows the specifications for a PCS1900 amplifier used in a BTS:

Ouput power	offset to the carrier frequency / dB					
	200 kHz	250 kHz	400 kHz	600 kHz	1.2 MHz	1.8 MHz
≥43 dBm	-30	-33	-56	-70	-73	-75
41dBm	-30	-33	-56	-68	-71	-73
39 dBm	-30	-33	-56	-66	-69	-71

Table 1.3: Specification of the RF-modulation-spectrum of a PCS-BTS- amplifier

In figure 1.6 the RF spectrum mask and a GSM2+ modulated signal are shown.

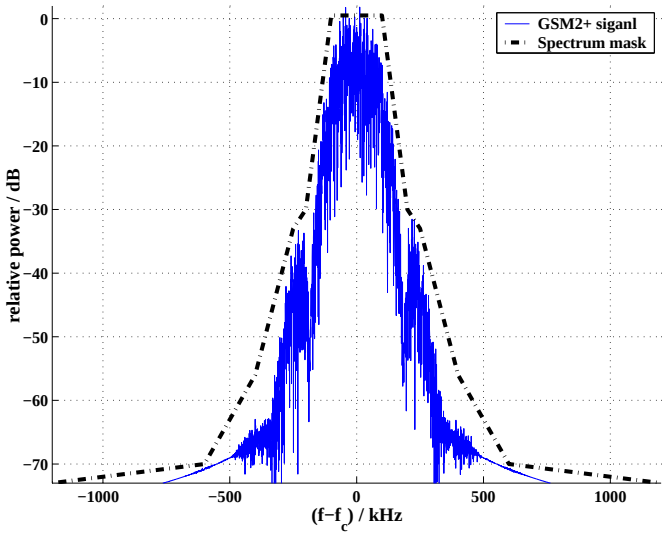

Figure 1.6: RF spectrum mask and GSM2+ modulated signal

1.3 Crest-factor

The CF (**C**rest **F**actor) is a important measures for describing the statistics of signal in a matter which is useful for amplifier specification [Ken00, chap. 2.6], [Pot99, chap. 2.4]:

$$\mathrm{CF} = \frac{\max\{s(t)\}}{\sqrt{\lim_{T\to\infty}\frac{1}{2T}\int_{-T}^{T}|s(t)|^2 dt}} \tag{1.13}$$

A similar definition based on the peak and the average power leads to the PAR (**P**eak To **A**verage **R**atio). Both figures of Merritt are connected by the relationship $\mathrm{PAR} = \mathrm{CF}^2$. In [Pot99] the peak power is called PEP (**P**eak **E**nvelope **P**ower). The crest-factor has a very practical relevance, because it marks the amplitude, where the amplitude-CCDF (**C**omplimentary **C**umulative **D**ensity **F**unction) first time approaches zero. Systems which are capable of handling the average signal power + crest-factor (both measured in dB) will not compress the output signal. Figure 1.7 shows the amplitude statistic of a GSM2+ 8PSK modulated signal and marks the crest-factor value. Finally it should be mentioned, that a relationship between signal bandwidth

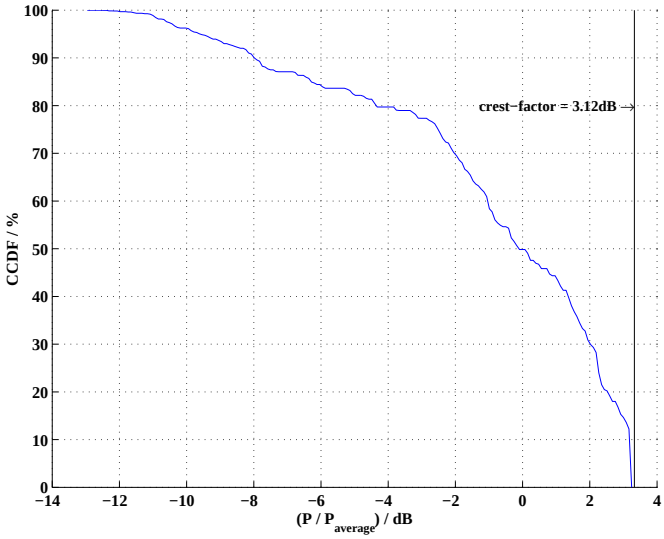

Figure 1.7: Amplitude-CCDF of a GSM2+ 8PSK modulated signal

of a GSM2+ modulated signal and CF exists. The more reduction of the signal bandwidth is achieved by filtering[2], the more the CF of this signal will arise.

[2] e.a. changing the bandwidth of the linearized GMSK-pulse-filter

Chapter 2

Feedforward linearization technique basics

2.1 Introduction

The feedforward linearization technique was invented by Harold S. Black in October 1928 [Bla28]. About nine years later he also invented the feedback linearization technique [Bla37]. Due to the inherent simplicity of the feedback technique, feedforward was of low practical interest for a long period of time. With the construction of RF-amplifiers requiring high output power, large bandwidth and a high degree of linearity, feedforward amplifier started to be a reasonable solution in improving the properties of an RF-amplifier.

In this chapter the basic properties, advantages and disadvantages of this linearization technique will be pointed out. The concept is based on [Ken00, chap. 5] and [Pot99, chap. 4.5 and chap. 5]. Both books provide an evident and well understandable introduction into the theory and the design aspects of feedforward amplifiers.

2.2 Feedforward structure

A simplified form of an amplifier enhanced with the feedforward linearization technique is shown in figure 2.1. The functionality of this amplifier may be seen clearly by presenting the response on a two-tone input signal at various points of the structure. The input signal is split in two identical parts and sent along the two branches of the amplifier. The upper branch which includes the main amplifier, two directional couplers and a delay element is called the amplifier path. The lower branch which includes the error amplifier, a subtracter and a delay element is called the reference path. The signal in the upper branch is amplified by the main amplifier and the nonlinearities in this amplifier results in intermodulation and harmonic distortion which are added to the scaled input signal.

By the use of the directional coupler a sample of the main amplifier output signal is taken and applied into the subtracter, where a time-delayed portion of the input signal is subtracted. The resulting signal consists of the distortion information of the main amplifier. This error signal

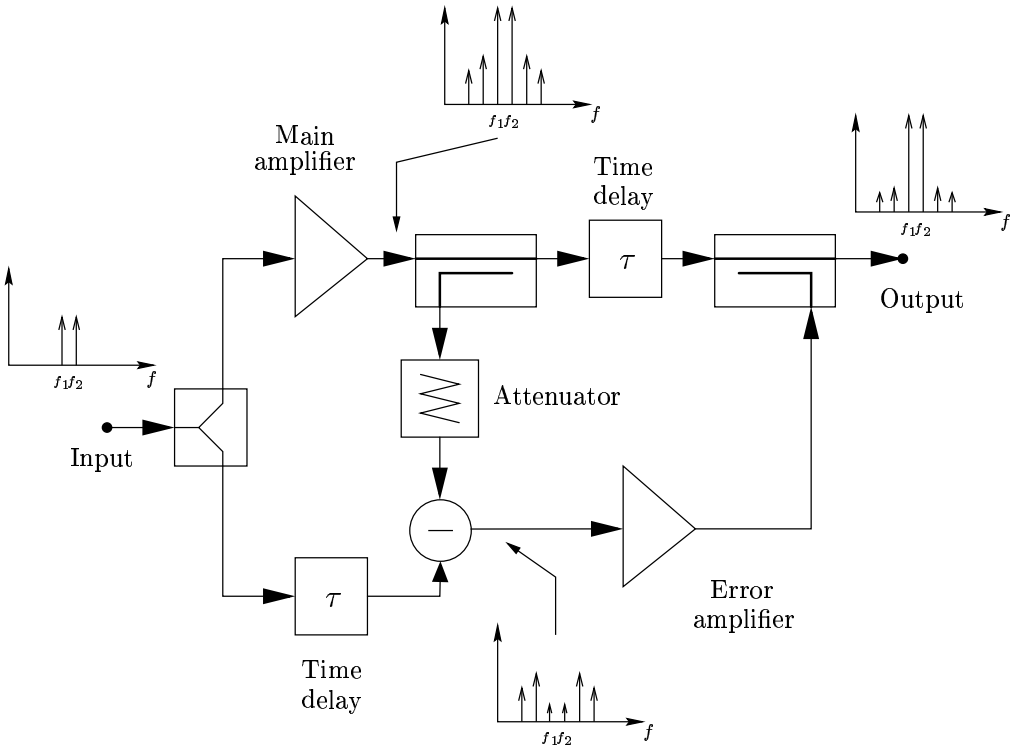

Figure 2.1: Basic configuration of a feedforward amplifier

is then linearly amplified to cancel the distortion in the main path passed through the output coupler.

As shown in the example above, two significant points exist within a feedforward amplifier:

- Carrier cancellation point:

  The perfect subtraction of the input signal from the sample taken at the output of the main amplifier is called carrier cancellation.

- Distortion cancellation loop:

  The perfect remove of the intermodulation and harmonic distortion from the main amplifier output signal is called distortion cancellation.

Figure 2.2 indicates the position of the both cancellation point and the corresponding loops.

Discussing the feedforward amplifier linearization technique the following advantages can be shown:

- Feedforward linearization technique does not reduce the gain of the main amplifier (assuming perfect operation)

- Feedforward linearization technique is unconditionally stable

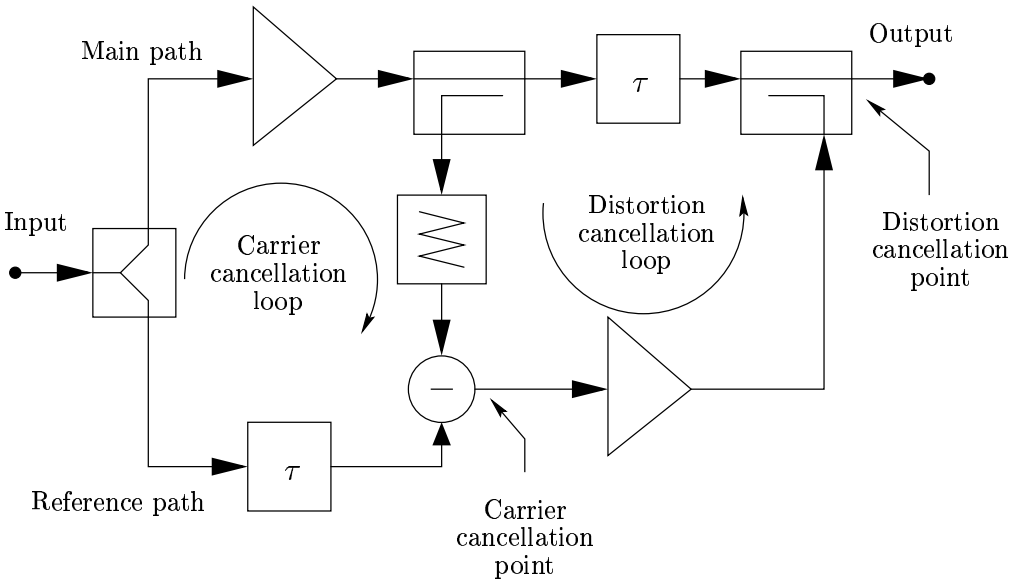

Figure 2.2: Feedforward nomenclature

- The gain-bandwidth product is conserved
- Correction is independent of the amplifier's delay within the system
- Correction is not attempted based on past events
- The error amplifier only needs to process the distortion of the main amplifier (ideally) and thus can be of lower power than the main amplifier

Feedforward also suffers from some major disadvantages:

- Changes of the device characteristic are not compensated
- Matching between the circuit elements in amplitude, phase and time-delay must be maintained to a very high degree over the bandwidth of interest
- Circuit complexity is generally very high compared to feedback systems. This usually results in greater size and cost
- Cost is the main limiting factor on achievable correction level

Additionally to the removal of intermodulation and harmonic distortion an additional benefit can be found. Feedforward can also be used to correct the linear distortion of an amplifier as it is needed, for example, for instrumentation amplifiers. In [KB96] theoretical and practical results about the reduction of linear distortion are presented.

2.3 Signal cancellation

The advantages mentioned in the last chapter come at the expense of the requirement for a high degree of matching in amplitude, phase and time-delay. This matching must be maintained over the whole bandwidth of interest. To estimate the effects of a mismatch in amplitude, phase and/or time-delay the model presented in figure 2.3 is used: In this model the input signal is

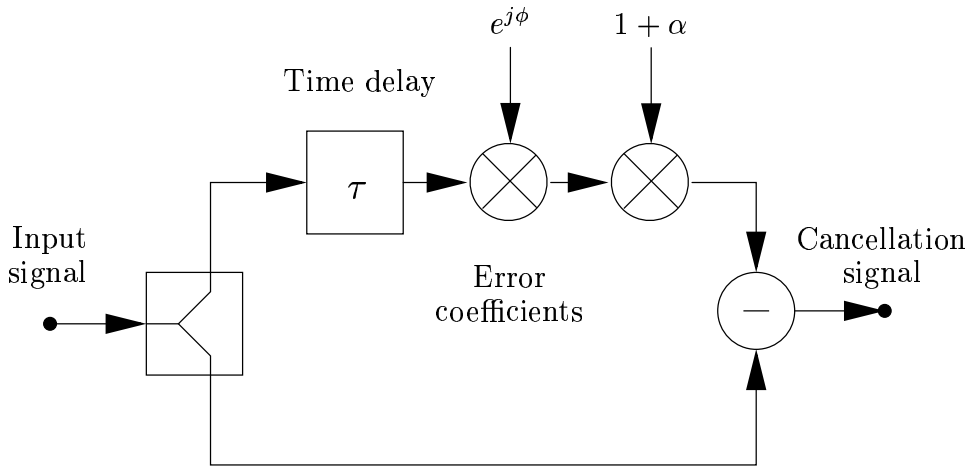

Figure 2.3: Signal cancellation model

split in two identical parts. The signal in the lower branch is directly passed to the subtracter. The signal in the upper branch is altered by the error coefficients. In case of a single-tone input signal, the time-delay τ and the phase-shift $e^{j\phi}$ can be merged together to a new phase-shift $e^{j\phi'}$.

2.3.1 Amplitude and phase matching

To calculate the effects of an amplitude and/or phase mismatch the vector representation of a single tone input signal is advantageous. In figure 2.4 the two signal vectors at the cancellation point of figure 2.3 are shown. The length of the lower branch signal is set to unity. The upper branch signal is altered by the amplitude mismatch α and rotated by the phase-shift $e^{j\phi}$. The effects of a time-delay are neglected. After the subtraction of the signals the cancellation signal r can be calculated as:

$$\begin{aligned} \text{lower branch signal} &= 1 \\ \text{upper branch signal} &= (1+\alpha)\cdot e^{-j\phi} = (1+\alpha)\cdot cos(\phi) - j(1+\alpha)\cdot sin(\phi) \\ \mathrm{r} &= -1 + (1+\alpha)\cdot cos(\phi) - j(1+\alpha)\cdot sin(\phi) \\ |\mathrm{r}|^2 &= 1 + (1+\alpha)^2 - 2\cdot(1+\alpha)\cdot cos(\phi) \\ \mathrm{CP} = |\mathrm{r}| &= 10\cdot\log_{10}\Big(1 + (1+\alpha)^2 - 2\cdot(1+\alpha)\cdot cos(\phi)\Big) \end{aligned} \tag{2.1}$$

In equation 2.1 the CP (**C**ancellation **P**erformance) is introduced as a figure of merit for the quality of the amplitude and phase matching in a cancellation loop. For a perfect matched cancellation loop CP tends to $-\infty$ dB . Figure 2.5 shows the amount of suppression which can be achieved for a given degree of phase and amplitude matching.

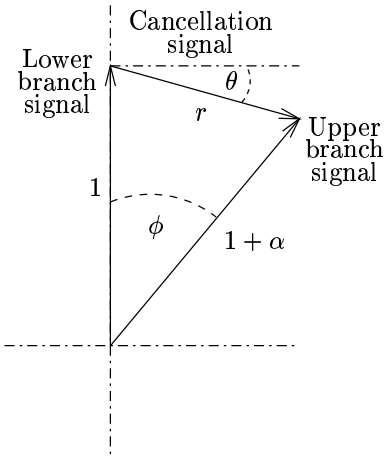

Figure 2.4: Vector representation of the signals in a cancellation loop

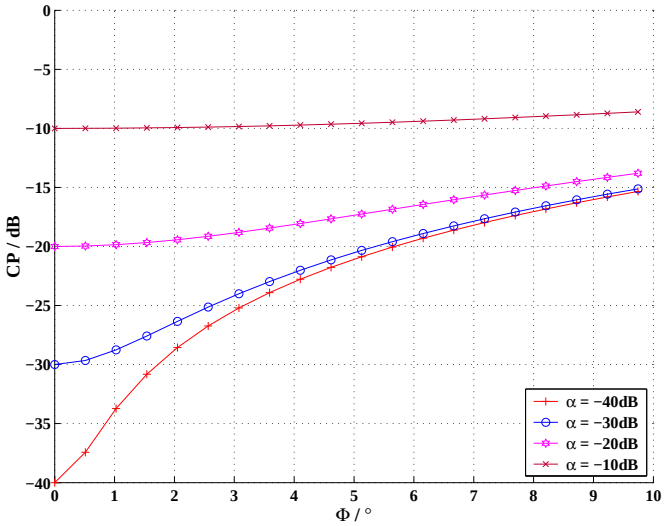

Figure 2.5: Cancellation performance as a function of the amplitude and phase mismatch

2.3.2 Time-delay matching

As a first approximation the delay[1] of a network can be calculated as:

$$\tau = \frac{\Delta\Phi}{\Delta\omega} \tag{2.2}$$

where $\Phi = \Phi(f)$ is the phase of the system and ω is the angular frequency. Systems with a nonlinear phase do not delay all frequencies components by the same amount. According to [BG64, chap. 4.4.2] the delay of such systems is called envelope or group delay and calculated

[1] correct only if the system can be modeled with a linear phase

as:

$$\tau_g(\omega) = \frac{d\Phi}{d\omega} \tag{2.3}$$

which can be evaluated at the frequencies of interest.

To handle the problem of varying group delay over the bandwidth a trade-off has to be found. In practice this will introduce an impairment to the cancellation performance. For extremely broadband systems dispersion compensation networks will help to reduce the effects of varying group delay [SSL90].

For the calculation of the effect of a delay mismatch the same approach as for an amplitude or phase mismatch can be used [KLY97]:

$$\begin{aligned}
\mathrm{r} = & -\left[1-(1+\alpha)\cdot\cos\left(\phi+2\pi\left(f-f_c\right)\tau\right)\right. \\
& \left.+j\,(1+\alpha)\cdot\sin\left(\phi+2\pi\left(f-f_c\right)\tau\right)\right] \\
= & -\left[1-(1+\alpha)\cdot\cos\left(\phi+2\pi\left(\tfrac{\lambda_{err}}{\lambda_o}\right)\left(1-\tfrac{f}{fc}\right)\right)\right. \\
& \left.+j\,(1+\alpha)\cdot\sin\left(\phi+2\pi\left(\tfrac{\lambda_{err}}{\lambda_o}\right)\left(1-\tfrac{f}{fc}\right)\right)\right] \\
|\mathrm{r}|^2 = & \ 1+(1+\alpha)^2-2\cdot(1+\alpha)\cdot\cos\left(\phi+2\pi\left(\tfrac{\lambda_{err}}{\lambda_o}\right)\left(1-\tfrac{f}{fc}\right)\right) \\
\mathrm{CP}=|\mathrm{r}| = & \ 10\cdot\log_{10}\left[1+(1+\alpha)^2-2\cdot(1+\alpha)\right. \\
& \left.\cdot cos\left(\phi+2\pi\left(\tfrac{\lambda_{err}}{\lambda_o}\right)\left(1-\tfrac{f}{fc}\right)\right)\right]
\end{aligned} \tag{2.4}$$

In the equations 2.4 the phase mismatch introduced by a time-delay $(f-f_c)\cdot\tau$ was converted to a relative measure $(\frac{\lambda_{err}}{\lambda_o})(1-\frac{f}{fc})$. Figure 2.6 shows the cancellation performance over the normalized frequency f/f_c for several time-delay mismatches. Phase and amplitude mismatch were neglected in this simulation.

2.3.3 Combination of delay mismatch, gain and phase error

The combination of all three error coefficients reveal another unwanted effect. Assume that the system if adjusted to have the best cancellation performance at the frequency $f = f_c$. When the value of the phase-shift ϕ is changing, the point of best performance is shifted away from the originally adjusted frequency. This is due to the argument $\phi + 2\pi\left(\frac{\lambda_{err}}{\lambda_o}\right)\left(1-\frac{f}{fc}\right)$ which introduces a frequency depending phase to the original argument ϕ. Figure 2.7 documents this effect for a fixed time delay and a varying phase mismatch.

2.4 Gain of a feedforward amplifier

The gain of a matched feedforward amplifier depends on the nonlinearities in the main and the error amplifier. The following derivation will show this dependency in detail. Figure 2.8 depict the gains and losses of the individual components of a simple feedforward system. The abbreviation used in figure 2.8 are:

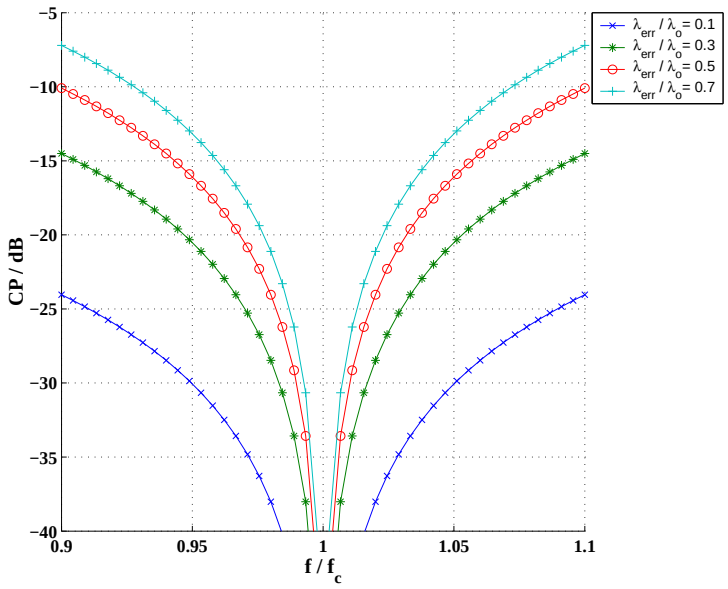

Figure 2.6: Degradation of the cancellation performance due to time-delay mismatch

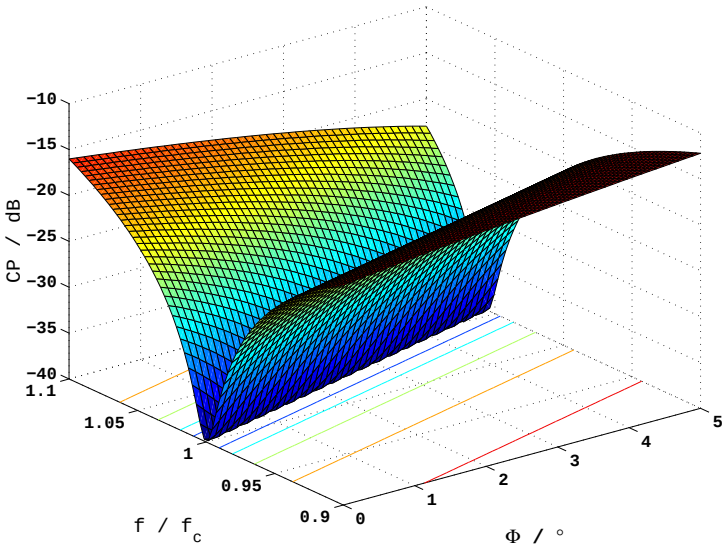

Figure 2.7: Influence of time-delay and phase mismatch on the cancellation performance at $\frac{\lambda_{err}}{\lambda_o} = 0.25$

PS	...	Powersplitter
MA	...	Main amplifier
EA	...	Error amplifier
DC	...	Directional coupler
A	...	Attenuator
D	...	Delayline

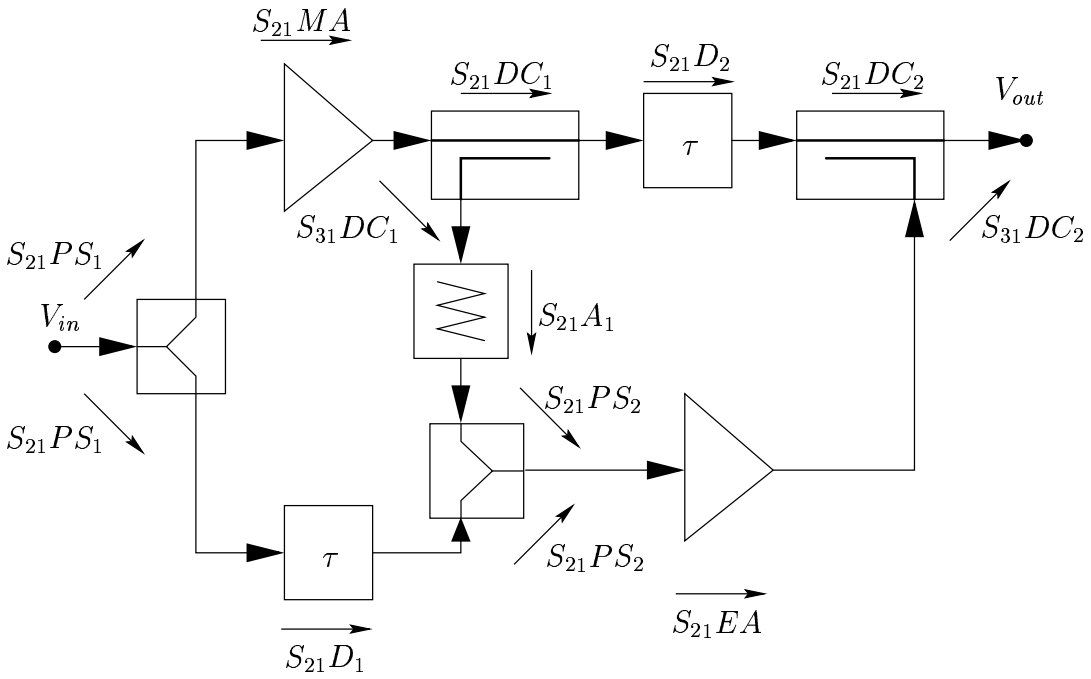

Figure 2.8: Feedforward gain analysis

For the power splitters PS_1 and PS_2 no difference was made between the ports, because all have the same magnitude of the transmission coefficient. So the distinction between the ports was neglected and all transmission coefficients are called $S_{21}PS$ independent of the connected ports.

The gain of a the structure is defined as:

$$\mathrm{G_{ff}} = \frac{V_{out}}{V_{in}} \tag{2.5}$$

The output voltage can be written as:

$$\begin{aligned} \mathrm{V_{out}} &= \mathrm{S_{21}PS_1 \cdot S_{21}MA \cdot S_{21}DC_1 \cdot S_{21}D_2 \cdot S_{21}DC_2 \cdot V_{in}} + \\ &+ \mathrm{S_{31}DC_2 \cdot S_{21}EA \cdot S_{21}PS_1 \cdot S_{21}PS_2 \cdot (S_{21}D_1 - S_{21}MA \cdot S_{31}DC_1 \cdot S_{21}A) \cdot V_{in}} \end{aligned} \tag{2.6}$$

Assuming that perfect cancellation is adjusted :

$$\mathrm{S_{21}MA} = \frac{\mathrm{S_{21}D_1}}{\mathrm{S_{31}DC_1 \cdot S_{21}A}} \tag{2.7}$$

Substituting 2.6 and 2.7 in 2.5:

$$\mathrm{G_{ff}} = \frac{\mathrm{S_{21}PS_1 \cdot S_{21}DC_1 \cdot S_{21}DC_2 \cdot S_{21}D_1 \cdot S_{21}D_2}}{\mathrm{S_{31}DC_1 \cdot S_{21}A_1}} \tag{2.8}$$

The same result can be reached assuming that the distortion cancellation loop is perfectly adjusted. Equation 2.8 depends now only on passive components. But the assumption of a adjusted loop forces all changes in the gain of an amplifier (either main amplifier or error amplifier)

to be compensated by one of the passive components in the same loop. Changes in the gain of one of the amplifiers will changes the gain of the complete structure.

Under the assumption of adjusted loops the gain of the feedforward amplifier can be varied by changing the value of the attenuator A_1. In[Pot99, chap. 5.1] it was mentioned that trimming the value of the attenuator A_1 is a practical solution for building feedforward amplifiers within a certain tolerance in a production environment.

2.5 Loop instabilities

As already pointed out in chapter 2.2 one of the key advantages of a feedforward system is its ability to achieve unconditional stability, hence allowing it to provide high degrees of linearity improvement over a broad bandwidth. Taking real components into account it is still possible to get a unstable feedforward amplifier [KWW97].

2.5.1 Loop instabilities in the carrier cancellation loop

In contrary to the standard operation described in chapter 2.2, a different path of the signal is possible as indicated by the arrows in figure 2.9. In an ideal system the directional couplers

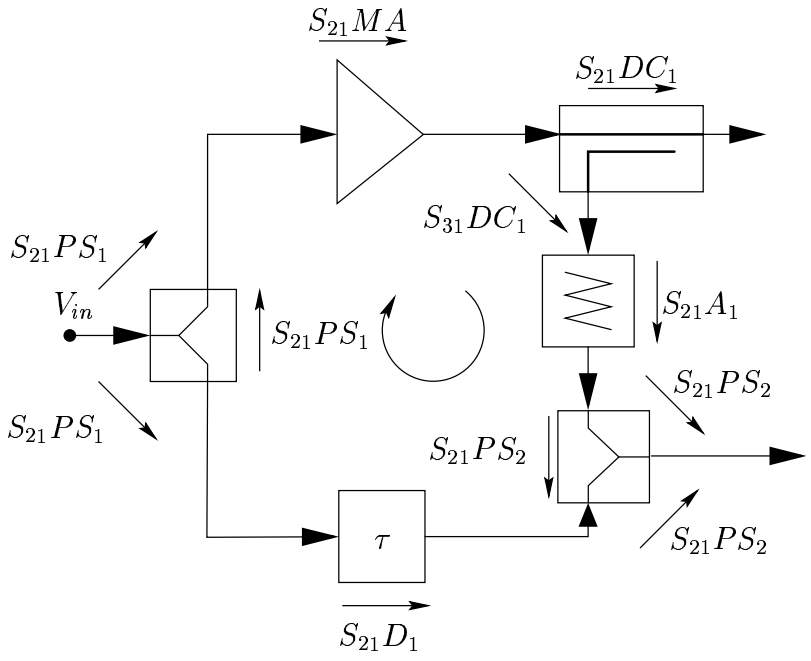

Figure 2.9: Carrier cancellation loop, showing possible oscillation mechanism

would have infinite directivity and hence no signal would flow in the 'reverse' direction. If some of the signal can take the reverse path, it is clearly possible for the main amplifier to have a path from it's output back to the input. Assuming a balanced loop the gain of the main amplifier can be calculated according to equation 2.7 . The gain coefficient defined in [KWW97] can be used

to apprise in the stability :

$$\mathrm{C_{Carrier\ cancellation}} = (\mathrm{S_{21}PS_1})^2 \cdot \mathrm{S_{21}MA} \cdot \mathrm{S_{31}DC_1} \cdot \mathrm{S_{21}A_1} \cdot \mathrm{S_{21}D_1} \cdot (\mathrm{S_{21}PS_2})^2 \tag{2.9}$$

This gain coefficient should be $|C_{Carrier\ cancellation}| < 1$ to guarantee stability and should preferably be, for example, $\frac{1}{4} \doteq -6$ dB in order to allow some margin for main amplifier gain changes to temperature, etc.

2.5.2 Loop instabilities in the distortion cancellation loop

A signal path in 'reverse' direction could also appear in the distortion cancellation loop. Figure 2.10 indicates the reverse path and names the devices. For a balanced distortion cancellation loop

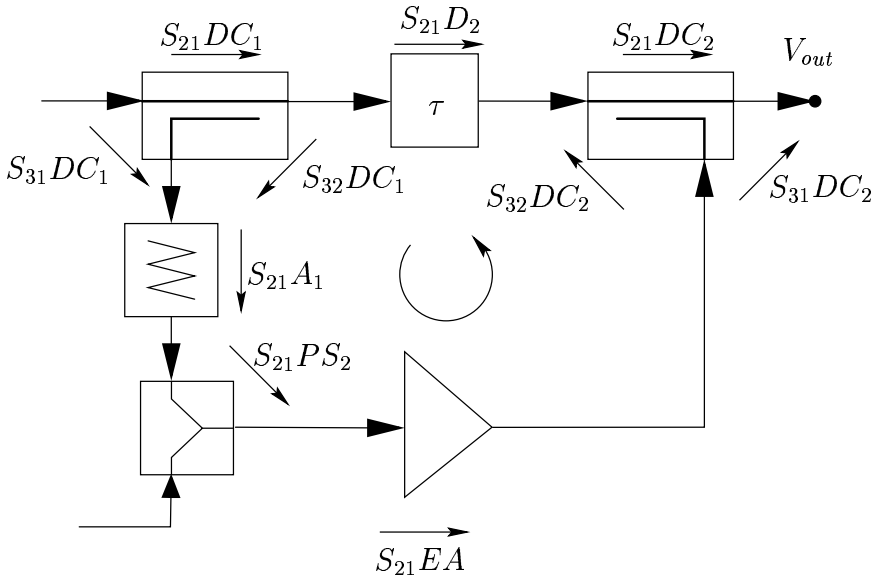

Figure 2.10: Distortion cancellation loop, showing possible oscillation mechanism

the gain of the error amplifier can be calculated as:

$$\mathrm{S_{21}EA} = \frac{\mathrm{S_{21}DC_1} \cdot \mathrm{S_{21}D_2} \cdot \mathrm{S_{21}DC_2}}{\mathrm{S_{31}DC_1} \cdot \mathrm{S_{21}A_1} \cdot \mathrm{S_{21}PS_2} \cdot \mathrm{S_{31}DC_2}} \tag{2.10}$$

The gain coefficient for the distortion cancellation loop is defined as:

$$\mathrm{C_{Distortion\ cancellation}} = \mathrm{S_{31}DC_1} \cdot \mathrm{S_{21}A_1} \cdot \mathrm{S_{21}PS_2} \cdot \mathrm{S_{21}EA} \cdot \mathrm{S_{32}DC_2} \cdot \mathrm{S_{21}D_2} \cdot \mathrm{S_{32}DC_1} \cdot \mathrm{S_{31}DC_2} \tag{2.11}$$

Also this gain coefficient should be within $|C_{Distortion\ cancellation}| < 1$ to guarantee stability and should preferably be about $\frac{1}{4} \doteq -6$ dB to keep some safety margin.

In addition to the problem of loop instability more 'secret traps' can be found within the feedforward structure. In [Bar00] problems like crosstalk due to improper shielding and inadequate input match of the used components are discussed. Another problem is the injection of distortion signals into the output of the feedforward amplifier, for example because of a broken antenna cable. Some aspects of these problems can be found in [Ken00, chap. 5.14].

2.6 Signal bandwidth and crest-factor

This section presents the bandwidth and crest-factor at various points of the feedforward structure for a two-tone input signal. In figure 2.2 the underlying structure and the sample points are presented. The whole demonstration is based on a simulation of the feedforward amplifier with

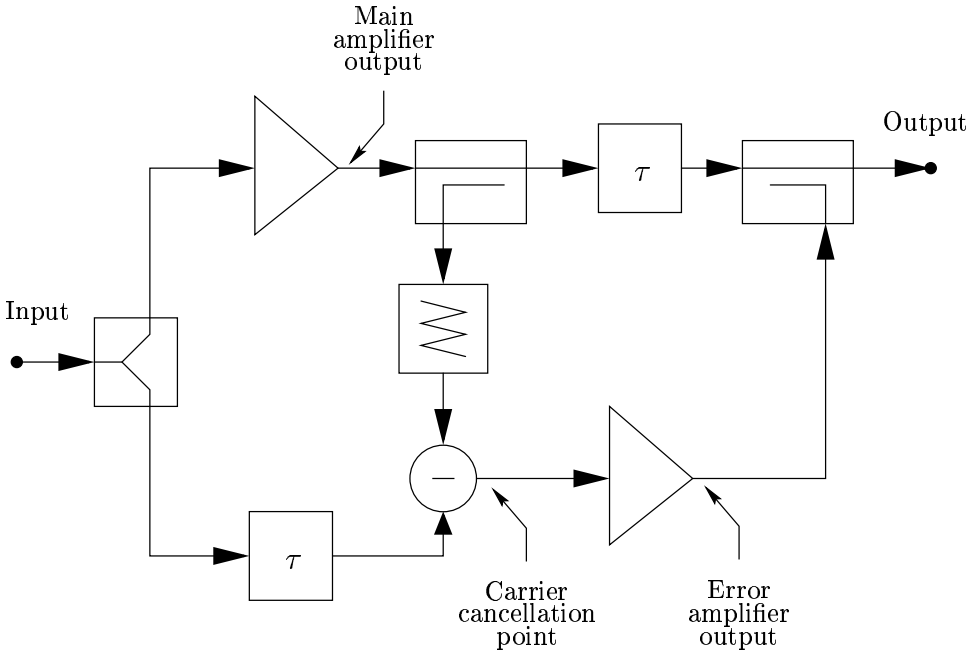

Figure 2.11: Structure used for the simulation of the signal bandwidth and the crest-factor

a nonlinear main and error amplifier. The 1 dB compression point for both of the amplifiers is set to 43 dBm. The input signal is a 200 kHz two-tone signal. The simulation only treated the narrow band intermodulation, broadband effects like harmonic distortion are neglected.

Figure 2.12 shows the signals, powers and crest-factors at the sample-points: Concerning the crest-factor following important facts can be seen in figure 2.12:

- The nonlinear characteristic of the main amplifier creates new frequency components and also reduces the crest-factor (figure (a) and (b))
- The carrier cancellation signal (c) shows a significantly increased crest-factor compared to the input (a) and the main amplifier output signal (b). This fact will rise the requirements for the error amplifier.

The additional frequency components created by the amplifier nonlinearity increases the signal bandwidth. The bandwidth of the signal amplified by a nonlinear device can be estimated by:

$$\mathrm{B}_{\mathrm{nonlinear}} \approx \frac{n+1}{2}\mathrm{B} \tag{2.12}$$

where n names the highest considered intermodulation product and B is the bandwidth of the amplifier input signal. Using equation 2.12 for the estimating of the main amplifier output signal bandwidth leads to $B_{nonlinear} = 800$ kHz, if the main amplifier is simulated by a 7^{th}-order power series. This fact shows another rise in the requirements for the error amplifier, because he must be able to handle a input signal, which has larger bandwidth as the main amplifier input signal.

Table 2.1 shows a summary of the crest-factors for the given example and for a GSM2+ input signal.

	Two-tone siganl CF / dB	GSM 2+ signal CF / dB
Input signal	3	3
Main amplifier output signal	1.7	2
Carrier cancellation point	4.3	8.6
Error amplifier output siganl	4.4	8
Ouput signal	3.1	3.3

Table 2.1: Crest-factors for a two-tone and a GSM2+ input signal

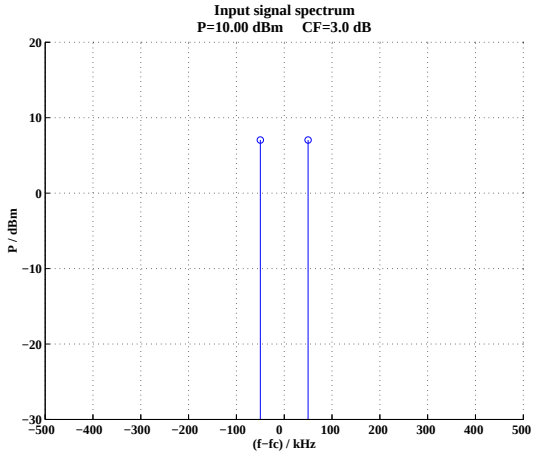

(a)

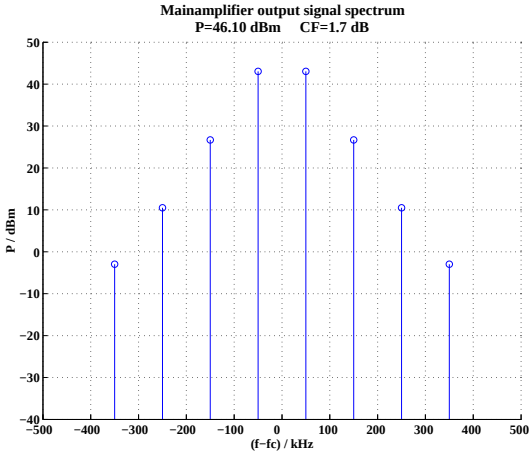

(b)

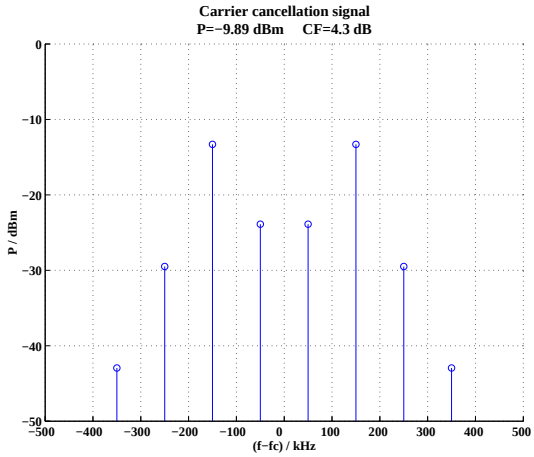

(c)

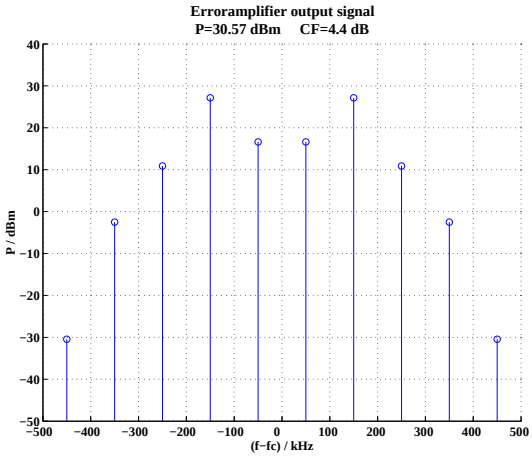

(d)

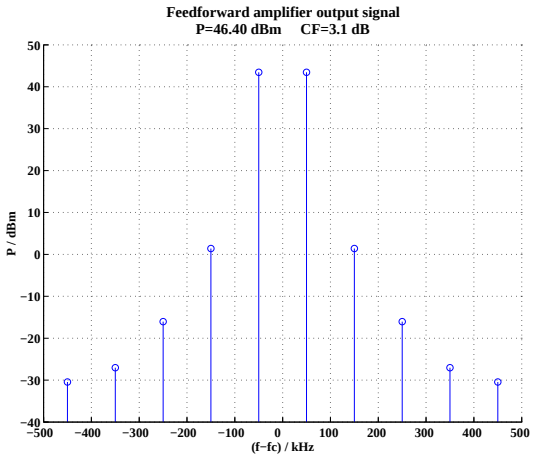

(e)

Figure 2.12: Signal spectrum at the sample points

Chapter 3

Amplifier modeling

3.1 Introduction

In section 2.6 a simulation of an FFA (**F**eed**f**orward **A**mplifier) was presented. In this charter it should be discussed, how to derive a suitable amplifier model for such a simulation. This chapter discusses the models and concepts used in this diploma thesis. In chapter 4 a comparison between the measurement and the model is presented.

The basic idea behind the models used, was to describe the intermodulation distortion added by the amplifier. The physical mechanism behind the distortion generation was not considered. The chosen models are the classical approach to characterize a black box device. A good introduction into this subject can be found in [Ken00, chap. 2].

3.2 Memoryless amplifier model, AM–AM Conversion

A perfect amplifier would have a linear instantaneous transfer characteristic, where the output voltage is a scalar multiple of the input voltage:

$$\mathrm{v_{out}}\,(\mathrm{t}) = k_1 \mathrm{v_{in}}\,(\mathrm{t}) \tag{3.1}$$

where k_1 is the voltage gain of the amplifier. If a nonlinear amplifier is considered equation 3.1 has to be extended to:

$$\mathrm{v_{out}}\,(\mathrm{t}) = \sum_{n=1}^{N} k_n \cdot \mathrm{v_{in}^n}\,(\mathrm{t}) \tag{3.2}$$

where $k_n \in \mathbb{R}$ is the i-th order voltage gain and N is the order of the model. Of course the shape of the output signal differs from the shape of the input signal. The nonlinear relationship between the input power and the output power is often termed as *AM–AM-conversion,* since it is a conversion between the amplitude modulation present at the input signal and the modified amplitude modulation present on the output signal.

3.2.1 Third-order characteristic

When talking about a third-order characteristic the usage of following model is assumed:

$$v_{out}(t) = k_1 v_{in}(t) + k_2 v_{in}^2(t) + k_3 v_{in}^3(t) \tag{3.3}$$

Figure 3.1 shows the behavior of this model for a single tone input signal $V_{in}(t)$ and for different values of the parameter k_x . v_{1st} is an example for the perfect linear model presented

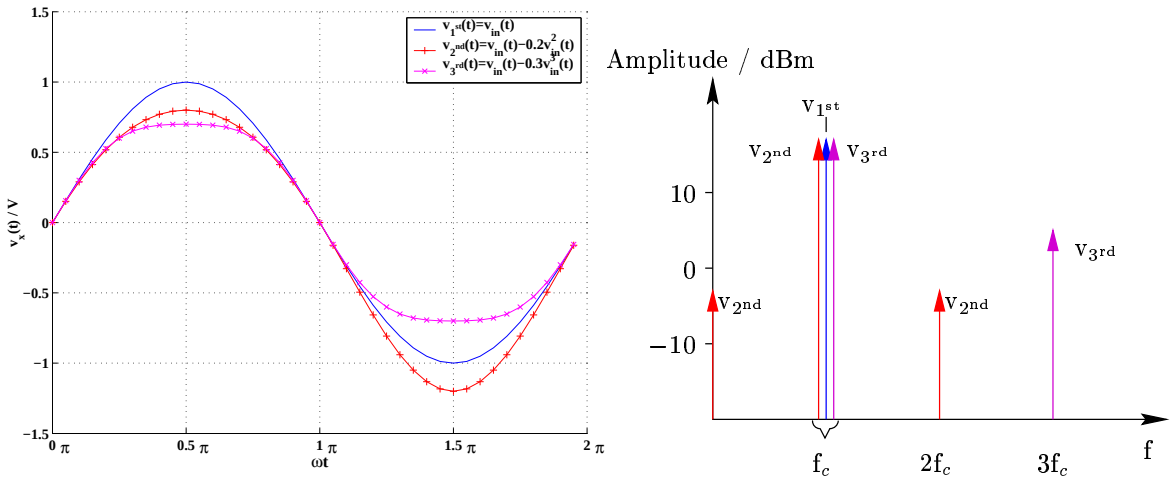

Figure 3.1: Output signal of a third-order model with different parameters k_x

in equation 3.1 with $k_1 = 1$. v_{2nd} shows the effect of a purely even order distortion. Two new frequency components are created at the frequencies $f = 0$ and $f = 2f_c$. v_{3rd} represents a purely odd-order distortion. The distortion creates a new frequency component at $f = 3f_c$ and alters the magnitude of the original output signal by the factor $\frac{3}{4}\frac{k_3}{k_1}$.

3.2.2 1 dB compression point

The 1 dB compression point of an amplifier refers to the output level at which the amplifiers transfer characteristic derivate from that of an ideal, linear characteristic by 1 dB. The 1 dB compression point of an amplifier is illustrated in figure 3.2 . More troubles with this figure of merit arise when it should be used for realistic amplifier. The problem is to define the ideal, linear transfer characteristic of the amplifier. In figure 3.2 the blue dashed line represents the ideal characteristic, as the slope of the real characteristic of the amplifier at the origin. Figure 3.3 shows the difficulties when trying to specify the 1 dB compression point for a realistic amplifier. Due to a complex relationship between the input and the output power, the gain of a power amplifier is analyzed around the considered operation point. In [Cav95] an interesting approach for the calculation of the amplifier gain was suggested.

By the use of the complex baseband representation the gain for a the selected input signal at a chosen power-level is calculated. $\widetilde{G}\left(|\widetilde{s}_{in}(t)|^2\right)$ names the complex envelope transfer characteristic. The difference between the instantaneous and the envelope transfer characteristic is

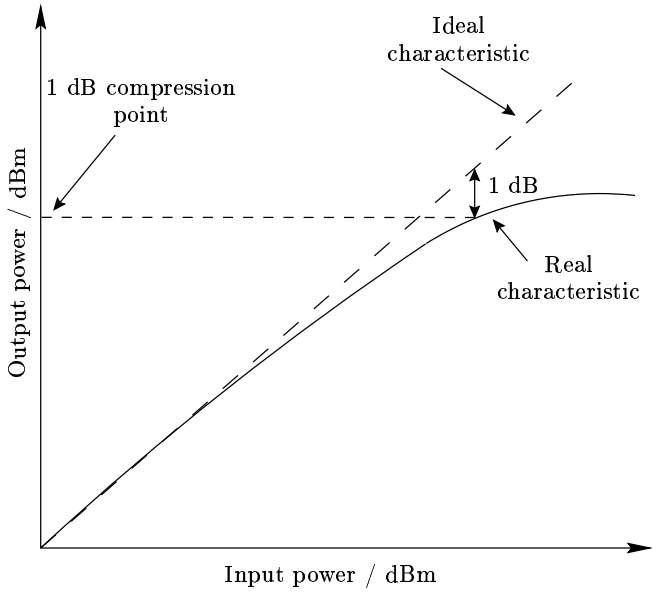

Figure 3.2: 1 dB compression point of a amplifier

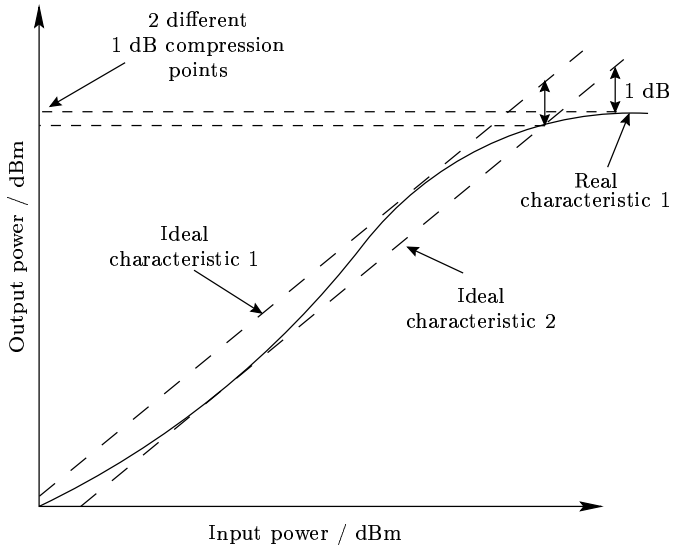

Figure 3.3: Problem with the specification of the 1 dB compression point

shown in section 3.3. The relationship between the input and the output signal can be found as:

$$\widetilde{s}_{out}(t) = \widetilde{s}_{in}(t)\,\widetilde{G}\left(\left|\widetilde{s}_{in}(t)\right|^2\right) \tag{3.4}$$

where $\widetilde{s}_{in}(t)$ and $\widetilde{s}_{out}(t)$ are the input signal and output signal. Knowing the amplitude-pdf (**P**robability **D**ensity **F**unction) of the input signal $p_{\widetilde{s}_{in}}$ the operating point of the amplifier can

be specified:

$$\widetilde{\mathrm{G}}_{\mathrm{s_{in}}} = \frac{1}{\mathrm{P_m}} \int_0^\infty \zeta \widetilde{\mathrm{G}}\left(\zeta\right) p_{\widetilde{\mathrm{s}}_{\mathrm{in}}}\left(\zeta\right) d\zeta \tag{3.5}$$

where $\mathrm{P_m}$ specifies the average power-level of the input signal $\widetilde{\mathrm{s}}_{\mathrm{in}}\left(\mathrm{t}\right)$. Equation 3.5 shows that the gain of an amplifier always depends on how the amplifier will be used. After the evaluation of the envelope gain $\widetilde{\mathrm{G}}_{\mathrm{s_{in}}}$ the instantaneous gain $\mathrm{G}_{\mathrm{s_{in}}}$ can be achieved. Now it is possible to determine the 1 dB compression point. This figure of merit is only valid for the selected input signal and the chosen input power-level.

3.2.3 Intercept point

The third-order characteristic can be very instructive to show another indicator of a RF-amplifier. Analyzing all parts of equation 3.3 separately using logarithmic units leads to:

$$\begin{aligned} \mathrm{P}_{1^{\mathrm{st}}} &= \mathrm{K}_1 + \mathrm{P}_{\mathrm{in}} \\ \mathrm{P}_{2^{\mathrm{nd}}} &= \mathrm{K}_2 + 2\mathrm{P}_{\mathrm{in}} \\ \mathrm{P}_{3^{\mathrm{rd}}} &= \mathrm{K}_3 + 3\mathrm{P}_{\mathrm{in}} \end{aligned} \tag{3.6}$$

where $\mathrm{P_{in}}$ and P_x are measured in dBm and the K_x are the values of k_x given in dB. The linear structure of equation 3.6 is due to the simple third-order model. The ideal shapes and also a more realistic versions of P_x are shown in figure 3.4. The point of intercept between the ideal fundamental and the ideal second-order characteristic is called second-order intercept point. It is common to use the output power level of the intercept point as specification from this characteristic value. The intercept point is used as a figure of merit for the linearity performance. The advantage of using an intercept point is that it is a fixed quantity from which the distortion level at a particular operation point may be predicted. The same concept as for the second-order intercept point can be used for the third-order intercept point. In difference to the second-order intercept point the third-order intercept point can only be measured by the use of a test signal with two or even more tones.

The example given in figure 3.4 is only comprehensible as long as the model parameter K_x for a real amplifier can be found. In the case of power amplifiers, other figures of merit like the IMD (**I**nter**m**odulation **D**istance), ACPR (**A**djacent **C**hannel **P**ower **R**atio), the NPR (**N**oise **P**ower **R**atio) or the shoulder distance are used to measure the linearity performance. The intermodulation distance will be explained in section 3.2.5. The definitions for the ACPR, NPR and shoulder distance are given in [Ken00, chap. 2.5]and *[CP99]* together with the equation for the conversion between these figures of merit.

3.2.4 First zone filter

As shown in figure 3.1 by the use of the third-order model 3.3 the distortion introduced by the factors $k_2\mathrm{v}_{\mathrm{in}}^2\left(\mathrm{t}\right)$ and $k_3\mathrm{v}_{\mathrm{in}}^3\left(\mathrm{t}\right)$ adds new spectral components to the output signal. Similar effects can be observed when using a two-tone input signal. Figure 3.5 shows the response of the third-order model on a two-tone input signal. It is obvious that the distortion components

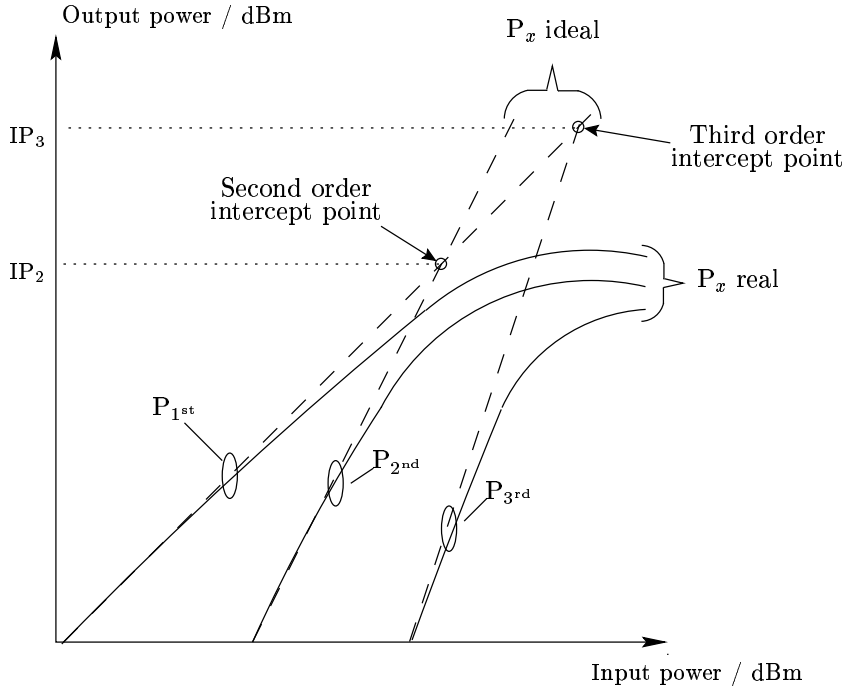

Figure 3.4: Locating of the intercept points

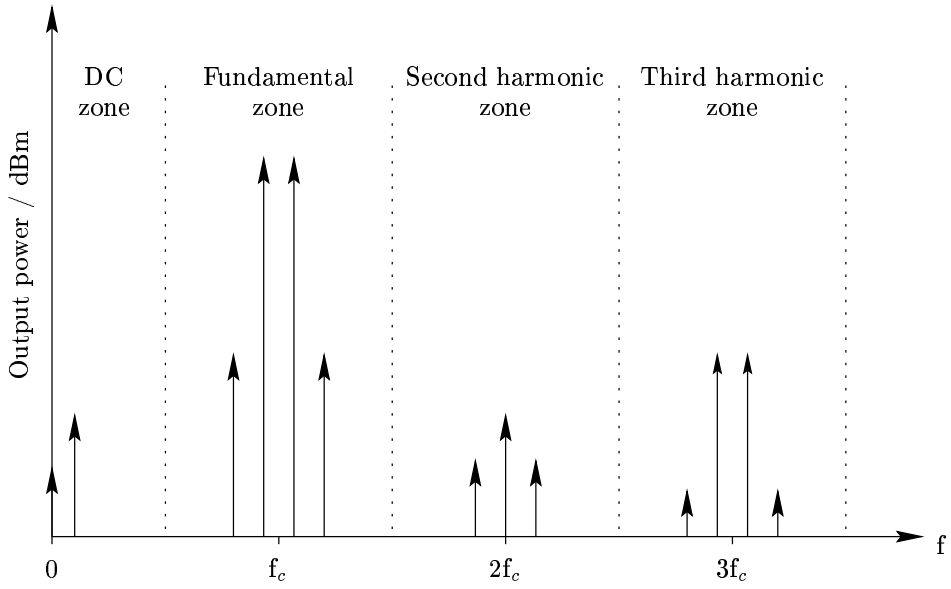

Figure 3.5: Frequency response of the third-order model supplied with a two-tone input signal

occupy a wide frequency range albeit the easy model is used. Especially in the case of mobile communication systems, the amplifiers can be modeled as a narrow-band device which only treat frequency components located in the fundamental zone (compare section 1.2.4). For all

further calculations, the distortion located outside the fundamental zone is neglected. In a theoretical analysis the negligence of the higher order harmonics is called a first-zone filter [JBS92, chap. 2.11.5.3] .

3.2.5 Intermodulation distance

The two-tone test is an almost accepted method of assessing the amplifier linearity. The effect of the two-tone test is to vary the envelope of the input signal over a wide range in order to test the amplifier transfer characteristic. In the general case a nonlinearity will create new frequency components when supplied with a two-tone input signal. They will have the shape:

$$f_{\mathrm{IM}} = mf_1 \pm nf_2, \quad m,n \in \mathbb{N}_o,\ m+n = \text{order of distortion} \tag{3.7}$$

Thus for the third-order model the additional output frequencies are:

$$\begin{array}{rlrl} m+n= & 2: & m+n= & 3: \\ \mathrm{f}_{\mathrm{IM2}_1}= & 2\mathrm{f}_1 & \mathrm{f}_{\mathrm{IM3}_1}= & 3\mathrm{f}_1 \\ \mathrm{f}_{\mathrm{IM2}_2}= & 2\mathrm{f}_2 & \mathrm{f}_{\mathrm{IM3}_2}= & 3\mathrm{f}_2 \\ \mathrm{f}_{\mathrm{IM2}_3}= & \mathrm{f}_1+\mathrm{f}_2 & \mathrm{f}_{\mathrm{IM3}_3}= & 2\mathrm{f}_1+\mathrm{f}_2 \\ \mathrm{f}_{\mathrm{IM2}_4}= & \mathrm{f}_1-\mathrm{f}_2 & \mathrm{f}_{\mathrm{IM3}_4}= & \mathrm{f}_1+2\mathrm{f}_2 \\ & & \mathrm{f}_{\mathrm{IM3}_5}= & 2\mathrm{f}_1-\mathrm{f}_2 \\ & & \mathrm{f}_{\mathrm{IM3}_6}= & \mathrm{f}_1-2\mathrm{f}_2 \end{array} \tag{3.8}$$

The complete output spectrum of the third-order model suppled with a two-tone input signal was already presented in figure 3.5.

The IMD_x is defined as the ratio of the amplitude of the highest intermodulation product of order x to one of the main tones. Figure illustrates the measurement of the IMD_x and shows the behavior as a function of the input power. The value of the third-order intermodulation distance IMD_3 can be also achieved when the third-order intercept point is known:

$$\mathrm{IMD}_3 = \left(\frac{\mathrm{P}_{\mathrm{in}_1}}{\mathrm{IP}_3}\right)^2 \tag{3.9}$$

where $\mathrm{P}_{\mathrm{in}_1}$ specifies the power of one tone of a two-tone signal.

3.3 Memoryless Amplifier model, AM-AM and AM-PM Conversion

The amplifier models presented up to now created only AM-AM distortion. Another effect which is also present in amplifiers, is the conversion from the amplitude modulation at the input signal to a phase modulation at the output signal of the amplifier, known as AM–PM conversion. Considering a memoryless bandpass nonlinearity with amplitude and phase distortion, the input signal:

$$\mathrm{V}_{\mathrm{in}}(\mathrm{t}) = \nu\cos(\omega_c \mathrm{t} + \varphi_c) \tag{3.10}$$

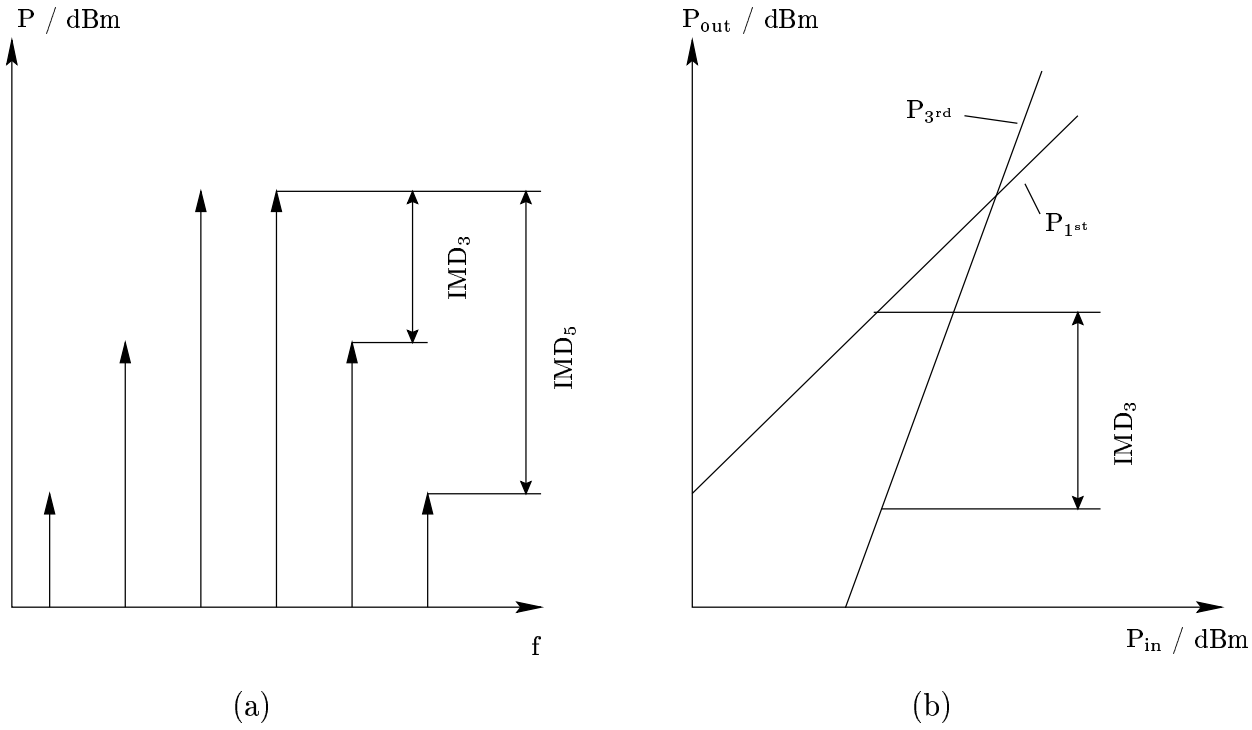

Figure 3.6: Measurement of IMD_3 and IMD_5 (a) and IMD_3 as a function of the input power (b)

is converted to:

$$V_{out}(t) = f\{\nu\}\cos(\omega_c t + \varphi_c + g\{\nu\}) \tag{3.11}$$

According to [Ken00, chap. 2.13.5] and [JBS92, chap. 2.11.5] equation 3.10 and equation 3.11 can be also applied to narrow-band modulated input signal as well:

$$\begin{aligned} V_{in}(t) &= \nu(t)\cos(\omega_c t + \varphi_c) \\ V_{out}(t) &= f\{\nu(t)\}\cos(\omega_c t + \varphi_c + g\{\nu(t)\}) \end{aligned} \tag{3.12}$$

That means that the instantaneous transfer characteristic can be applied to both narrow-band modulated and continuous carrier signals. The relationship presented in equation 3.12 is usually called envelope nonlinearities. If the described system should be modeled in the baseband, only the in-band distortion can be considered, because the harmonic frequencies of the envelope in the baseband differ from the passband harmonic frequencies. An equality between the passband and the baseband description of a nonlinear system is given when the fundamental zone is considered, e.a. a first-zone filter according to section 3.2.4 is used. Additionally the input signal must be also narrow-band, so that the device transfer characteristic is essentially frequency independent over the bandwidth of the input signal. Otherwise equation 3.12 has to be extended to frequency-dependent nonlinearity [JBS92, chap. 2.6.11],[Ken00, chap. 2.13.11].

Figure 3.7 shows the block model for AM-AM and AM-PM bandpass nonlinearity [Ken00, figure 2.28]. In figure 3.8 the equivalent baseband model is illustrated according to [JBS92,

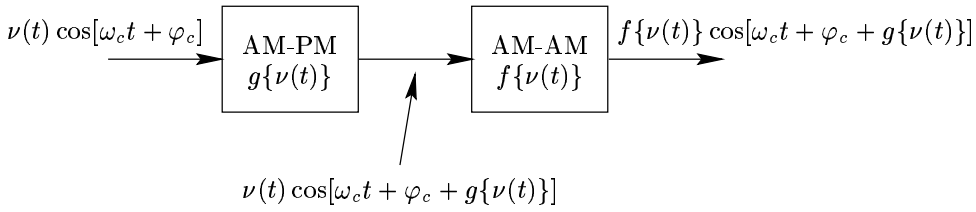

Figure 3.7: AM-AM and AM-PM bandpass nonlinearity passband model

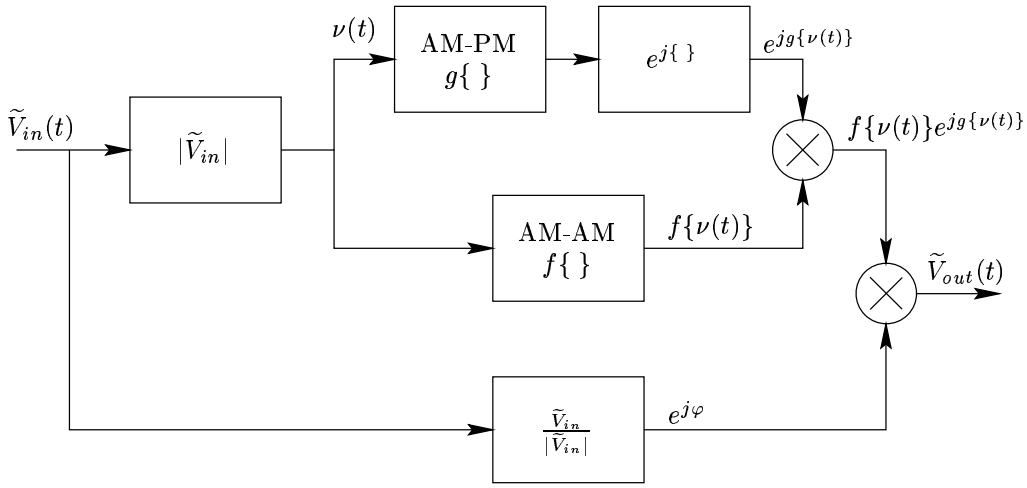

Figure 3.8: AM-AM and AM-PM bandpass nonlinearity baseband model

figure 2.59]. In the block models presented in figure 3.7 and figure 3.8 amplitude and phase distortion are treated separately, which is called the polar form of a memoryless nonlinear model. In a similar manner to the polar model, an equivalent Cartesian model can be found. This model has the advantage that it can be constructed from two nonlinear amplitude models, $\mathrm{I}\{\nu(\mathrm{t})\}$ and $\mathrm{Q}\{\nu(\mathrm{t})\}$, thereby avoiding the potential complexity of an AM-PM conversion. Equation 3.12 may be expanded to:

$$\begin{aligned} \mathrm{V_{out}}(\mathrm{t}) = \; & f\{\nu(\mathrm{t})\}\cos(g\{\nu(\mathrm{t})\})\cos(\omega_c \mathrm{t}+\varphi_c) \\ & -f\{\nu(\mathrm{t}))\}\sin(g\{\nu(\mathrm{t})\})\sin(\omega_c \mathrm{t}+\varphi_c) \end{aligned} \tag{3.13}$$

This equation can also be expressed in quadrature components as:

$$\mathrm{V_{out}}(\mathrm{t}) = \mathrm{I}\{\nu(\mathrm{t}))\}\cos(\omega_c \mathrm{t}+\varphi_c) - \mathrm{Q}\{\nu(\mathrm{t})\}\sin(\omega_c \mathrm{t}+\varphi_c) \tag{3.14}$$

The block models for the Cartesian representation can be found in [Ken00, figure 2.33] and [JBS92, figure 2.60].

3.3.1 Relationship between instantaneous and envelope transfer characteristic

Up to now no transformation equations between the instantaneous and the envelope transfer characteristic was given. When talking about the instantaneous transfer characteristic of a system following relationship is assumed:

$$\mathrm{V_{out}}\,(\mathrm{t}) = F\left\{\mathrm{V_{in}}\,(\mathrm{t})\right\} \tag{3.15}$$

where $\mathrm{V_{in}}\,(\mathrm{t})$ is in our case mostly a narrow-band modulated carrier:

$$\mathrm{V_{in}}\,(\mathrm{t}) = \nu\,(\mathrm{t})\cos\left(\omega_c \mathrm{t} + \Phi(\mathrm{t})\right) \tag{3.16}$$

The envelope transfer characteristic provides the relationship between the generally complex-valued signals $\widetilde{\mathrm{V}}_{\mathrm{in}}\,(\mathrm{t})$ and $\widetilde{\mathrm{V}}_{\mathrm{out}}\,(\mathrm{t})$:

$$\widetilde{\mathrm{V}}_{\mathrm{out}}\,(\mathrm{t}) = \widetilde{F}\left\{\widetilde{\mathrm{V}}_{\mathrm{in}}\,(\mathrm{t})\right\} \tag{3.17}$$

The derivation of the envelope transfer characteristic $\widetilde{F}\left\{\cdot\right\}$, starting from the instantaneous transfer characteristic $F\left\{\cdot\right\}$ is shown below.

According to [JBS92, chap. 2.11.7.2], the instantaneous characteristic $F\left\{\cdot\right\}$ is a memoryless nonlinear function of the input. Considering a bandpass input signal as shown in equation 3.16 and making the substitution:

$$\beta = \omega_c \mathrm{t} + \Phi\,(\mathrm{t})\,, \quad \nu = \nu\,(\mathrm{t}) \tag{3.18}$$

The output can be considered as a function of β:

$$\mathrm{V_{out}} = F\left\{\nu\cos\left(\beta\right)\right\} \tag{3.19}$$

Equation 3.19 is a periodic function in β and hence can be expanded in a Fourier series:

$$\mathrm{V_{out}} = a_o + \sum_{k=1}^{\infty}\left(a_k\cos\left(k\beta\right) + b_k\sin\left(k\beta\right)\right) \tag{3.20}$$

Assuming the use of a first-zone filter:

$$\mathrm{V_{out}} = f_1\left\{\nu\,(\mathrm{t})\right\}\cos\left(\omega_c \mathrm{t} + \Phi\,(\mathrm{t})\right) - f_2\left\{\nu\,(\mathrm{t})\right\}\sin\left(\omega_c \mathrm{t} + \Phi\,(\mathrm{t})\right) \tag{3.21}$$

where the coefficients are given by:

$$\begin{aligned} a_1 = f_1\left\{\nu\,(\mathrm{t})\right\} &= \tfrac{1}{\pi}\int_0^{2\pi} F\left\{\nu\cos\left(\beta\right)\right\}\cos\left(\beta\right)\,d\beta \\ b_1 = f_2\left\{\nu\,(\mathrm{t})\right\} &= -\tfrac{1}{\pi}\int_0^{2\pi} F\left\{\nu\cos\left(\beta\right)\right\}\sin\left(\beta\right)\,d\beta \end{aligned} \tag{3.22}$$

To produce AM-AM and AM-PM distortion two quadrature nonlinearities are needed. Comparing equations 3.13 and 3.21 shows that $\widetilde{\mathrm{I}}\left\{\cdot\right\} = f_1\left\{\cdot\right\} = a_1$ and $\widetilde{\mathrm{Q}}\left\{\cdot\right\} = f_1\left\{\cdot\right\} = b_1$. After evaluating the two amplitude nonlinearities, the envelope transfer characteristic can be set together as $\widetilde{F}\left\{\cdot\right\} = \widetilde{\mathrm{I}}\left\{\cdot\right\} + j\widetilde{\mathrm{Q}}\left\{\cdot\right\}$.

3.3.2 Generalized complex power series

The complex power series, describing the envelope transfer characteristic of a memoryless nonlinear device, is given by:

$$\widetilde{\mathrm{V}}_{\mathrm{out}}(\mathrm{t}) = \sum_{n=1}^{N} a_n \widetilde{\mathrm{V}}_{\mathrm{in}}^{n}(\mathrm{t}) \tag{3.23}$$

with $a_n \in \mathbb{C}$ and N is the order of the model. It should be mentioned that the baseband description of a passband nonlinearity assumes the use of a first-zone filter. In difference to the Taylor series presented in equation 3.2 the generalized complex power series can be used to model a memoryless nonlinear device including AM-AM and AM-PM conversion. Substituting $a_n = a_{\mathrm{I}_n} + j a_{\mathrm{Q}_n}$ into equation 3.23 leads to:

$$\widetilde{\mathrm{V}}_{\mathrm{out}}(\mathrm{t}) = \sum_{n=1}^{N} a_{\mathrm{I}_n} \widetilde{\mathrm{V}}_{\mathrm{in}}^{n}(\mathrm{t}) + j \sum_{n=1}^{N} a_{\mathrm{Q}_n} \widetilde{\mathrm{V}}_{\mathrm{in}}^{n}(\mathrm{t}) = \mathrm{I}\left\{\widetilde{\mathrm{V}}_{\mathrm{in}}(\mathrm{t})\right\} + j\mathrm{Q}\left\{\widetilde{\mathrm{V}}_{\mathrm{in}}(\mathrm{t})\right\} \tag{3.24}$$

where $\mathrm{I}\{\cdot\}$ and $\mathrm{Q}\{\cdot\}$ are the two amplitude nonlinearities used for the Cartesian representation of a nonlinear model.

The easy manageable structure of the generalized power series can be profitably used to calculate the relationship between the instantaneous and the envelope transfer characteristic without solving the integrals in equation 3.22 . Following the concept of [JBS92, chap. 2.11.7.2] the input signal is defined as:

$$\mathrm{V}_{\mathrm{in}}(\mathrm{t}) = \nu(\mathrm{t}) \cos\left(\omega_c \mathrm{t} + \Phi(\mathrm{t})\right) = \Re\left\{\nu(\mathrm{t})\, e^{j\Phi(\mathrm{t})}\, e^{j\omega_c \mathrm{t}}\right\} = \Re\left\{\widetilde{\mathrm{V}}_{\mathrm{in}}(\mathrm{t})\, e^{j\omega_c \mathrm{t}}\right\} \tag{3.25}$$

Using the instantaneous transfer characteristic 3.2:

$$\begin{aligned} \mathrm{V}_{\mathrm{out}}(\mathrm{t}) &= \sum_{n=1}^{N} k_n \mathrm{V}_{\mathrm{in}}^{n}(\mathrm{t}) \\ \mathrm{V}_{\mathrm{in}}^{n}(\mathrm{t}) &= \left(\tfrac{1}{2}\widetilde{\mathrm{V}}_{\mathrm{in}}(\mathrm{t})\, e^{j\omega_c \mathrm{t}} + \tfrac{1}{2}\widetilde{\mathrm{V}}_{\mathrm{in}}^{*}(\mathrm{t})\, e^{j\omega_c \mathrm{t}}\right)^n \end{aligned} \tag{3.26}$$

$\mathrm{V}_{\mathrm{in}}^{n}(\mathrm{t})$ can be rearrange by the use of binomial expansion:

$$\mathrm{V}_{\mathrm{in}}^{n}(\mathrm{t}) = \frac{1}{2^n} \sum_{m=0}^{n} \binom{n}{m} \left(\widetilde{\mathrm{V}}_{\mathrm{in}}(\mathrm{t})\right)^m \left(\widetilde{\mathrm{V}}_{\mathrm{in}}^{*}(\mathrm{t})\right)^{n-m} e^{j(2m-n)\omega_c \mathrm{t}} \tag{3.27}$$

After first-zone filtering terms can contribute only if n is odd and $2k - n = \pm 1$. This condition further simplifies equation 3.27 to:

$$\mathrm{V}_{\mathrm{in}_{1z}}^{n}(\mathrm{t}) = \frac{1}{2^{n-1}} \binom{n}{\frac{n+1}{2}} \left|\widetilde{\mathrm{V}}_{\mathrm{in}}(\mathrm{t})\right|^{n-1} \widetilde{\mathrm{V}}_{\mathrm{in}}(\mathrm{t})\, e^{j\omega_c \mathrm{t}} \tag{3.28}$$

Hence the baseband equivalent of equation 3.26 is:

$$\widetilde{\mathrm{V}}_{\mathrm{out}}(\mathrm{t}) = \widetilde{\mathrm{V}}_{\mathrm{in}}(\mathrm{t}) \sum_{n=0}^{\frac{N-1}{2}} \frac{k_{2n+1}}{2^{2n}} \binom{2n+1}{n+1} \left|\widetilde{\mathrm{V}}_{\mathrm{in}}(\mathrm{t})\right|^{2n} \tag{3.29}$$

Now the coefficients of equation 3.23 and equation 3.29 can be compared to find the conversion function between the instantaneous transfer characteristic and the envelope transfer characteristic:

$$\begin{aligned} a_{2n+1} &= k_{2n+1}\frac{2^{2n}n!(n+1)!}{(2n+1)!} \\ a_{2n} &= 0 \end{aligned} \tag{3.30}$$

Chapter 4

Measurement of key-components

4.1 Introduction

Up to now the theory of an FFA and the modeling of nonlinear RF-devices were discussed. Now the attention should be turned on the devices used in the FFA. Most expenditure was given to the measurement of the amplifiers and the vector attenuators.

A PCB (**P**rinted **C**ircuit **B**oard) was built access the vector attenuator module. After measuring the realized units a MATLAB®-function was written, which sets the driving-current according to the selected attenuation value.

In the next part of this chapter the measurements of the amplifiers are presented. Several measurements were performed to characterize the preamplifier, main and error amplifier.

4.2 Vector attenuator

The chosen VA (**V**ector **A**ttenuator) MPT 1820VA is a hybrid-MIC produced by MPT (**M**icro-**P**recision **T**echnologies Inc.). This VA is specified to operate at a frequency range between 1.8 and 2.0 GHz. Two current loops are used to adjust the real and the imaginary part of the attenuation. This VA consists of two pin-diodes used as variable attenuators between two I/Q-hybrids [MPT97]. Figure 4.1 depicts the principle structure of the VA. The MPT 1820VA is built in a 18-pin surface mount package measuring 1.0" x 0.9". The electrical characteristics are presented in table 4.1 [MPT00].

4.2.1 Circuit schematic

The circuit schematic is based on the available evaluation board. To preserve full flexibility, all four current inputs I_{I1}, I_{I2}, I_{Q1} and I_{Q2} are separately accessible. The whole circuit is built on a FR4 Epoxy Laminate base material, 63 mil thick, with two-sided copper coating. The shielding enclosure should consist out of multipoint socket connector strips soldered on the PCB. The cover, kept by the multi-point socket connector strips, consists of a copper plate with a silver coating. By the use of PCB-mounted 90° SMA-connectors the RF-signals are passed through the shielding enclosure. A coplanar-ground transmission line provides the connection of the RF-signals from

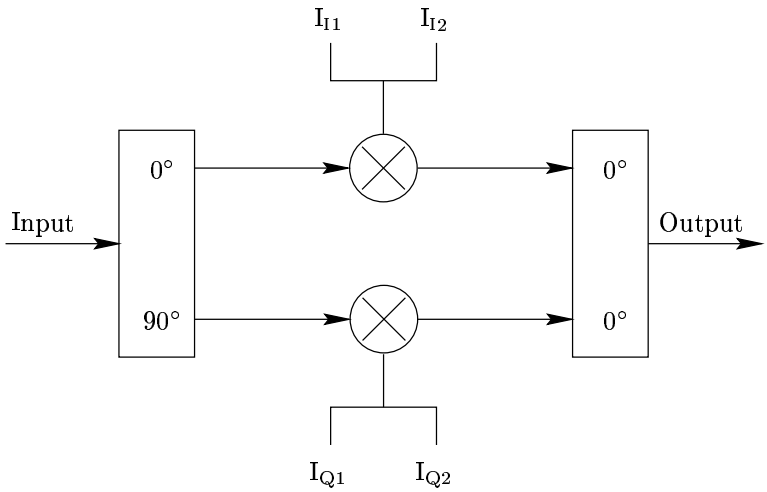

Figure 4.1: Structure of a vector attenuator

max. RF-input signal power	20 dBm
minimum insertion loss	10 dB
typical attenuation range	20 dB
$\|S_{11}\|$	-19 dB
$\|S_{22}\|$	-14 dB
IP_3	>40 dBm
max. Input current for I_{I1},I_{I2},I_{Q1},I_{Q2}	50 mA

Table 4.1: Electrical characteristics of the vector attenuator MPT 1820VA

the SMA-connectors to the MPT 1820VA. Feed-through capacities make the interconnect for the driving currents. RF-chokes and blocking capacities keep the driving currents free of RF-signals. A batch of 100 Ω-resistors should assure equal currents in each branch, if the inputs are connected in parallel. Figure 4.2 shows the complete circuit diagram for the VA-interface board. The electronic devices used in the circuit diagram are listed in table 4.2.

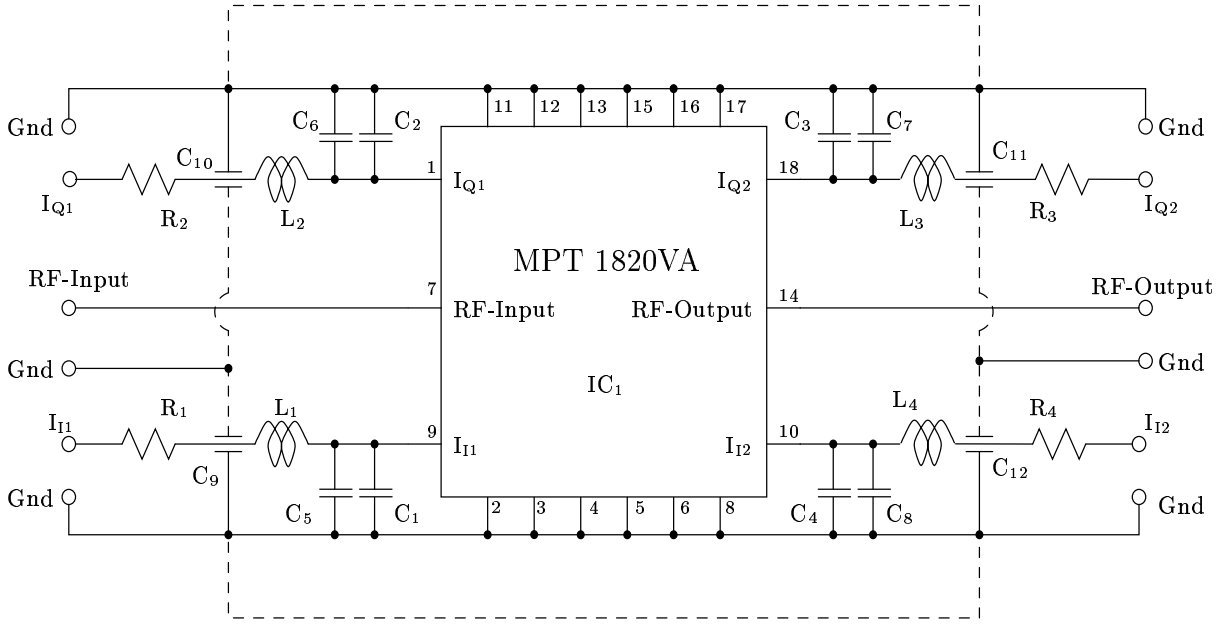

Figure 4.2: Circuit diagram of the VA-interface board

IC_1		MPT 1820VA Vector attenuator
$C_1 - C_4$	68 pF	Ceramic SMD Chip capacities 0603
$C_5 - C_8$	820 pF	Ceramic SMD Chip capacities 0603
$C_9 - C_{12}$	10 nF	Feed through capacities
$L_1 - L_4$	18nH	SMD Chip inductivities 0805
$R_1 - R_4$	100 Ω	metal oxide resistors
not shown in the circuit diagram:		
2 pcs		90° SMA connectors for PCB mounting
201 mm		multipoint socket connector strip
1 pce		40 mm x 60,5mm cover plate
6 pcs		soldering pins

Table 4.2: Electronic devices used for the VA-interface board

4.2.2 PCB-design

The only critical part in the design of the PCB was to dimension the transmission line, which should be matched to 50 Ω. The defaults for the dimensioning of the transmission line were:

- FR4 has to be used for the PCB, which has an $\epsilon_r \approx 4.2$ at 2 GHz
- The PCB is manufactured with a thickness of 1.6 mm $\approx$ 63 mil cladded with 35 μm $\approx$ 1.4 mil copper
- The signal trace of the transmission line should be smaller than 100 mil to fit between connector-pins of the SMA-connector
- The transmission line is used at 2 GHz

The estimation of the transmission line parameters was done by the use of the programs TX-Line 2001 and LineGauge Basic 1.01. Both programs are tools to calculate the dimension of classical transmission lines. Figure 4.3 illustrates the structure of the two simulated transmission lines.

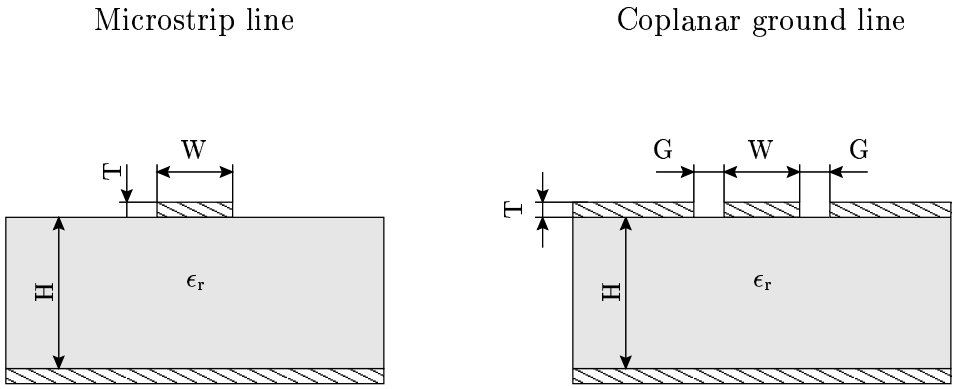

Figure 4.3: Structure of a microstrip and a coplanar ground transmission line

As first transmission line a microstrip line was evaluated. But due to the quite low ϵ_r of the base-material, the width of the track was too wide to fit between the connector-pins of the SMA-connector (W $\approx$ 126 mil).

The alternative to the microstrip line was the CPG-line (**Co**planar **G**round). The first evident advantage of the CPG-line are the two ground planes beside the signal-track. The construction of the chosen SMA-connector advises the use of a structure, where the signal-trace is located between two ground planes. The disadvantage of the CPG-line is the high sensitivity on the ratio between the width of the signal-track and the width of the gap $\frac{G}{W}$. This ratio is used to adjust the characteristic impedance of the transmission line. Table 4.3 presents the set of suitable parameters.

The characteristic impedance results in a return-loss $|S_{11}|$ of better more than -20 dB at the considered frequency. The uncertainty of the PCB's ϵ_r let the result seem acceptable. For a further improvement of the return loss without increasing the width W of the signal trace a significantly higher accuracy requirement for the ratio $\frac{G}{W}$ would be needed.

The final layout for the PCB is illustrated in figure 4.4. The component placement, illustrated in figure 4.5, helps to find the correct location of the electronic components. The PCB's were produced without a solder resist mask, because this dielectric layer could alter the properties of the transmission line.

H =	63 mil	$\approx$1.6 mm
W =	70 mil	$\approx$1.78 mm
G =	14 mil	$\approx$356 μm
T =	1.4 mil	$\approx$36 μm
ϵ_r =	4.2	
f =	2 GHz	
Z_o =	59.5 Ω	

Table 4.3: Physical dimension of the CPG-line

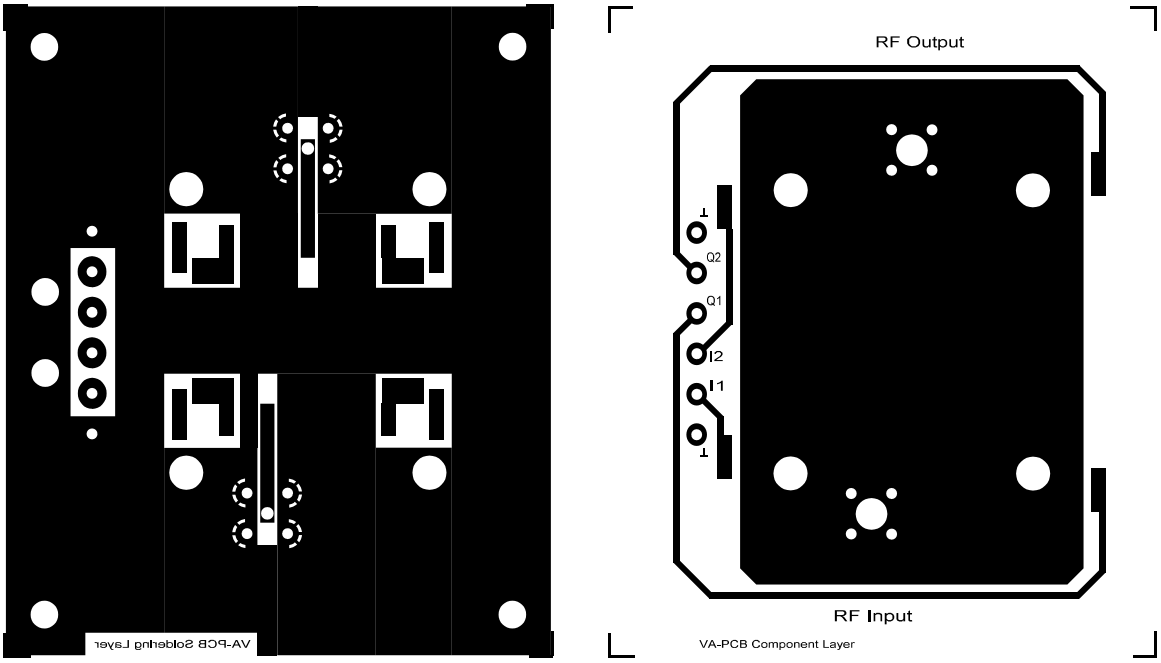

(a) (b)

Figure 4.4: Soldering layer (a) and component layer (b) of the PCB , scaled 1:1

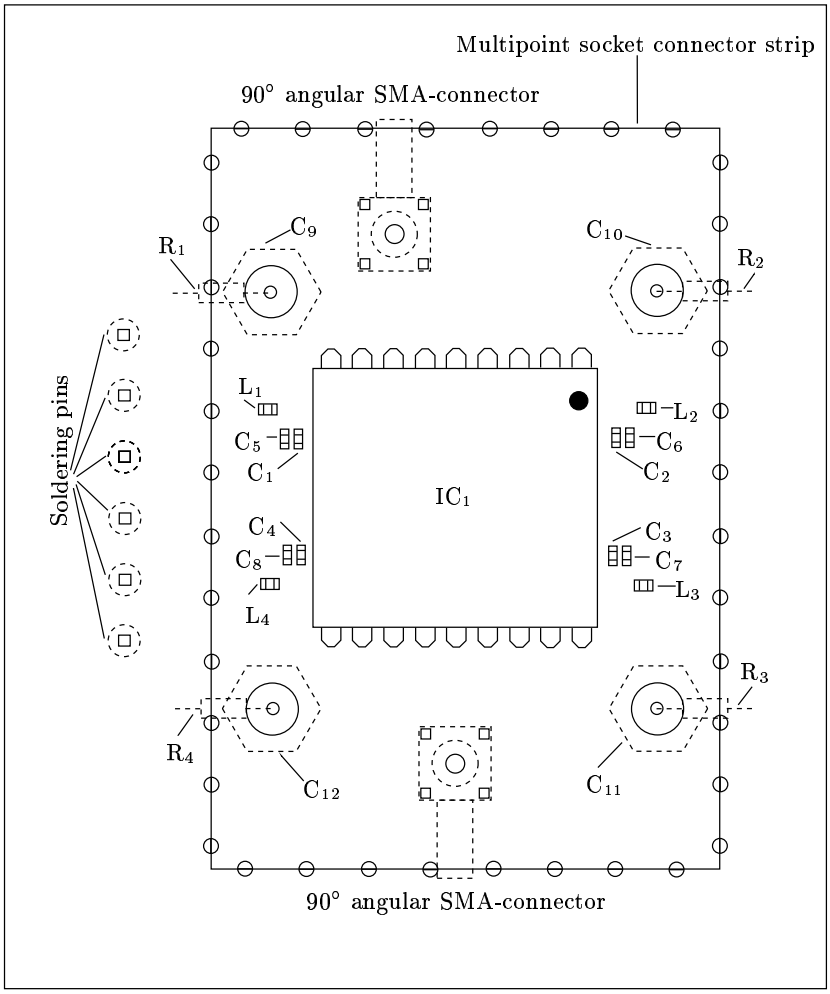

Figure 4.5: Component placement shown from the soldering side of the PCB

4.2.3 Vector attenuator measurement

Two vector attenuator boards were assembled, further on called VA1 and VA2. Together with the MPT-evaluation board, the behavior of three vector attenuator boards were analyzed. After some tests with the VA1-board it turned out, that the current inputs I_{I1} and I_{I2} and the current inputs I_{Q1} and I_{Q2} can be connect in parallel without any performance degradation. For all three boards, the magnitude of the reflection coefficient at the input and the output of the circuit were measured. For this measurement all current inputs were supplied with a current to provide a defined operation point for the pin-diodes. Afterwards the controlling function $S_{21}(I_I, I_Q)$ was evaluated for several I, Q -current values, where $I_I = I_{I1} + I_{I2}$ and $I_Q = I_{Q1} + I_{Q2}$. For the measurement of the controlling function the MATLAB® script "VAmeasure_V3" was used, which is described in the appendix A.1.1.

All three boards show quite similar measurement results for the controlling function and the return loss. Due to this reason only the measurement results for the VA1-board are mapped into this thesis. Table 4.4 presents the results of the return loss measurement. Figure 4.6 depicts

Input current $I_{I1}, I_{I2}, I_{Q1}, I_{Q2}$	$\lvert S_{11}\rvert$/ dB	$\lvert S_{22}\rvert$/ dB
1 mA	< -18 dB	< -21 dB
20 mA	< -17 dB	< -17.5 dB

Table 4.4: VA1 return loss for a frequency range of 1.8 - 2.0 GHz

$|S_{11}|$ over a frequency range from 1.8 to 2.0 GHz at a drive current of 1 mA for each input.

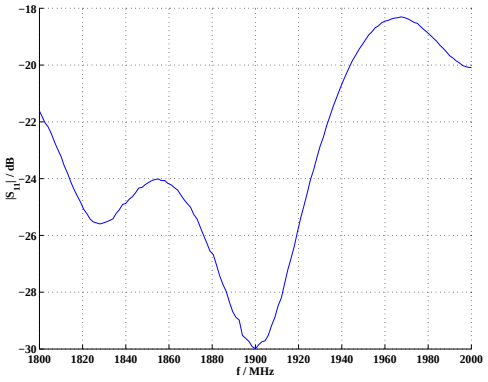

Figure 4.6: $|S_{11}|$ of the VA1-board

The behavior of the controlling function for a set of inphase and quadrature currents is illustrated in figure 4.7. Figure 4.8 shows the inphase and the quadrature control current as a function of the complex-valued transfer function.

4.2.4 Attenuation–current transformation

The application for the VA is to tune a cancellation loop according to the commands given by the loop controller. The attenuation–current transformation makes the connection between the

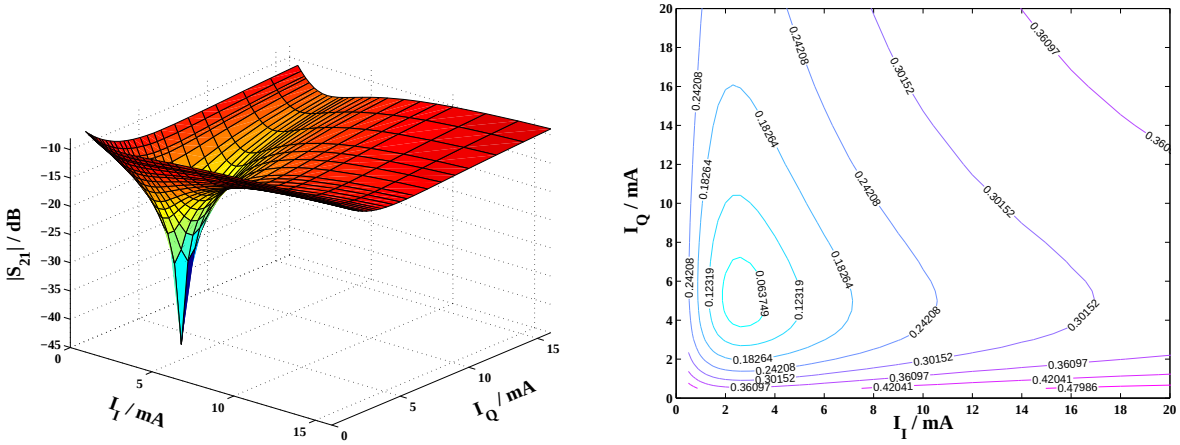

(a) (b)

Figure 4.7: |S21(I, Q)| measured at 1960 MHz

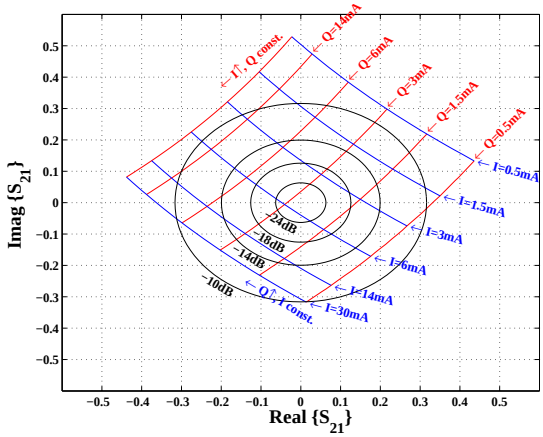

Figure 4.8: Control current as a function of the transfer characteristic from the VA1-board at 1960 MHz

output of the loop controller and the driving currents which are used to adjust the VA.

The transformation uses the measured controlling function values $|S21(I_I, I_Q)|$ as fulcrums. In a first step the fulcrum with the shortest distance to the desired attenuation value VA_o is determined. As second step the neighbors in inphase and quadrature direction to the fulcrum are evaluated. By the use of linear interpolation the output currents will be estimated.

Figure 4.9 illustrates the locating of the measurement points in the complex attenuation plane. The points which are indexed by the inphase and the quadrature currents are afterwards

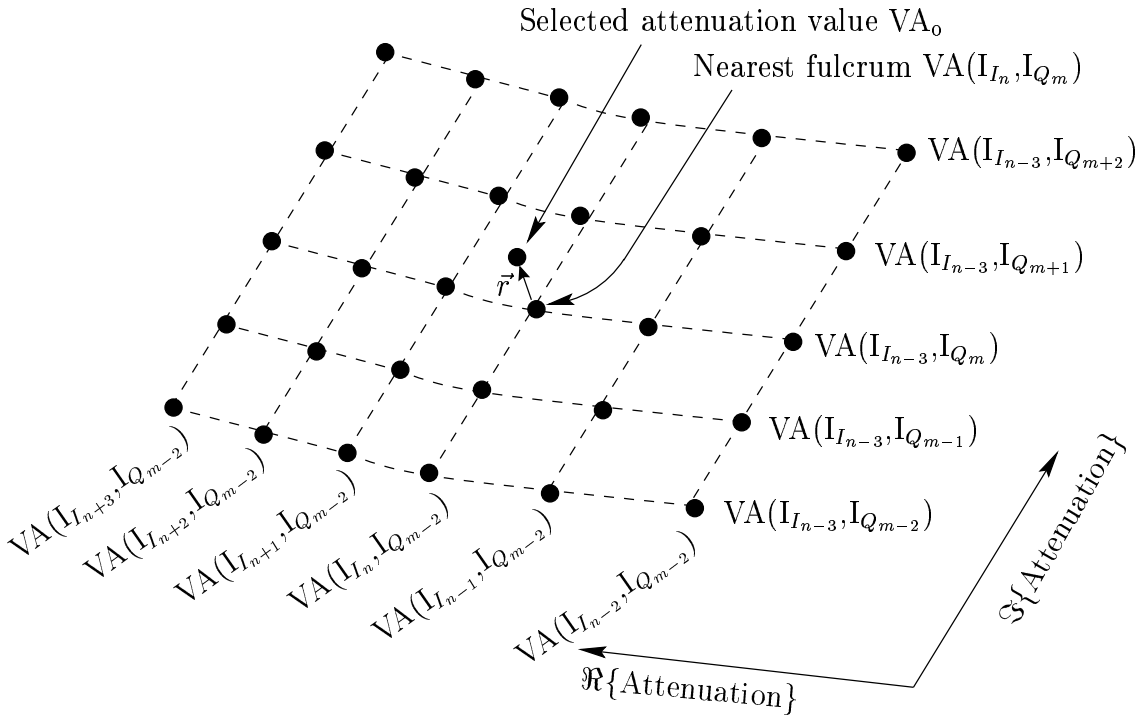

Figure 4.9: Measurement points of the vector attenuator used as fulcrum for the attenuation-to-current transformation

used as fulcrum for the transformation. In the drawing the measurement points are named $VA(I_{meas}(n), I_{meas}(m))$. The vector $I_{meas}(\cdot)$ keeps all k current-elements at which the vector attenuator was measured. The elements in the I_{meas}-vector are sorted in ascending order. Hence the measured controlling function in the example shown in figure 4.9 is a $k \times k$ squared matrix. The attenuation value $VA_o = VA(I_{I_o}, I_{Q_o})$ specifies the attenuation for which the corresponding control-currents should be found. The nearest fulcrum to this attenuation value, called $VA(I_{I_n}, I_{Q_m})$. The control-currents used to set $VA(I_{I_n}, I_{Q_m})$ can be interpreted as a first approximation for the searched control-current values.

Due to the ascending order of the currents in the vector I_{meas} the searched current-values must be located within the following limits:

$$\begin{array}{ll} I_{I_{n-1}} < I_{I_o} \leq I_{I_n} & , for \ \left|VA(I_{I_{n-1}}, I_{Q_m}) - VA_o\right| \leq \left|VA(I_{I_{n+1}}, I_{Q_m}) - VA_o\right| \\ I_{I_n} < I_{I_o} < I_{I_{n+1}} & , else \end{array} \tag{4.1}$$

$$\begin{array}{ll} \mathrm{I_{Q_{m-1}}} < \mathrm{I_{Q_o}} \leq \mathrm{I_{Q_m}} & , for \ \left|\mathrm{VA(I_{I_n}, I_{Q_{m-1}})} - \mathrm{VA_o}\right| \leq \left|\mathrm{VA(I_{I_n}, I_{Q_{m+1}})} - \mathrm{VA_o}\right| \\ \mathrm{I_{Q_m}} < \mathrm{I_{Q_o}} < \mathrm{I_{Q_{m+1}}} & , else \end{array} \tag{4.2}$$

After the four surrounding fulcrums of the attenuation value $\mathrm{VA_o}$ are known, the approximation for the control-current can be improved. Postulating a linear relationship between the attenuation values and the control-currents within the four surrounding fulcrums results in the structure presented in figure 4.10. The vector $\overrightarrow{\mathrm{VA_I}}$ connects the two fulcrums $\mathrm{VA\,(I_{I_n}, I_{Q_m})}$ and

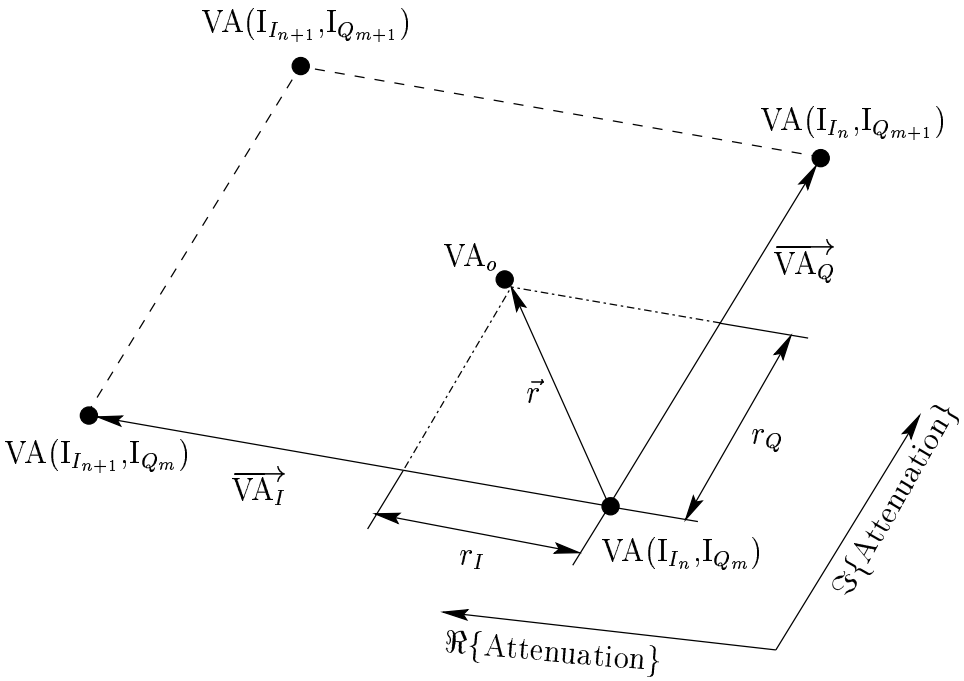

Figure 4.10: $\mathrm{VA_o}$ surrounded by four fulcrums

$\mathrm{VA\,(I_{I_{n+1}}, I_{Q_m})}$. Any point along this line can be found by varying the inphase current. The same relationships are valid for the vector $\overrightarrow{\mathrm{VA_Q}}$. The projection of the vector $\overrightarrow{r}$ onto the vector $\overrightarrow{\mathrm{VA_I}}$ gives a correction-factor which can be used to approximate the inphase control-current. The linear estimation of the control-currents for an attenuation value $\mathrm{VA_o} = \mathrm{VA(I_{I_o}, I_{Q_o})}$ is thus:

$$\begin{aligned} \mathrm{I_{I_o}} &= \mathrm{I_{I_n}} + \frac{\left(\overrightarrow{r}, \overrightarrow{\mathrm{VA_I}}\right)}{\left|\overrightarrow{\mathrm{VA_I}}\right|} \cdot \left(\mathrm{I_{I_{n+1}}} - \mathrm{I_{I_n}}\right) \\ \mathrm{I_{Q_o}} &= \mathrm{I_{Q_m}} + \frac{\left(\overrightarrow{r}, \overrightarrow{\mathrm{VA_Q}}\right)}{\left|\overrightarrow{\mathrm{VA_Q}}\right|} \cdot \left(\mathrm{I_{Q_{m+1}}} - \mathrm{I_{Q_m}}\right) \end{aligned} \tag{4.3}$$

where $\left(\vec{a}, \vec{b}\right)$ means the scalar product of the two vectors.

It is obvious that the quality of this estimation depends on the current vector $\mathrm{I_{meas}}$. For a

constant accuracy the following requirements must be fulfilled:

$$\frac{\partial \mathrm{VA}\left(\mathrm{I_{I_o}}, \mathrm{I_{Q_o}}\right)}{\partial \mathrm{I_{I_o}}} = \frac{\partial \mathrm{VA}\left(\mathrm{I_{I_o}}, \mathrm{I_{Q_o}}\right)}{\partial \mathrm{I_{Q_o}}} = constant \tag{4.4}$$

This means that the distance between two current values $\mathrm{I_{I_n}}$ and $\mathrm{I_{I_{n+1}}}$ must be set according to the requirement of the change in the attenuation values $\mathrm{VA}\left(\mathrm{I_{I_n}}, \mathrm{I_{Q_m}}\right)$ and $\mathrm{VA}\left(\mathrm{I_{I_{n+1}}}, \mathrm{I_{Q_m}}\right)$.

4.3 Preamplifier

A wideband amplifier manufactured by MINI-CIRCUITS® ZHL-42W was used as a preamplifier for the measurement of the main amplifier and the FFA. The specifications printed in the data-sheet are shown in table 4.5. To characterize the behavior of this amplifier a single-tone and

DC-power supply:	15 V, 0.8 A
Frequency band:	10 - 4200 MHz
Gain:	min. 30 ±1.5 dB
1 dB compression point:	28 dBm
$\mathrm{IP3_{output}}$:	38 dBm

Table 4.5: Preamplifier specification

a two-tone measurement was performed. The single-tone measurement was carried out from -25 dBm to 0 dBm by the use of the amplifier "gainmeasurement"-script, described in the appendix, section A.2. Figure 4.11 shows the gain of the preamplifier over the frequency-power-plane. It

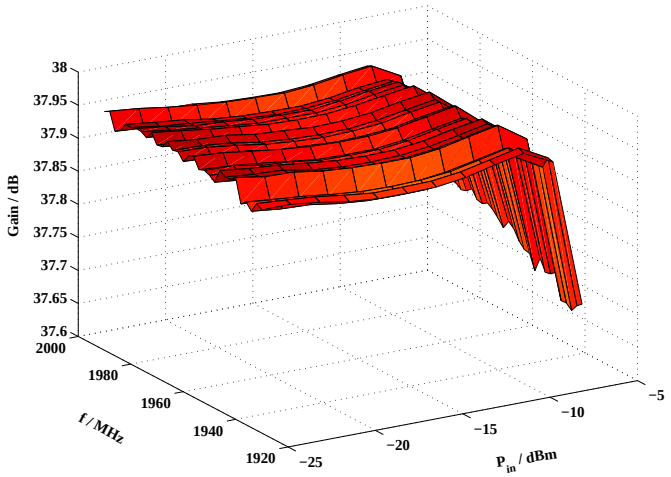

Figure 4.11: Gain of the preamplifier

illustrates, that the gain of this amplifier varies by 0.1 dB (37.9 dB - 38.0 dB) in the interesting frequency band. According to section 3.2.2, the 1 dB compression point was evaluated at an output power level of 31.92 ±0.03 dBm.

In a next step the response on a two-tone input signal was measured by the use of the "TwoTone"-script, which is also documented in the appendix, section A.3 . Figure 4.12 illus-

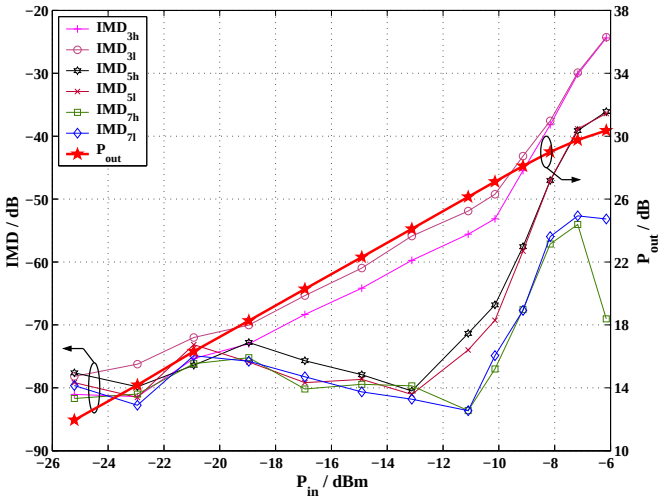

Figure 4.12: IMD of the preamplifier for a two-tone input signal at 1930 MHz

trates that the preamplifier can be used up to a output power of 28 dBm, when a minimum intermodulation distance of 50 dB must be adhered. By the use of the two-tone measurement, the third-order intercept point was evaluated: $IP3_{output}$=38.7 dBm.

DC-power supply:	15 V, 0.7 A
Measured frequency band:	1930 - 1990 MHz
Gain:	37.8 ±0.16 dB
1 dB compression point:	31.92 ±0.03 dBm
$IP3_{output}$:	38.7 dBm

Table 4.6: Preamplifier measurement summary

4.4 Main amplifier

Three power amplifiers were supplied by SIEMENS AG VIENNA for the main amplifier of the FFA. For all amplifiers a single-tone measurement and a two-tone measurement were performed. Based on these measurements one amplifier was selected and additional measurements according to the GSM2+ standard were carried out. The supplied amplifiers were power amplifiers for BTS's, called EPWRSTPV1 (**E**dge **P**ower**st**age **P**CS-band **V1**), able to fulfill the GSM2+ specification at an output power of 34W. Additionally these amplifiers are equipped with a isolator and a directional coupler at the output.

In this thesis only the measurement results of the selected main amplifier are printed. Figure 4.13 shows the single-tone measurement of the EPWRSTPV1 amplifier. According to this single-tone

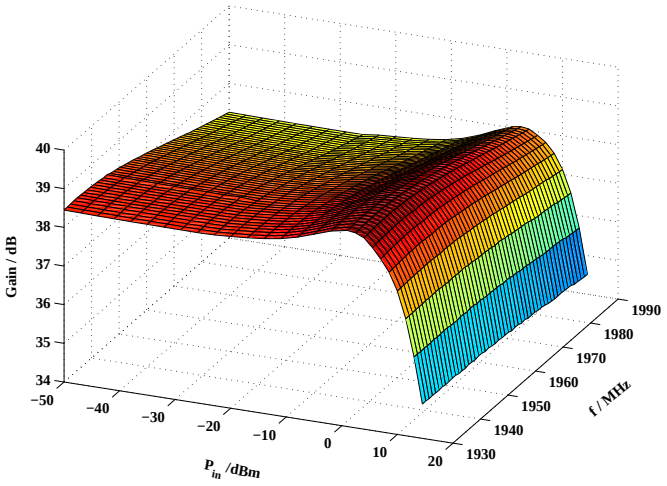

Figure 4.13: Gain of the main amplifier

measurement the gain of the amplifier is $36.2^{+2.8}_{-0.8}$ dB. The 1 dB compression point was found at 48.1 dBm ±0.2 dB.

Additionally the gain of the amplifier can be calculated for a GSM2+ input signal can be found. After converting the instantaneous transfer characteristic to the envelope characteristic as shown in section 3.3.2 the gain was calculated according to equation 3.5. Table 4.7 presents the results for three different input signal powers. The evaluation was performed with the following

Mean input signal power	Gain
10 dBm	36.4 dB
11 dBm	35.7 dB
12 dBm	34.9 dB

Table 4.7: Gain of the main amplifier for a GSM2+ input signal

defaults:

- The instantaneous gain was approximated by a 9th-order complex power series
- The carrier frequency of the input signal was set to 1960 MHz

Figure 4.14 illustrates the behavior of the amplifier when a two-tone input signal is supplied. Based on this measurement the third order intercept point was evaluated: $IP3_{output}$=53.1 dBm.

Additionally to the gain and the intermodulation performance the PAE (**P**ower **A**dded **E**fficiency) , the GSM2+ compliance test and a measurement of the internal of the main amplifier were performed. The power added efficiency is defined as [Mag98]:

$$\eta_{\mathrm{PAE}} = \frac{\mathrm{P_{out}} - \mathrm{P_{in}}}{\mathrm{P_{DC}}} \cdot 100\% \tag{4.5}$$

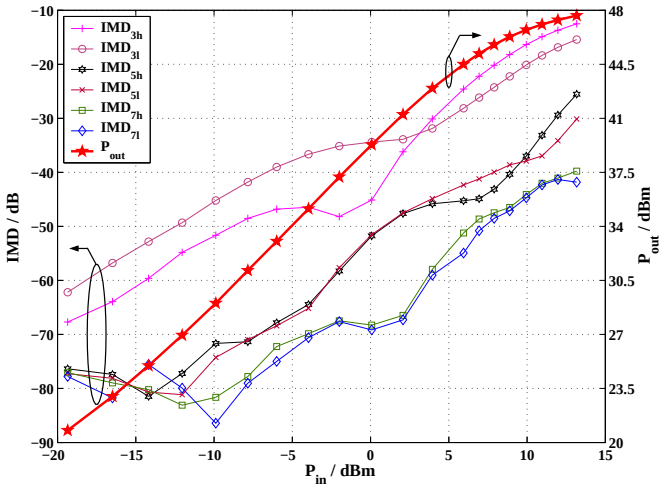

Figure 4.14: Intermodulation distance of the main amplifier for a two-tone input signal at 1960 MHz

where P_{in} and P_{out} are the RF-input and output power and P_{DC} is the consumed DC-power. Figure 4.15 shows the PAE over the frequency-output power-plane for a single-tone input signal. The GSM2+ compliance test was performed by the use of an AGILENT TECHNOLOGIES VSA

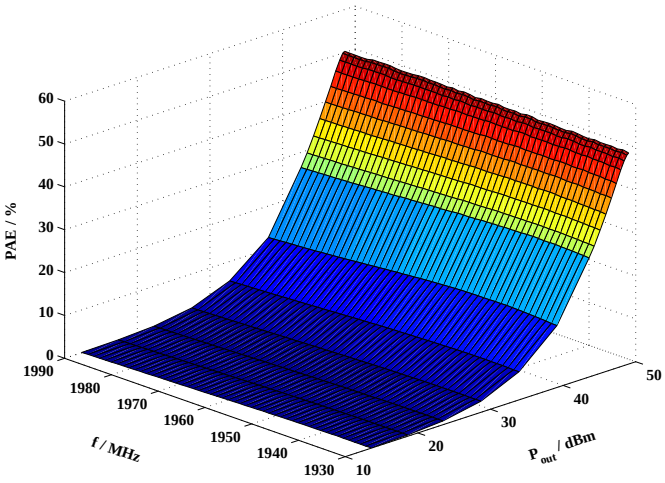

Figure 4.15: Power added efficiency of the main amplifier

(**V**ector **S**ignal **A**nalyzer) transmitter tester including the GSM2+ software option. Following measurements were performed:

- EVM

  The EVM specification includes the following parts, as presented in section 1.2.3:

  - EVM 95 : th percentile
  - EVM_{rms}
  - Maximum EVM_{rms}
  - Peak EVM

- I/Q offset suppression

  The I/Q offset suppression, which is also called Origin Offset Suppression, is a part of the EVM-specification. The calculation of the Origin Offset Suppression is shown in section 1.2.3 .

- GSM2+ spectrum mask

  The specification of the limits set for the spectrum mask are presented in table 1.3, section 1.2.4.

The GSM2+ input signal was generated by the use of the arbitrary signal generator AMIQ and shifted into the passband by the use of the vector signal generator SMIQ (both products are manufactured by ROHDE&SCHWARZ). The GSM2+ input signal included power-ramping.

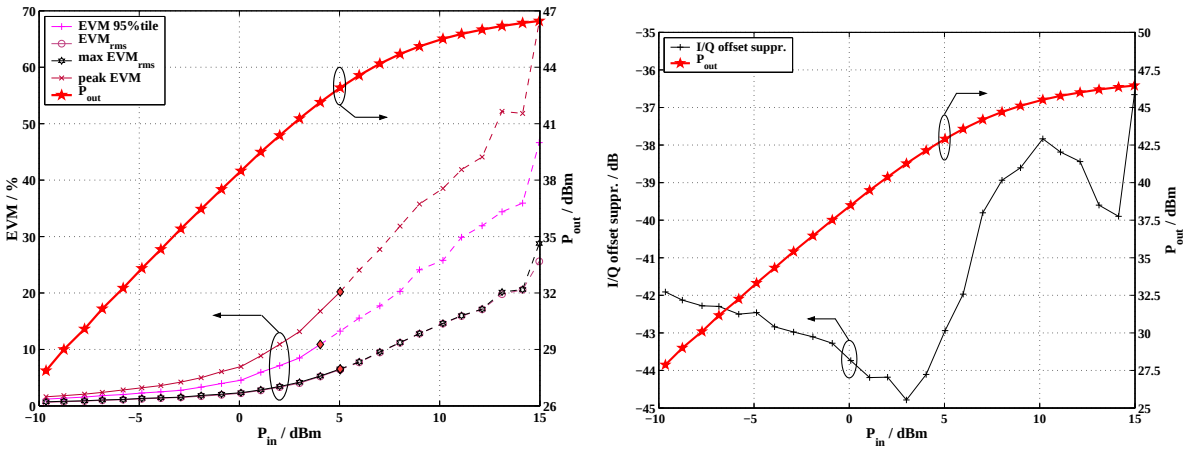

(a) (b)

Figure 4.16: Measurement of the EVM (a) and the I/Q offset suppression (a) at 1960 MHz

The dashed line-style in the EVM-measurement in figure 4.16 shows the area where the amplifier exceeds the limits given by the GSM2+ standard starting from the diamond shaped marker. The I/Q offset suppression is below the limit of -35 dB over the whole input power range. The same system as in figure 4.16 is also used in figure 4.17 to indicate, when the transmit-signal of the amplifier exceeds the limits given by the GSM2+ spectrum mask.

The last measurement presented for the main amplifier is the characterization of the directional coupler at the output of the main amplifier. This device was measured within two steps. As first step the gain of the amplifier was measured. Next, the "gain" between the input of the main amplifier and the directional coupler output were quantified. The quotient between the

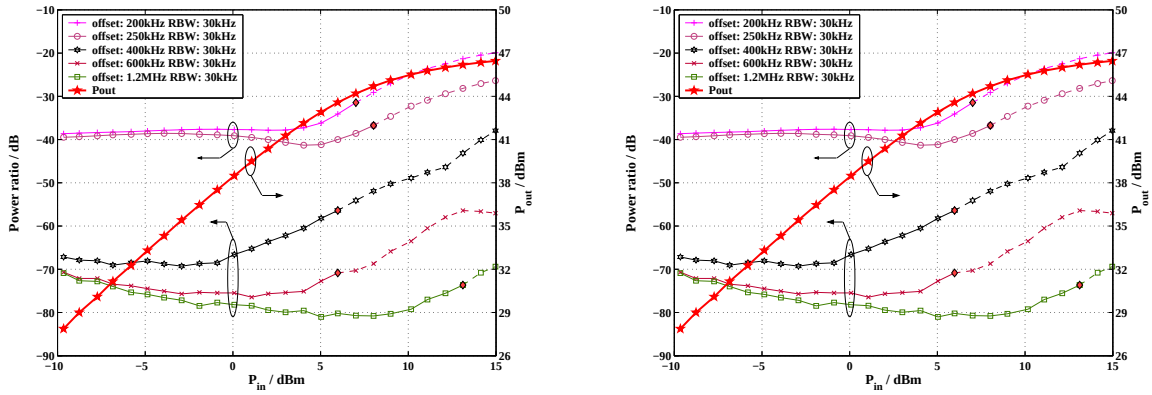

Figure 4.17: Measurement of the lower (a) and upper (b) sideband of the spectrum mask at 1960 MHz

two measurements shows the characteristic of the directional coupler. Figure 4.18 presents the measurement result. The average coupling factor of the directional coupler is -24.9 dB.

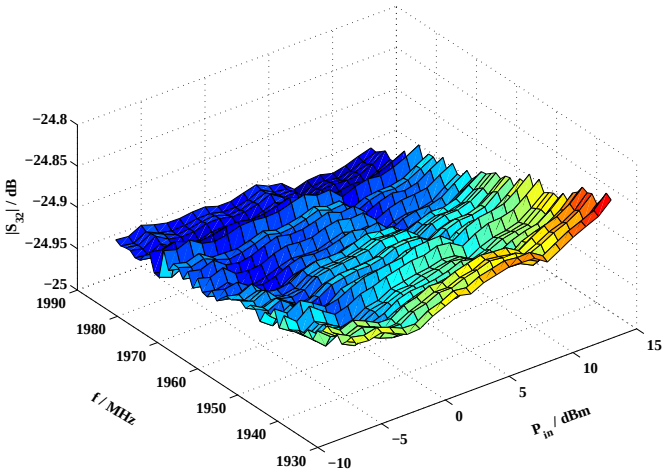

Figure 4.18: Characteristic of the directional coupler included into the main amplifier

4.5 Error amplifier

The defaults for the error amplifier are significantly influenced by the properties of the main amplifier and by the structure of the FFA. The properties of the main amplifier were ample discussed in the last chapter. The presentation of the features of the realized feedforward structure will be given in chapter 6.

The defaults for the error amplifier were:

DC-power supply:	27 V, 7 A
Measured frequency band:	1930 - 1990 MHz
Gain:	$36.2^{+2.8}_{-0.8}$ dB
1 dB compression point:	48.1 ±0.2 dBm
$IP3_{output}$:	53.1 dBm
$\|S_{31}\|$ directional coupler:	-24.9 dB

Table 4.8: Main amplifier measurement summary

- Gain: 80 dB
- P_{in}= -44 dBm
- Crest-factor of the input signal: 8.6 dB

To cope with the extremely high gain of this amplifier a three stage structure were chosen. The first two stages were realized by two ZFL-2500 amplifiers manufactured by MINI-CIRCUITS®. Table 4.9 presents the specifications as shown in the data sheet.

DC-power supply:	5 V, 220 mA
Frequency band:	500 - 2500 MHz
Gain:	min. 28 ±1.5 dB
1 dB compression point:	15 dBm
$IP3_{output}$:	27 dBm

Table 4.9: MINI-CIRCUITS® ZFL-2500 specification

The last stage of the error amplifier will be a power amplifier, which again was supplied by SIEMENS AG VIENNA. This amplifier, called PWRSTMPV2 (**P**ow**erst**age **M**icroBTS **P**CS-band **V2**), is capable to deliver 10 W RF-output power. Similar to the main amplifier the output of the error amplifier is protected by an isolator. Additionally a directional coupler is included to sample the output signal.

Table 4.10 shows the measurement result of the two MINI-CIRCUITS® amplifier. The same

	First amplifier	Second amplifier
Gain	32.3 ±0.5 dB	33.1 ±0.6 dB
1 dB compression point	17.5 ±0.2 dBm	17.5 ±0.2 dBm
$IP3_{output}$	28.8 dBm	27.6 dBm

Table 4.10: MINI-CIRCUITS® ZFL-2500 measurement results

measurements were also performed for the PWRSTMPV2. The measurement results are presented in table 4.11.

Connecting all three amplifiers together would result in an amplifier with a gain of around 100 dB. It is clear that a 20 dB-attenuator has to be used to adjust the gain to the desired value.

Gain:	$33.4^{+3.1}_{-1.4}$ dB
1 dB compression point:	42.0 ±0.8 dBm
$IP3_{output}$:	56.8 dBm

Table 4.11: PWRSTMPV2 measurement results

The PWRSTMPV2 amplifier needs an input power of around 5 dBm to bet set to the operation point. As the ZFL-2500 amplifier can only deliver 17 dBm output power, a possible attenuator must not be placed between the second amplifier and the power amplifier. Placing the attenuator between the two ZFL-2500 amplifiers has no effect on the intermodulation performance and also helps to reduce the noise effects of the attenuator. The noise-figure of a chain of devices can be calculated by the use of FRII's-formula:

$$F_{ges,n} = F_1 + \frac{F_2 - 1}{G_1} + \frac{F_3 - 1}{G_1 G_2} + \cdots + \frac{F_n - 1}{G_1 G_2 \cdots G_{n-1}} \tag{4.6}$$

where F_x,G_x are the noise figure and gain of the x-th device and n specifies the number of devices. An elaboration of the noise effects in RF-devices can be found in the literature, for example: [Mag98, chapter 3.4]. As shown in equation 4.6, the gain of the first amplifier will help to reduce the noise added by the following attenuator. The final structure of the error amplifier is presented in figure 4.19 . Figure 4.20 shows the single-tone measurement of the error amplifier.

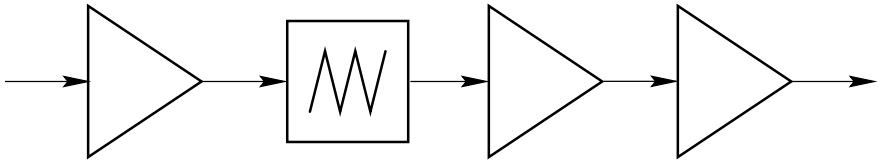

Figure 4.19: Structure of the error amplifier

According to this single-tone measurement the gain of the amplifier is $78.3^{+4.4}_{-2.7}$ dB. The 1 dB compression point was found at 44.8 dBm ±0.5 dB. Figure 4.21 illustrates the behavior of the amplifier when a two-tone input signal is supplied. By the use of this measurement the third order intercept point was evaluated: $IP3_{output}$=55.8 dBm.

DC-power supply:	27 V, 3.5 A; 5 V, 400 mA
Measured frequency band:	1930 - 1990 MHz
Gain:	$78.3^{+4.4}_{-2.7}$ dB
1 dB compression point:	44.8 dBm ±0.5 dB
$IP3_{output}$:	55.8 dBm

Table 4.12: Error amplifier measurement summary

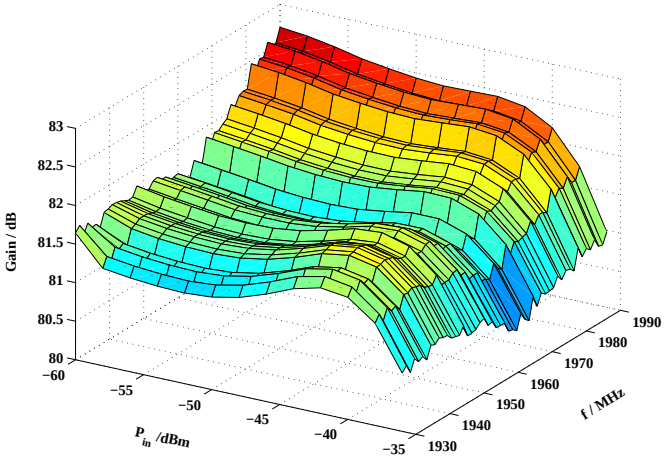

Figure 4.20: Gain of the error amplifier

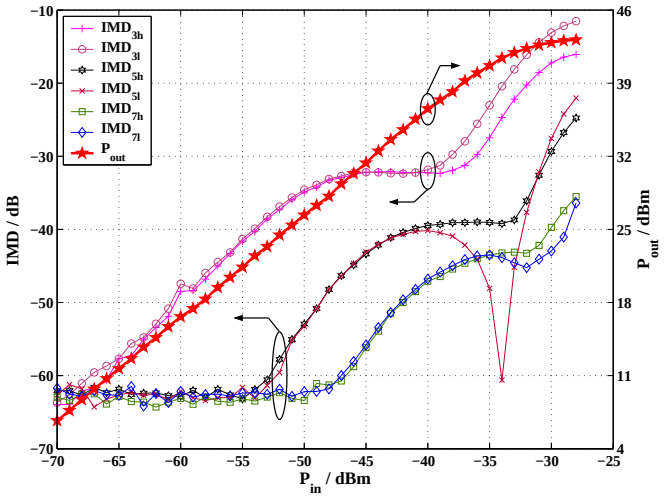

Figure 4.21: IMD of the error amplifier for a two-tone input signal at 1960 MHz

Chapter 5

Feedforward amplifier for GSM2+

5.1 Introduction

This chapter will present the realized FFA, the evaluation of the amplifier delay, the design of the loop controllers and the measurement results of the adaptive controlled feedforward amplifier.

5.2 Feedforward structure

For the design of a suitable feedforward structure the following defaults were given:

1. The main amplifier should operate at an input signal power of 10 dBm (≈45 dBm output power)
2. The insertion losses of all devices after the main amplifier have to be minimized
3. The VA must not operate with an input signal power above 20 dBm
4. The default attenuation of the VA is set to approximately 13 dB
5. The gain of the error amplifier should be kept as low as possible
6. The carrier cancellation loop should be adjusted by the use of a power sensor
7. The adjustment of the distortion cancellation loop is performed by the use of a pilot-tone

These specifications result in the structure presented in figure 5.1. The properties of this structure are now discussed:

Vector attenuator VA_1: Normally all nonlinear devices should be placed in the amplifier path. Due to the default condition 1 the VA_1 cannot be placed in front of the main amplifier, because the maximum allowed input power for this device would be exceeded. Shifting the VA_1 to the reference path will lead to following properties:

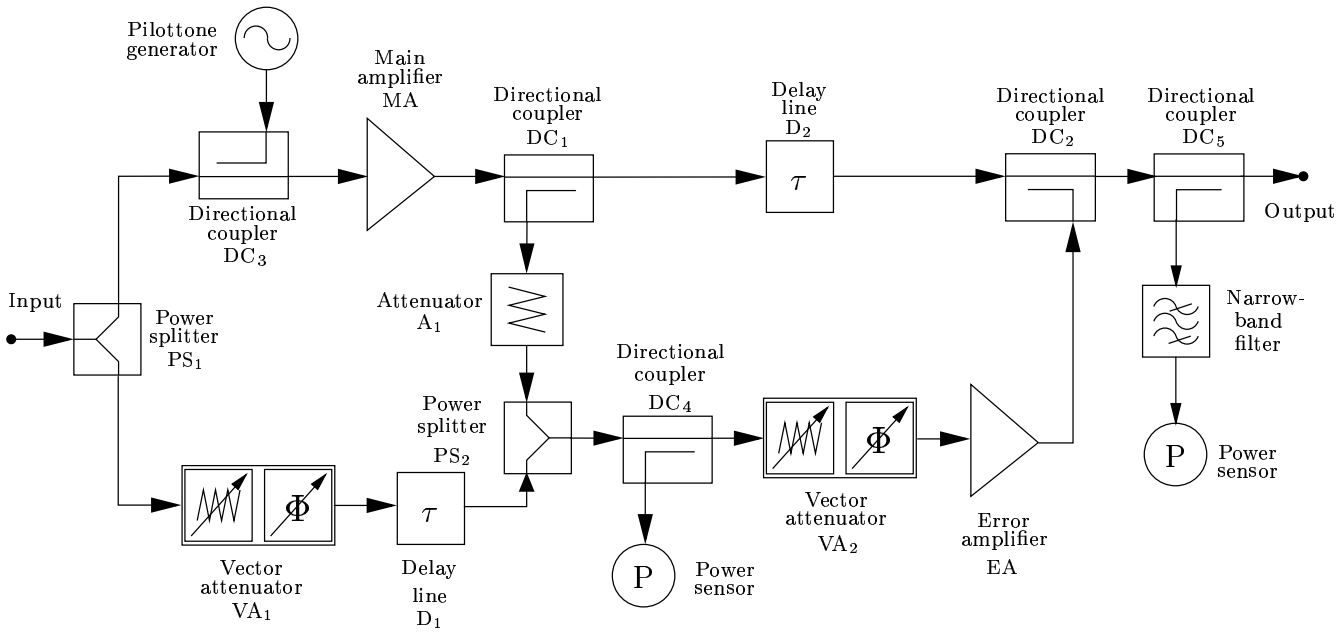

Figure 5.1: Realized feedforward structure

- Due to a maximum input signal power of 13 dBm the intermodulation products created by the VA_1 will have a minimum intermodulation distance of around -50 dB. This will be the performance limit for the assembled FFA.
- VA_1 can be used to disable the carrier cancellation.
- The output signal of the main amplifier is independent of the VA_1 adjustment.

Vector attenuator VA_2: Placing VA_2 after the attenuator A_1 would significantly decrease the gain of the error amplifier. Unfortunately this would also make an interconnect between the carrier and the distortion cancellation loop. Placing VA_2 right behind the error amplifier gives the possibility to disable the operation of the error amplifier.

Directional coupler DC_2: The task of the directional coupler DC_2 is to combine the main and the error amplifier output signal. The power level of both signals should not be reduced. These defaults lead to a nonreciprocal device. In the realized FFA a 10 dB directional coupler is used to combine the two signals. DC_2 will reduce the main amplifier signal by 0.65 dB.

Directional coupler DC_3: DC_3 combines the input signal and the pilot-tone signal. Together with directional coupler DC_5, the narrow-band filter and the power detector the performance of the distortion cancellation loop can be evaluated.

Directional coupler DC_4: DC_4 sense the carrier cancellation signal and passes it to the power sensor. This part of the structure is used for the controlling system of the carrier cancellation loop.

5.2.1 Calculation of the feedforward amplifier structure

Based on the theory presented in chapter 2 the selected structure is analyzed. Figure 5.2 names the parameters used for the calculations. The directional coupler DC_5 is neglected for the dimensioning of the structure.

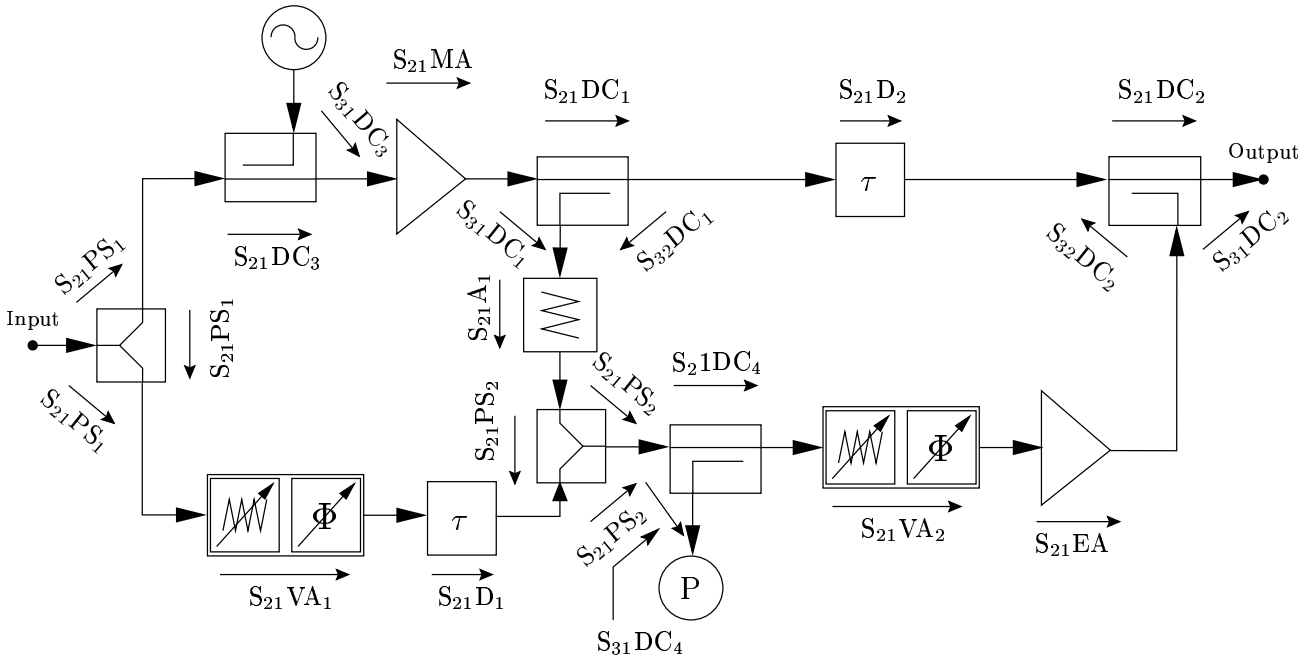

Figure 5.2: Declaration of the typical transfer characteristic values

Passive Devices:

All passive devices are assumed to be perfectly matched to 50 Ω and perfectly reciprocal. Table 5.1 shows the compilation of the nominal attenuation values of the passive devices.

$S_{21}PS_1$=	-6 dB	$S_{21}DC_3$=	-0.5 dB
$S_{21}PS_2$=	-6 dB	$S_{31}DC_3$=	-10 dB
$S_{21}D_1$=	-1 dB	$S_{21}DC_4$=	-0.5 dB
$S_{21}D_2$=	-1 dB	$S_{31}DC_4$=	-10 dB
$S_{21}DC_1$=	-0.05 dB	$S_{21}DC_5$=	-0.1 dB
$S_{31}DC_1$=	-25 dB	$S_{31}DC_5$=	-20 dB
$S_{21}DC_2$=	-0.65 dB		
$S_{31}DC_2$=	-10 dB		

Table 5.1: Nominal attenuation values of the passive devices

Active Devices:

Table 5.2 presents the compilation of the return losses and typical values of the transfer characteristic of the active devices.

$S_{21}MA=$	-35 dB	$S_{21}EA=$	-78 dB
$S_{11}MA=$	-13 dB	$S_{11}EA=$	-16 dB
$S_{21}VA_1=$	-14 dB	$S_{21}VA_2=$	-14 dB
$S_{11}VA_1=S_{22}VA_1=$	-17 dB	$S_{11}VA_2=S_{22}VA_2=$	-17 dB

Table 5.2: Return losses and transfer coefficients of the active devices

Carrier cancellation loop

For the carrier cancellation loop the following conditions must be fulfilled:

$$S_{21}PS_1 \cdot S_{21}DC_3 \cdot S_{21}MA \cdot S_{31}DC_1 \cdot S_{21}A_1 \cdot S_{21}PS_2 = S_{21}PS_1 \cdot S_{21}VA_1 \cdot S_{21}D_1 \cdot S_{21}PS_2 \quad (5.1)$$

$$S_{21}A_1 = \frac{S_{21}VA_1 \cdot S_{21}D_1}{S_{21}DC_3 \cdot S_{21}MA \cdot S_{31}DC_1} \doteq -26 \text{ dB} \quad (5.2)$$

It is clear that the attenuation of A_1 is influenced by the operation point chosen for the VA_1. The stability of the carrier cancellation loop can be analyzed by the use of the gain coefficient, as presented in section 2.5:

$$\begin{aligned} C_{\text{Carrier cancellation}} = \; & (S_{21}PS_1)^2 \cdot S_{21}DC_3 \cdot S_{21}MA \cdot S_{31}DC_1 \cdot \\ & \cdot S_{21}A_1 \cdot S_{21}D_1 \cdot S_{21}VA_1 \cdot (S_{21}PS_2)^2 \doteq -57 \text{ dB} \end{aligned} \quad (5.3)$$

The result of equation 5.3 showed, that the loop is far away from the instable area.

Signal flowchart of the carrier cancellation loop

The effects of the return losses of the different active devices should be analyzed now. To keep the effort within reasonable limits the following simplifications were assumed:

- The carrier cancellation loop is considered separated from the rest of the structure
- The directional couplers DC_3 and DC_4 are neglected
- The output of the main amplifier is perfectly matched

Figure 5.3 presents the simplified signal flowchart for the carrier cancellation loop. Analyzing the presented signal flowchart the following context is used [Mag98, chapter 2.4]:

$$\frac{S_{\text{Carrier canellation}}}{S_{\text{Input}}} = \frac{\sum_{i=1}^{n} SP_i \cdot \Delta^{(i)}}{\Delta G} \quad (5.4)$$

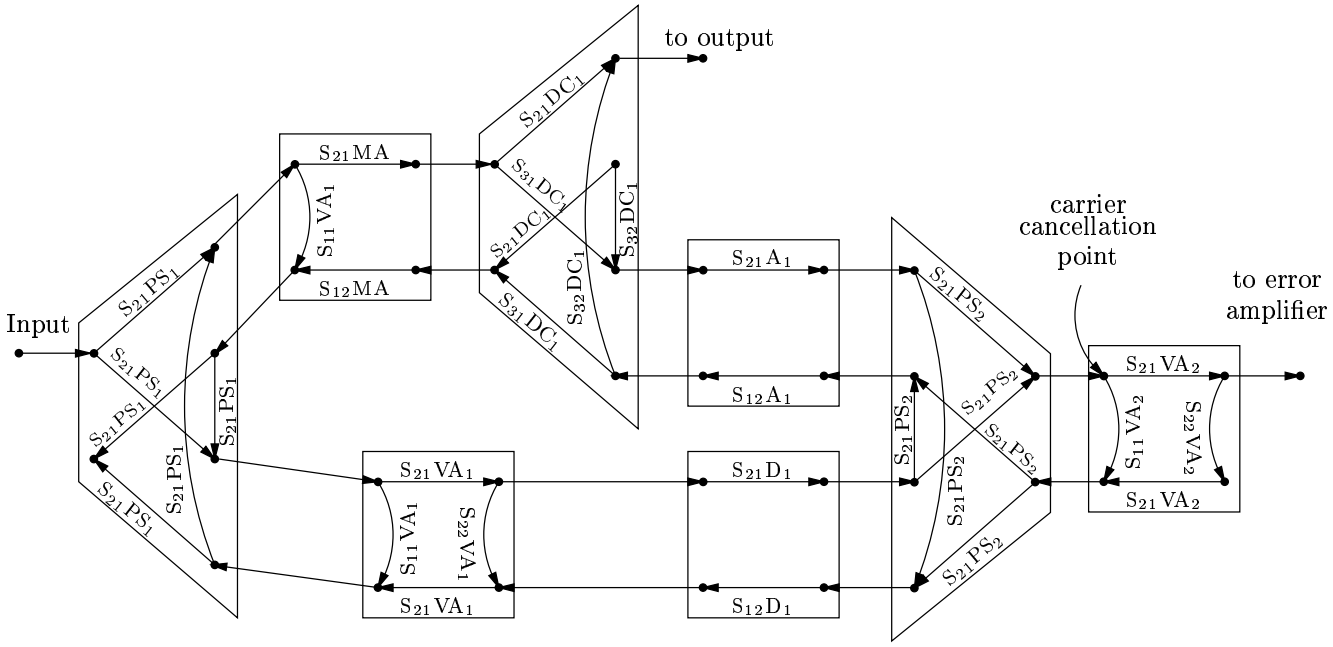

Figure 5.3: Signal flowchart carrier cancellation loop

where $S_{\text{Carrier canellation}}$ names the carrier cancellation signal, S_{Input} the input signal, SP_i the i$^{\text{th}}$ signal path between the input and the carrier cancellation point, $\Delta^{(i)}$ the i$^{\text{th}}$ path determinant and ΔG the graph determinant. The following signal paths SP_i can be found:

$$
\begin{aligned}
SP_1 &= \mathrm{S_{21}PS_1} \cdot \mathrm{S_{21}MA} \cdot \mathrm{S_{31}DC_1} \cdot \mathrm{S_{21}A_1} \cdot \mathrm{S_{21}PS_2} \\
\Delta^{(1)} &= 1 \\
SP_2 &= \mathrm{S_{21}PS_1} \cdot \mathrm{S_{21}VA_1} \cdot \mathrm{S_{21}D_1} \cdot \mathrm{S_{21}PS_2} \\
\Delta^{(2)} &= 1 \\
SP_3 &= \mathrm{S_{21}PS_1^2} \cdot \mathrm{S_{11}VA_1} \cdot \mathrm{S_{21}MA} \cdot \mathrm{S_{21}DC_1} \cdot \mathrm{S_{21}A_1} \cdot \mathrm{S_{21}PS_2} \\
\Delta^{(3)} &= 1 \\
SP^{(4)} &= \mathrm{S_{21}PS_1^2} \cdot \mathrm{S_{11}VA_1} \cdot \mathrm{S_{21}MA} \cdot \mathrm{S_{21}DC_1} \cdot \mathrm{S_{21}A_1} \cdot \mathrm{S_{21}PS_2^2} \cdot \mathrm{S_{21}D_1^2} \cdot \mathrm{S_{22}VA_1} \\
\Delta^{(4)} &= 1 \\
SP^{(5)} &= \mathrm{S_{21}PS_1^2} \cdot \mathrm{S_{11}MA} \cdot \mathrm{S_{21}VA_1} \cdot \mathrm{S_{21}D_1} \cdot \mathrm{S_{21}PS_2} \\
\Delta^{(5)} &= 1 \\
SP^{(6)} &= \mathrm{S_{21}PS_1} \cdot \mathrm{S_{21}MA} \cdot \mathrm{S_{31}DC_1} \cdot \mathrm{S_{21}A_1} \cdot \mathrm{S_{21}PS_2^2} \cdot \mathrm{S_{21}D_1^2} \cdot \mathrm{S_{22}VA_1} \\
\Delta^{(6)} &= 1
\end{aligned}
\tag{5.5}
$$

SP_1 and SP_2 are the two paths for the signal cancellation. All other signal paths create an additional distortion signal which falsify the original cancellation signal. To evaluate the effect of the additional signal path, a worst case estimate is performed. The complete distortion signal created by SP_3 to SP_6 is interpreted as a mismatch to the signal cancellation. Assuming that the paths SP_1 and SP_2 are perfectly balanced, the maximum cancellation performance which

can be reached is given by:

$$\mathrm{CP} = \sum_{i=3}^{6} \left| SP^{(i)} \cdot \Delta^i \right| = 9.7 \cdot 10^{-3} \doteq -40.3 \text{ dB} \tag{5.6}$$

This evaluation was only performed for the carrier cancellation loop due to the long winded calculation at the distortion cancellation loop.

Distortion cancellation loop

The bias-point of VA_2 must be chosen to balance the distortion cancellation loop:

$$\mathrm{S_{21}DC_1} \cdot \mathrm{S_{21}D_2} \cdot \mathrm{S_{21}DC_2} = \mathrm{S_{31}DC_1} \cdot \mathrm{S_{21}A_1} \cdot \mathrm{S_{21}PS_2} \cdot \mathrm{S_{21}DC_4} \cdot \mathrm{S_{21}VA_2} \cdot \mathrm{S_{21}EA} \cdot \mathrm{S_{31}DC_2} \tag{5.7}$$

$$\mathrm{S_{21}VA_2} = \frac{\mathrm{S_{21}DC_1} \cdot \mathrm{S_{21}D_2} \cdot \mathrm{S_{21}DC_2}}{\mathrm{S_{31}DC_1} \cdot \mathrm{S_{21}A_1} \cdot \mathrm{S_{21}PS_2} \cdot \mathrm{S_{21}DC_4} \cdot \mathrm{S_{21}EA} \cdot \mathrm{S_{31}DC_2}} \doteq -12.2 \text{ dB} \tag{5.8}$$

The gain coefficient of the distortion cancellation loop can be calculated according to section 2.5:

$$\begin{aligned} \mathrm{C_{Distortion\ cancellation}} = \ & \mathrm{S_{31}DC_1} \cdot \mathrm{S_{32}DC_1} \cdot \mathrm{S_{21}A_1} \cdot \mathrm{S_{21}PS_2} \cdot \mathrm{S_{21}DC_4} \cdot \\ & \cdot \mathrm{S_{21}VA_2} \cdot \mathrm{S_{21}EA} \cdot \mathrm{S_{32}DC_2} \cdot \mathrm{S_{21}D_2} \cdot \mathrm{S_{31}DC_2} \doteq -72.7 \text{ dB} \end{aligned} \tag{5.9}$$

Also this loop proofed to be very stable.

Gain of the FFA

The gain of the selected feedforward structure can be calculated according to equation 2.8 presented in section 2.4:

$$\mathrm{G_{ff}} = \frac{\mathrm{S_{21}PS_1} \cdot \mathrm{S_{21}VA_1} \cdot \mathrm{S_{21}DC_1} \cdot \mathrm{S_{21}DC_2} \cdot \mathrm{S_{21}D_1} \cdot \mathrm{S_{21}D_2}}{\mathrm{S_{31}DC_1} \cdot \mathrm{S_{21}A_1}} \doteq 26.8 \text{ dB} \tag{5.10}$$

The reduction of the gain compared to the main amplifier is due to the components located after the main amplifier and due to the power splitter at the input of the FFA.

5.2.2 Level characteristic of the selected feedforward structure

After dimensioning all devices used within the FFA a level diagram of the structure can be drawn. Also for this diagram directional coupler DC_5 was neglected. Figure 5.4 illustrates the behavior of the information signal and the intermodulation distortion in the amplifier path. After the directional coupler DC_2 the intermodulation distortion is reduced by 20 dB due to the distortion cancellation. One important fact is difficult to recognize in this drawing. After the main amplifier output the information signal is reduced by 1.7 dB, which means, that the amplifier output signal is lowered form 31 W down to 21 W. For the main amplifier an intermodulation distance of around 20 dB was assumed.

In a similar way figure 5.5 presents the level characteristic of the reference path. This drawing

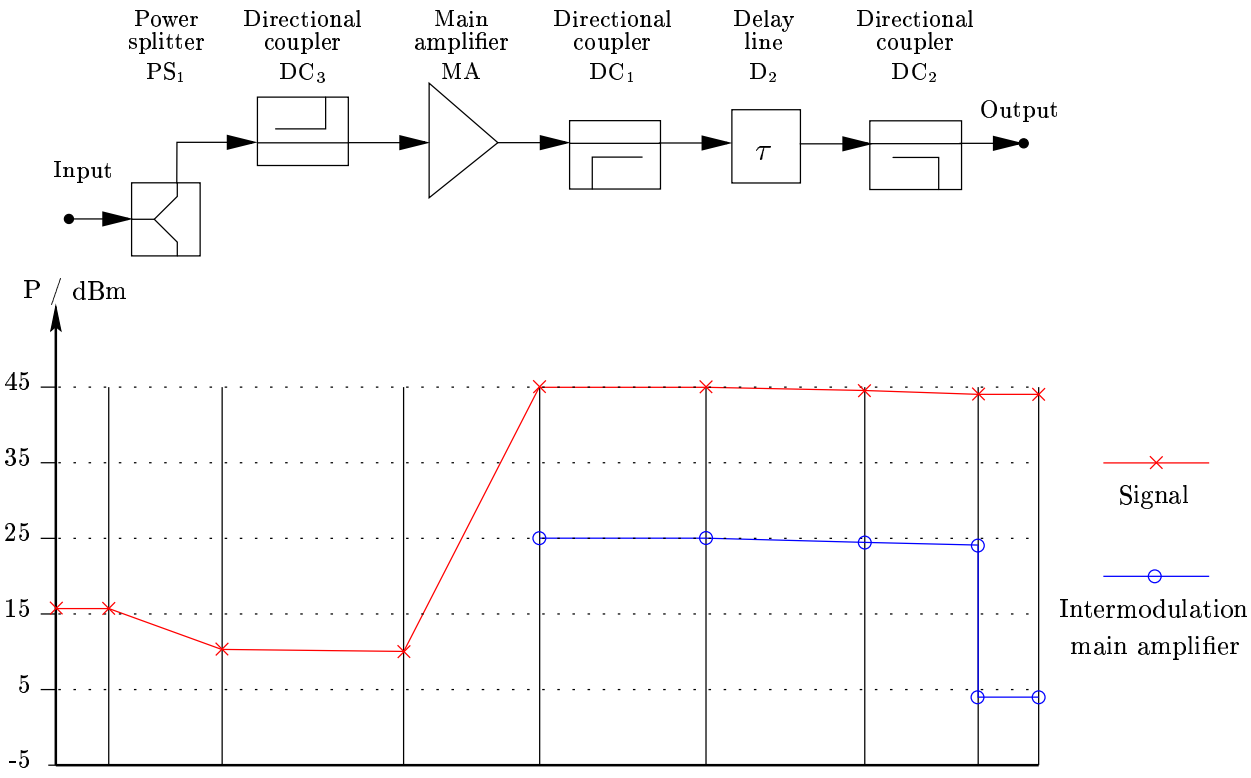

Figure 5.4: Level characteristic of the amplifier path

illustrates the extremely high dynamic range between the different signals in the FFA. For the selected structure about 100 dB difference between the input signal of the error amplifier and the output signal of the main amplifier can be observed. If the whole amplifier is built on one PCB this fact should be considered carefully. For the case of the realized FFA only devices covered by a shielding enclosure were used. Due to this reason no troubles occurred with the crosstalk of the different signals. After the power splitter PS_2 the information signal is reduced by 23 dB due to the carrier cancellation. The error amplifier operates with an intermodulation distance of around 22 dB.

5.3 Delay measurement and compensation

One of the important limitations to a broadband FFA is a delay mismatch introduced into the cancellation loop as presented in section 2.3.2. Hence the compensation of the time delay introduced by an amplifier is an important process during the erection of an FFA. Generally this process can be ascribed to the delay time measurement of a bandpass device. The goal out of this measurement is to specify the size of the time delay needed to balance the cancellation loop.

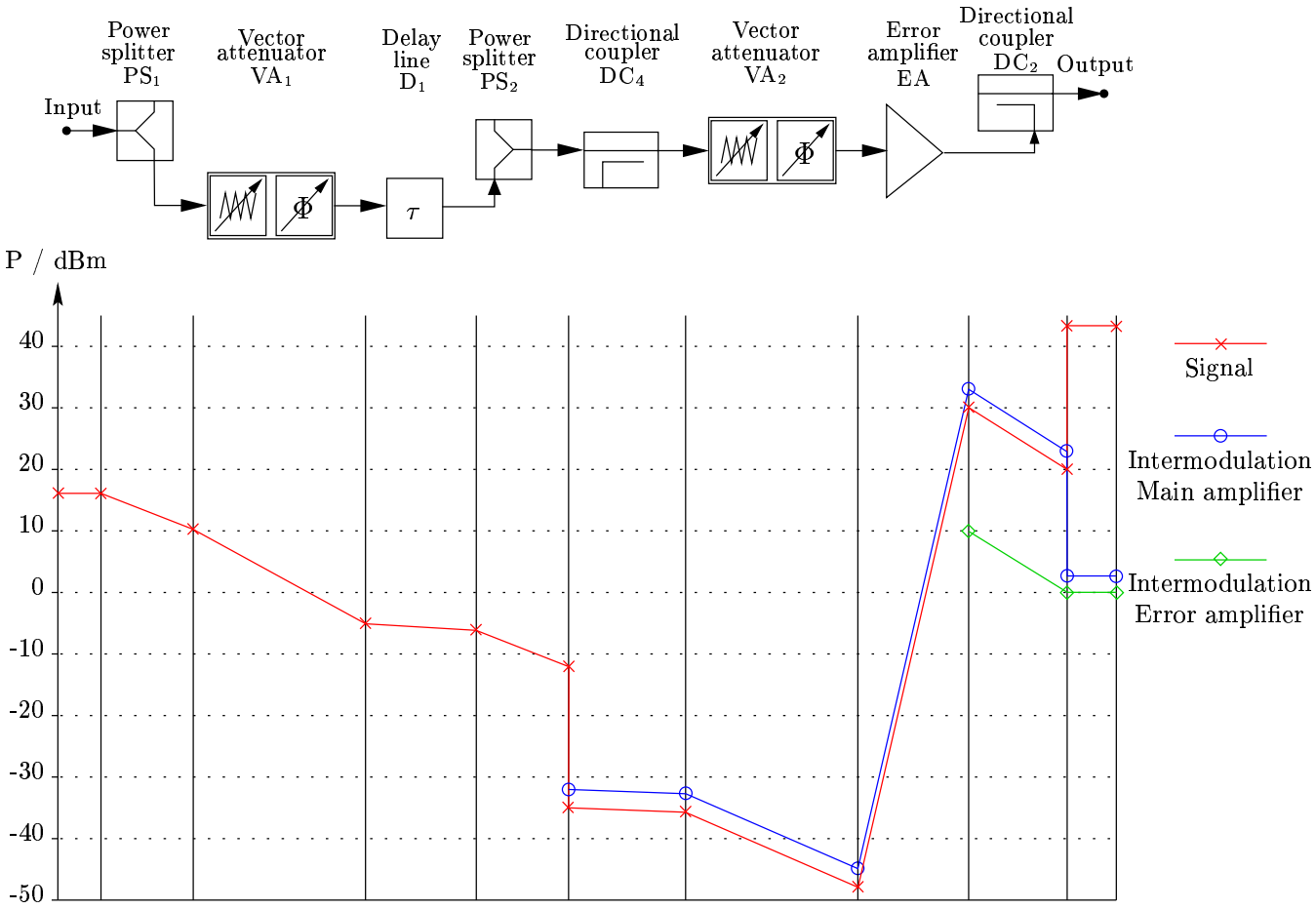

Figure 5.5: Level characteristic of the reference path

5.3.1 Delay time measurement

The measurement of the amplifier time delay cannot be performed directly. By the use of the following measurement process the quality of the delay matching for different time delays can be compared.By performing several iterations an acceptable compensation of the delay mismatch in a loop can be achieved.

The measurement is based on the frequency depending effects of a cancellation loop. If a perfectly balanced system is assumed the output signal is suppressed even if a frequency sweep is performed. A network analyzer can be used to accomplish the frequency sweep and to measure the cancellation signal. Figure 5.6 presents the measurement circuit for the delay time measurement of the carrier cancellation loop. To explain the measurement principle think of several frequencies at which the network analyzer measures the complex cancellation signal, i.e. the amplitude ratio and the phase difference between the input signal and the output signal of the cancellation loop. If we assume a perfect balanced loop (in phase, amplitude and time delay) no signal could be measured for all measurement frequencies. The network analyzer would

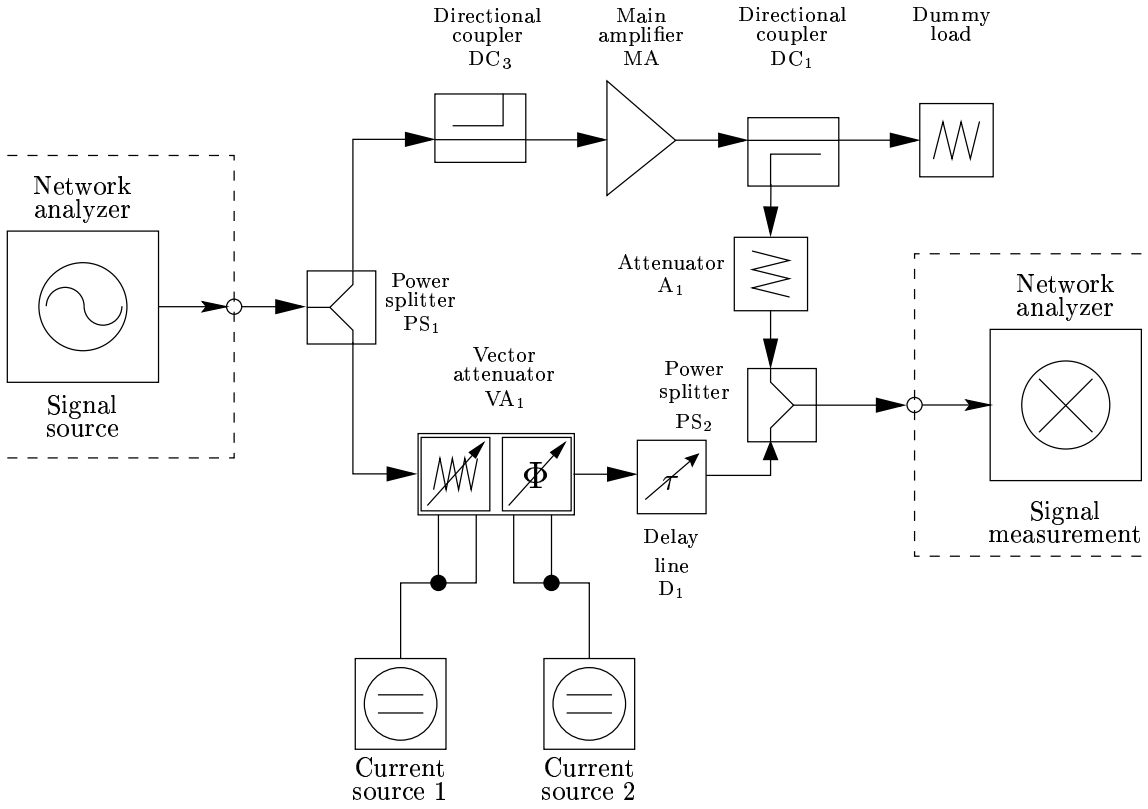

Figure 5.6: Time delay measurement circuit for the carrier cancellation loop

display only a dot in the origin (when it is set to a polar display). If an amplitude and/or a phase mismatch is introduced into the loop the dot will be moved away for the origin. Only when a time delay mismatch occurs within the cancellation loop the dot will be expanded to a curve connecting the measurement points for the selected frequencies. The length of this curve is directly related to the amount of delay mismatch set to the system [Pot99, chap. 5.5]. Figure 5.7 illustrates the output of the network analyzer for the different error cases. The function CP(α,ϕ,τ,f) describes the cancellation signal as a function of the amplitude, phase or time delay mismatch as presented in section 2.3 . The makers on the CP(α,ϕ,τ,f)-curve indicates the different measurement frequencies f_1 to f_{10}. If the length of the curve should be calculated equation 5.11 can be used:

$$\text{length} = \sum_{i=2}^{n} |\text{CP}(\alpha, \phi, \tau, f_i) - \text{CP}(\alpha, \phi, \tau, f_{i-1})| \tag{5.11}$$

where n specifies the number of frequency points at which the cancellation signal was measured.

For a practical measurement the following step has to be taken starting from a very short time-delay:

1. Evaluate the length of the cancellation signal for the actual time delay

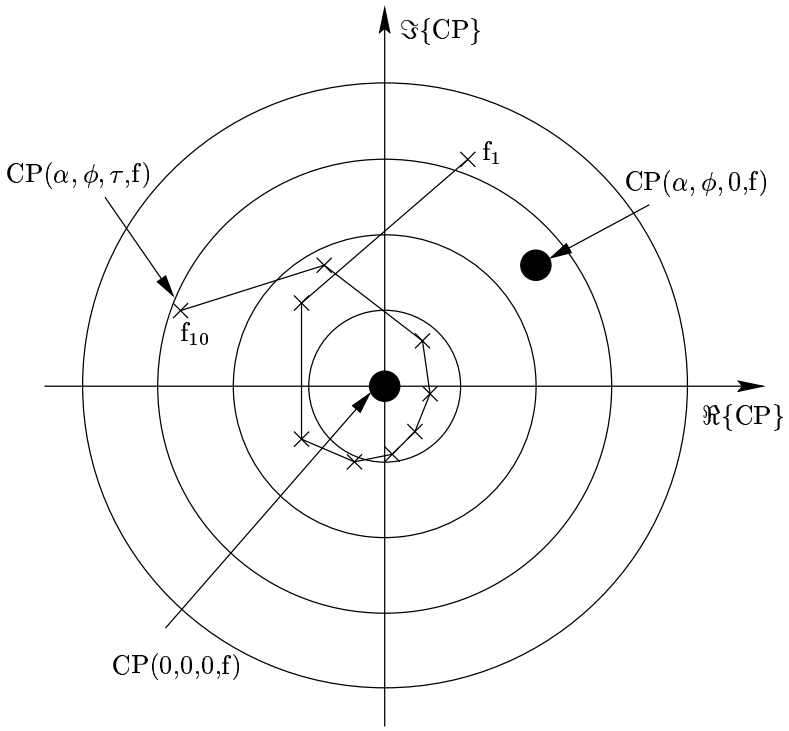

Figure 5.7: Output of the network analyzer for a cancellation signal

2. Increase the time delay
3. Find the correct setting for the vector attenuator to minimize the amplitude and phase error. In this case only the time delay mismatch should be the significant error source within the cancellation loop.
4. Evaluate the length of the measured cancellation signal curve
5. Compare the result with the measurement of step1. If the length of the curve is reduced, continue with step 2.

This process should iteratively approach to the correct time delay for the cancellation loop.

The procedure of minimizing the amplitude and phase mismatch and the evaluation of the length of the cancellation signal was automated by the use of a MATLAB®script. The usage of this script is presented in appendix A.4.

5.3.2 Delay time compensation

After the correct time delay was evaluated a semi-rigid cable has to be assembled causing the same time delay. The selected semi-rigid RF-cable is produced by HUBER&SUHNER named EZ-86. This cable has the following specifications:

- Operating frequency up to 20 GHz

- Outer diameter 2.20 mm
- Nominal attenuation (18 GHz, 25 °C) 3.2 dB/m
- Temperature range: -40 ... +125 °C

The connectors mounted on the cable were SMA-connectors (**S**ub**m**iniature **A**). Based on the broadband measurement of two semi-rigid cord sets the propagation constant of the cable and the delay of the SMA-connectors were evaluated:

Propagation constant: $a = \frac{1}{0.7 \cdot c_o}$, where c_o is the speed of light

Connector delay: $t_{Connector} = \frac{2.5\ mm}{0.7 \cdot c_o} = 11.9$ ps for each connector

Based on these measurement results a suitable semi-rigid cable can be assembled. The complete time delay of a cable can be calculated as

$$\tau = a \cdot \text{cable length} + 2 \cdot t_{Connector} \tag{5.12}$$

where cable length means the length of the cable to the first discontinuity. Figure 5.8 shows how the length of a cable is interpreted. Additionally it should be mentioned that if the cable is

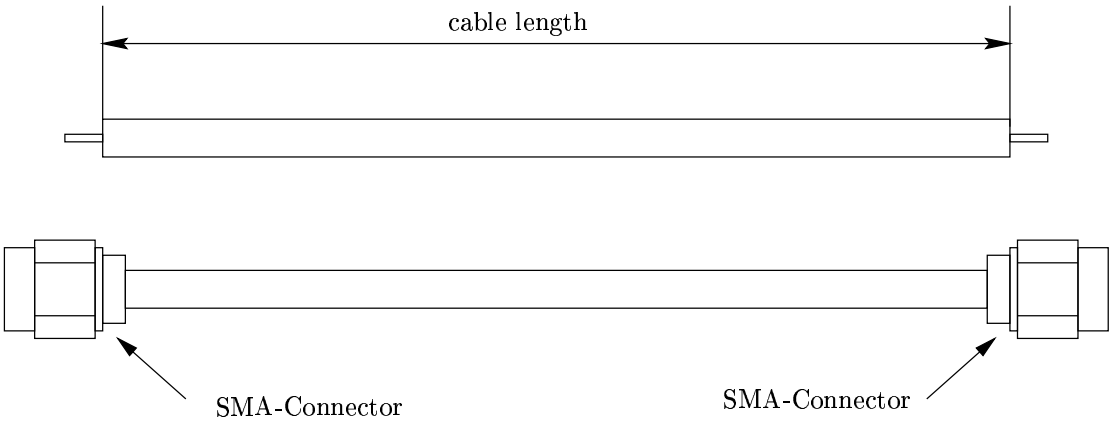

Figure 5.8: Length of a semi-rigid cable

winded up with diameter of about 40 mm a reduction of the time delay of about 2.5 % occurs.

The evaluated time-delays and cable length are presented in table 5.3. After the correct

	Time delay τ / ns	assoziated cable length cable length / m
Carrier cancellation loop	5.725	0.9702
Distortion cancellation loop	9.953	2.2317

Table 5.3: Time delay and cable length in the realized FFA

delay-lines are assembled the FFA can be tested in manual operation.

5.4 Loop controller

The adaptive controlling system should permit a secure operation of the FFA independent of outside influences. Following defaults were given for the design of the loop controllers:

- Only a power meter or a spectrum analyzer should be used to measure the cancellation signals, i.e. the loop controllers should operate without baseband processing
- The vector attenuators are set by the use of GPIB-controlled (**G**eneral **P**urpose **I**nterface **B**us) current sources

The loop controller must be able to excess the GPIB-bus to collect the measurement results and set the vector attenuators. Due to this reason the loop controllers were realized as MATLAB®-scripts. The complete controlling program was designed to handle all devices which are needed to operate the FFA.

5.4.1 Carrier cancellation loop

For the adjustment of the carrier cancellation loop the signal at the carrier cancellation point should only consist of the intermodulation distortion created by the main amplifier. This condition is fulfilled when the input signal and the carrier cancellation signal are uncorrelated [Cav95, CTC99]. The minimization of the power of the carrier cancellation signal is only a suboptimal criteria for the adjustment of this loop. The carrier cancellation signal with minimum power can still consist of both intermodulation distortion of the main amplifier and the input signal. Figure 5.9 shows the difference between the correlation and the power minimization criteria at the output of the loop for a two-tone input signal. Due to the need of baseband pro-

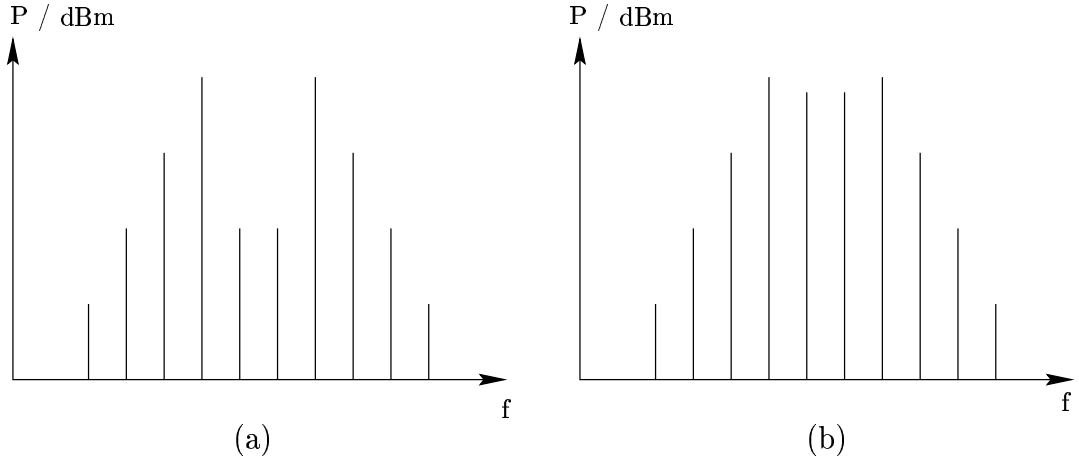

Figure 5.9: Carrier cancellation signal for a loop controller operating by the use of the correlation (a) and the power (b) minimization criteria

cessing for the evaluation of the correlation criteria, the loop controller of the carrier cancellation loop is based on the power minimization criteria. In the realized structure presented in figure 5.1

the directional coupler DC_4 is used to sense the carrier cancellation signal and to pass this signal to the power detector. Based on this power measurement the vector attenuator is adjusted.

5.4.2 Distortion cancellation loop

The problem for the distortion cancellation loop is the large difference between the power levels of the amplified input signal and the distortion signal. Due to this reason a minimization of the power cannot be used to adjust this loop. Again a correlation criteria can be found, but the need for baseband processing prevents the usage of these techniques. To handle this problem in our case a pilot-tone is added to the main amplifier input signal. This signal is treated by the distortion cancellation loop as a normal intermodulation created by the main amplifier. By the use of a narrow-band power measurement the suppression of the pilot-tone can be measured at the output of the FFA. Based on this measurement the loop controller for the distortion cancellation loop can evaluate the setting for the vector attenuator VA_2. In figure 5.1 DC_3 is used to pass the pilot-tone signal to the main amplifier input. The sample of the output signal taken by DC_5 is filtered by the narrow-band bandpass filter and measured by the power sensor. The goal of the loop control is to minimize the power level measured after the narrow-band bandpass filter.

5.4.3 Cartesian controller

As presented in section 5.4.1 and 5.4.2 the control of both loops is based on the minimization of the power level. Hence, the same controlling algorithm can be used to handle the carrier and the distortion cancellation loop.

The cartesian controller tries to solve the minimization problem by splitting the controlling process for the complex attenuation adjusted at the vector attenuator into two separately working real-valued processes. Figure 5.10 depict the block diagram of the cartesian controller. These real-valued controllers are operating with variable step size. Both controllers are equipped with a three-stage history saving the latest cancellation signal power levels $\mathrm{P}[n]$ to $\mathrm{P}[n-3]$. Based on the changes in the power levels $\mathrm{P}[n]$:

$$\Delta \mathrm{P}[n] = \mathrm{P}[n] - \mathrm{P}[n-1] \tag{5.13}$$

the output of this controller can be calculated:

$$\mathrm{A_{out}}[n] = \mathrm{A_{out}}[n-1] + \mathrm{a}[n] \cdot \mathrm{b}[n] \cdot \delta(\Delta \mathrm{P}[n]) \tag{5.14}$$

where $\mathrm{A_{out}}[n]$ is the output of the controller, $\mathrm{a}[n]$ selects one of the two orthogonal real-valued controllers, $\mathrm{b}[n]$ specifies the actual step size and the function $\delta(\cdot)$ chooses the direction for the next step according to the value of $\Delta \mathrm{P}[n]$. The function $\delta(\cdot)$ is defined as:

$$\delta(x) = \begin{cases} 1 & , x < 0 \\ -1 & , x \geq 0 \end{cases} \tag{5.15}$$

According to equation 5.14 and 5.13 the direction for the next step is changed, if the actual power level $\mathrm{P}[n]$ is bigger than the last one. The step size factor $\mathrm{b}[n]$ starts from an initial value

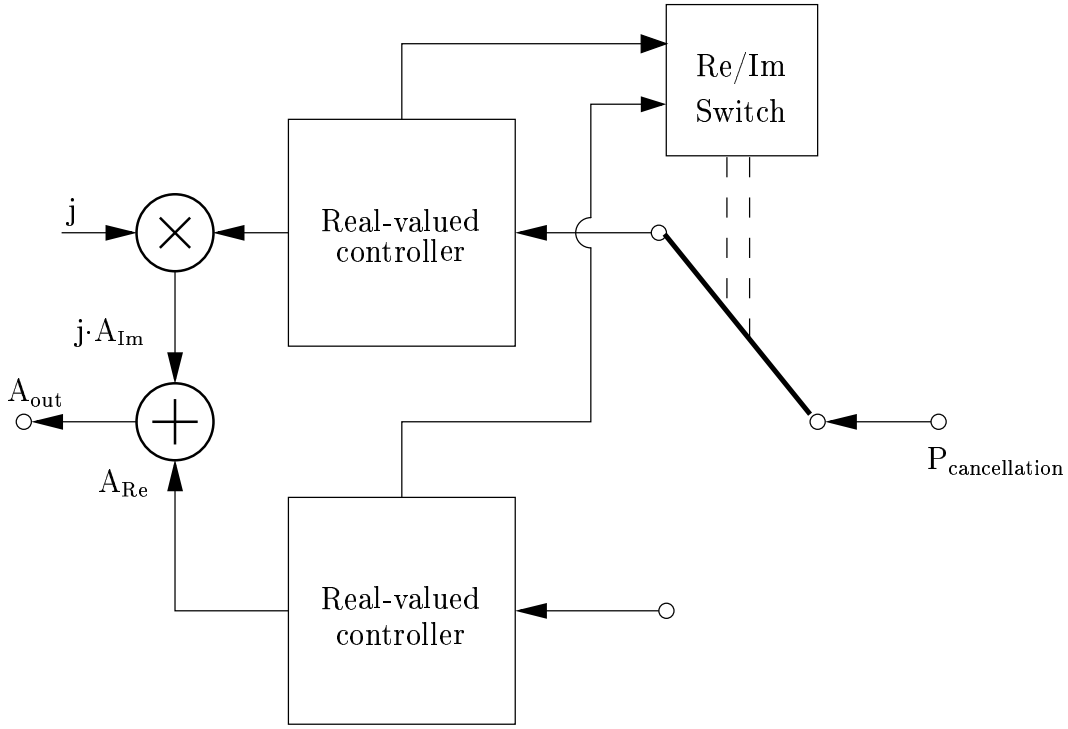

Figure 5.10: Block diagram of the cartesian controller

b[0] and is altered by the use of the following regulation:

$$\mathrm{b}[n] = \begin{cases} \frac{\mathrm{b}[n-1]}{2} & ,\Delta\mathrm{P}\,[\mathrm{n}] \geq 0 \\ 2\mathrm{b}[n-1] & ,\Delta\mathrm{P}\,[\mathrm{n}] < 0 \cap \Delta\mathrm{P}\,[\mathrm{n}-1] < 0 \cap \Delta\mathrm{P}\,[\mathrm{n}-2] < 0 \\ \mathrm{b}[n-1] & ,\mathrm{otherwise} \end{cases} \tag{5.16}$$

Equation 5.16 reduces the step size when a change in the step direction occurs. If no change in the step direction occurred for the last three times then the step size is increased. This structure is used to delay the exponential growing of the step size and should improve the convergence near the minimum point. Additionally an upper and a lower limit for the size of b[n] is defined. After each change in b[n] these limits are checked. The upper limit of the step size is used to set a maximum speed of the controller. The lower limit is needed to improve the response time on changes of P[n] when the controller is in the minimum point. Figure 5.11 presents the block diagram of the real-valued controller. The 'step direction'-block realizes the $\delta\,(\Delta\mathrm{P}\,[n])$-function. The 'step size correction'-unit calculates the weighting factor for the previous step size according to equation 5.16.

This concept presented up to now is sufficient to handle a real-valued control loop. The switching between real-part and the imaginary-part controller is performed by the use of the variable a[n]. In figure 5.10 the variable a[n] is realized by the 'Re/Im-switch'-unit. The problem is to find a good consideration for the switching between the two controllers. The chosen solution is based on the changes in the direction of the steps. For each time when the direction of the

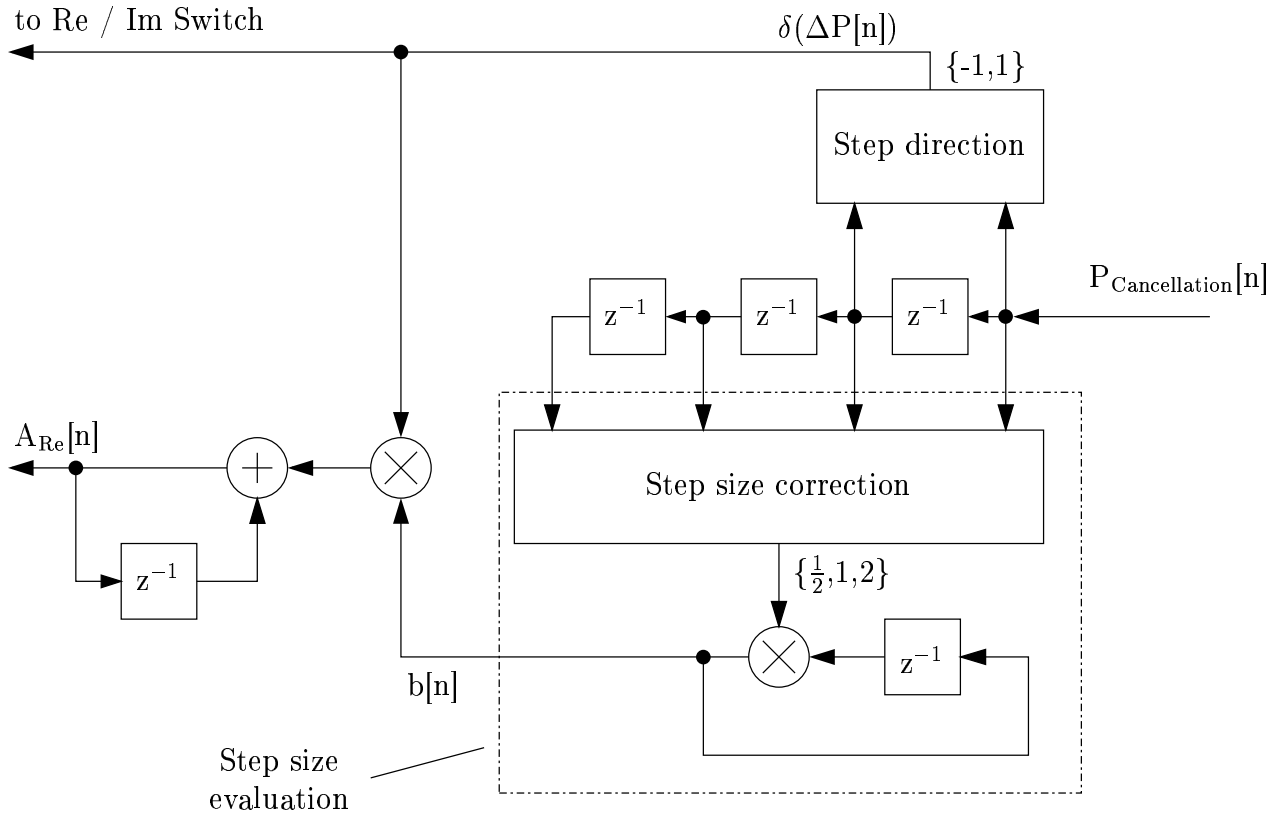

Figure 5.11: Block diagram of the real-valued controller

step changes a counter is increased:

$$\mathrm{c}\left[n\right] = \begin{cases} \mathrm{c}\left[n\right]+1 & ,\delta\left(\mathrm{P}\left[n\right]\right) \geq 0 \\ \mathrm{c}\left[n\right] & ,\text{otherwise} \end{cases} \tag{5.17}$$

After three changes in the direction of the steps for one controller, the other controller is activated:

$$\mathrm{a}\left[n\right] = \begin{cases} j & ,\mathrm{mod}\left(\mathrm{c}\left[n\right],3\right)=0 \cap \mathrm{a}\left[n-1\right]=j \\ 1 & ,\mathrm{mod}\left(\mathrm{c}\left[n\right],3\right)=0 \cap \mathrm{a}\left[n-1\right]=1 \\ \mathrm{a}\left[n-1\right] & ,\text{otherwise} \end{cases} \tag{5.18}$$

where mod (a, b) is the modulo division. Each controller has its own set of parameters b[n] and P[n] which is activated when a change between the controllers occur. Due to this reason both controllers can act completely independently from each other.

In the practical operation the advantages of the cartesian controller are the ability to act completely independent from the parameters of the input signal. His behavior does not change for different input signals or different input power levels. Additionally this type of controller has the ability to approach the minimum point of the cancellation power very closely. The disadvantages of this controller is the quite slow convergence compared to the gradient controller and the slow reaction on fast changes in the input power level. Figure 5.12 presents $\mathrm{A}_{\mathrm{out}}\left[n\right]$

for the cartesian controller adjusting the carrier cancellation loop for a two-tone and a GSM2+ input signal of 10 dBm input power. If the two results of figure 5.12 are compared it is noticeable

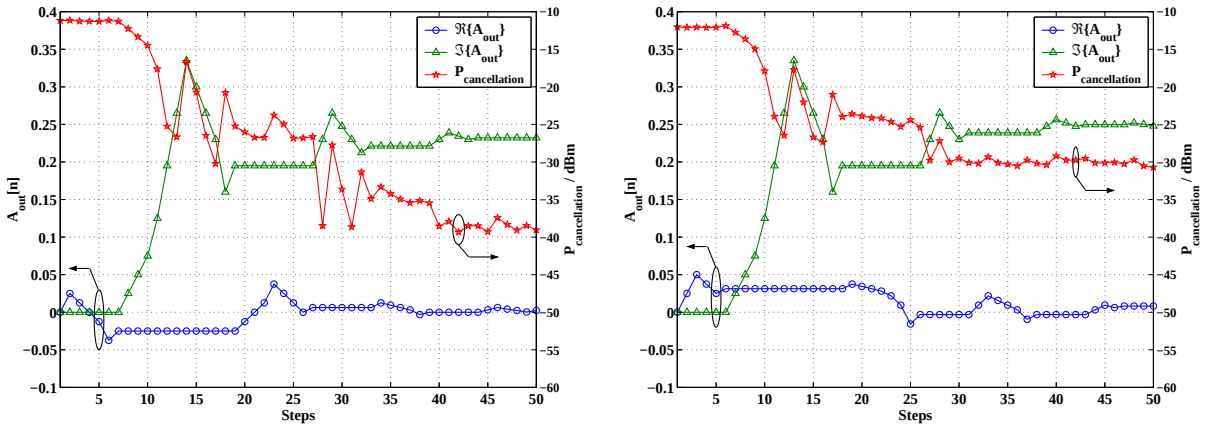

(a) (b)

Figure 5.12: Convergence of the cartesian controller for a two-tone (a) and a GSM2+ (b) input signal

that for two different input signals with the same input power levels the achievable minimization power is completely different.

5.4.4 Gradient controller

A major drawback in the design of the cartesian controller is the need to switch between the two controllers for the real and the imaginary-part. To avoid this problem a controller should be build which has the possibility to handle the complex attenuation even if he can only evaluate a real-valued result out of this operation.

To analyze the task for the controller the power level of the carrier cancellation signal over the complex attenuation plane was measured. Figure 5.13 presents the resulting control surface. Along this control surface the steepest decent for a given start point should be evaluated, which points directly to the minimum [ZCBK96]. In this case the calculation of the complex attenuation can be expressed as:

$$\mathrm{A_{out}}\,[n] = \mathrm{A_{out}}\,[n-1] - \alpha \frac{\partial \mathrm{P}\,[n-1]}{\partial \mathrm{A_{out}}\,[n-1]} \tag{5.19}$$

where $\mathrm{A_{out}}\ [n]$ specifies the actual attenuation value, α is the gradient coefficient and $\mathrm{P}[n]$ is the cancellation signal power level. Figure 5.14 depicts the block diagram for the gradient controller. The estimation of the power gradient is done by measuring the values of the cancellation signal power in two points around the actual known attenuation. Figure 5.15 illustrates the evaluation of the power gradient. The power levels $\mathrm{P_{Re}}[\mathrm{n}]$ and $\mathrm{P_{Im}}[\mathrm{n}]$ are measured at the attenuation values $\mathrm{A_{Re}} = \mathrm{A_{out}}\,[n-1] + \Delta\mathrm{A}$ and $\mathrm{A_{Im}} = \mathrm{A_{out}}\,[n-1] + j\Delta\mathrm{A}$. The value $\Delta\mathrm{A}$ is a constant parameter of the gradient controller. Due to this measurement the changes in the cancellation signal power

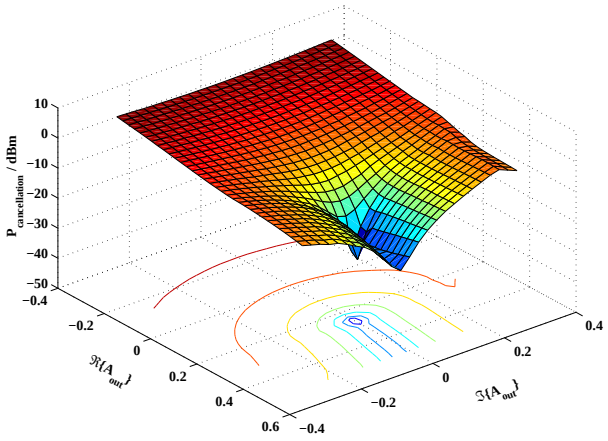

Figure 5.13: Carrier cancellation signal power over the complex attenuation

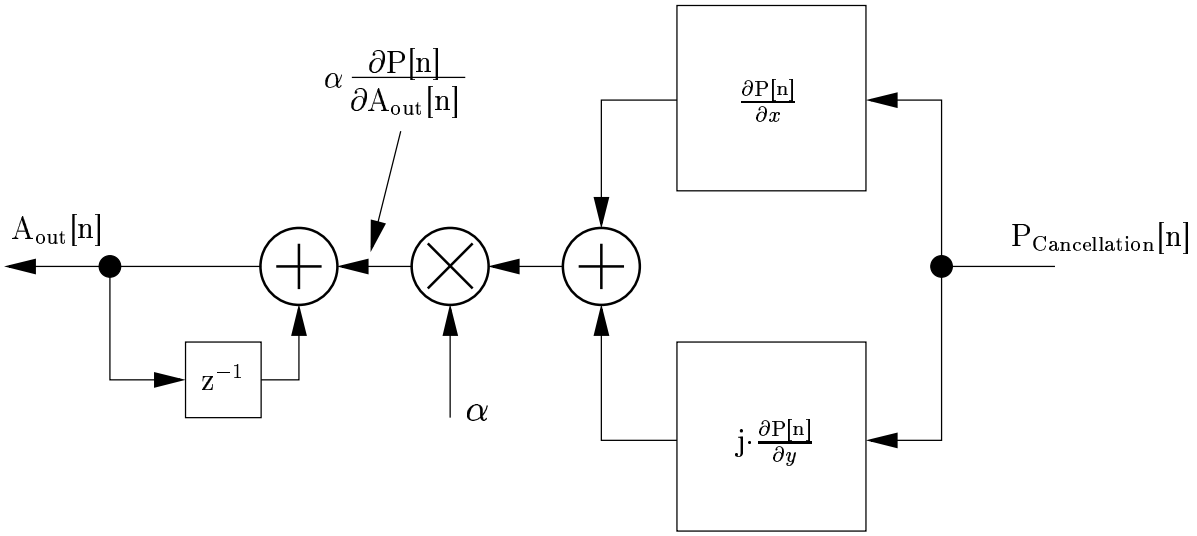

Figure 5.14: Block diagram for the gradient controller

are known and can be used to estimate the power gradient:

$$\alpha \frac{\partial \mathrm{P}\left[n-1\right]}{\partial \mathrm{A}_{\mathrm{out}}\left[n-1\right]} \approx \frac{\left(\mathrm{P}_{\mathrm{Re}}\left[n-1\right]-\mathrm{P}\left[n-1\right]\right)+j\left(\mathrm{P}_{\mathrm{Im}}\left[n-1\right]-\mathrm{P}\left[n-1\right]\right)}{\mathrm{P}_{\mathrm{norm}}} \tag{5.20}$$

where $\mathrm{P}_{\mathrm{norm}}$ is a proportional constant. Additionally a limitation of the length of the power gradient is introduced to set a maximum possible speed of the controller. Three measurements have to be performed for each step of the controller. Compared to the cartesian controller the convergence should be three times better. Figure 5.16 presents $\mathrm{A}_{\mathrm{out}}\left[n\right]$ for the gradient controller adjusting the carrier cancellation loop for a two-tone and a GSM2+ input signal of 10 dBm input power. If the measurement results of the cartesian and the gradient controller are compared to

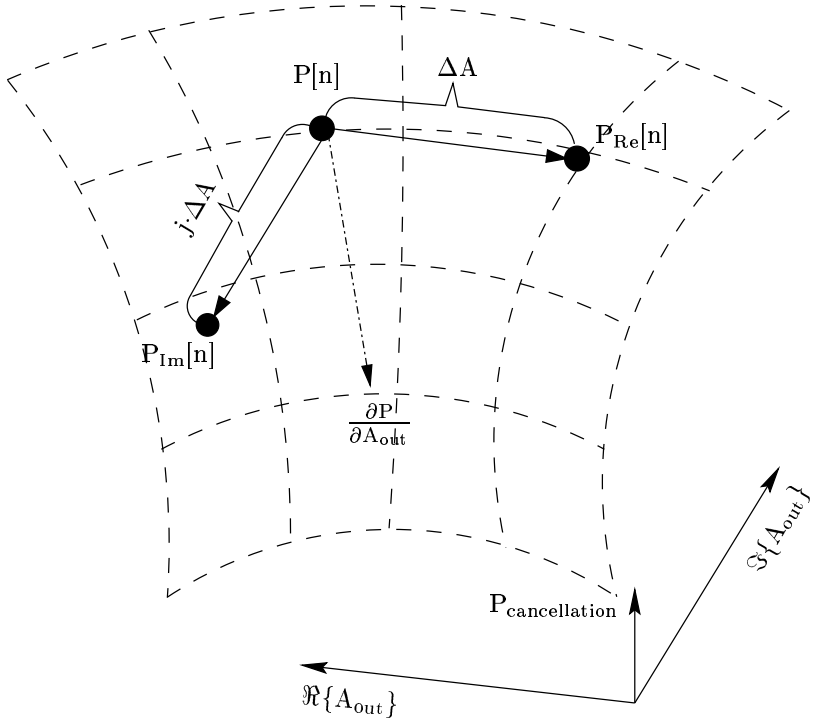

Figure 5.15: Estimation of the power gradient

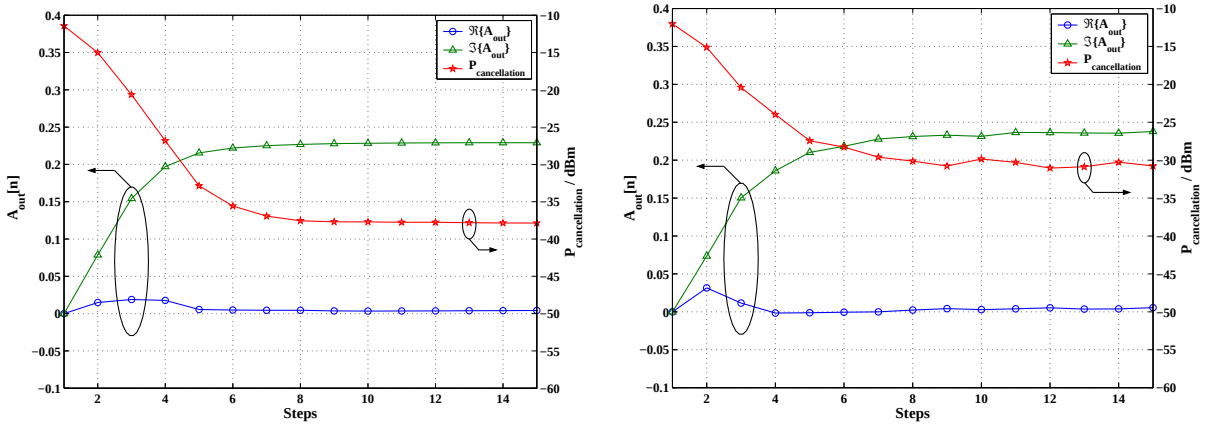

Figure 5.16: Convergence of the gradient controller for a two-tone (a) and a GSM2+ (b) input signal

each other the following conclusions can be drawn:

- For both types of input signals the convergence of the gradient controller is more than three times faster as the cartesian controller

- Both controllers achieve quite the same quality of signal suppression
- The gradient controller is more sensitive to noise effects. For a GSM2+ signal the stability of the gradient controller is lower than for the cartesian controller

Up to now a major disadvantage of the realized gradient controller is not discussed. The stability of this controller is mainly influenced by the chosen P_{norm}. To get a stable controller as presented in figure 5.16 P_{norm} must be set correctly. Unfortunately the value of P_{norm} is influenced by the input signal power and also by the type of input signal. To use the gradient controller over a wide range of input power levels P_{norm} must be adjusted by the use of a lookup table or an other suitable estimation process.

5.5 Measurement results of the FFA

The measurement procedure of the adaptive controlled FFA includes the adjustment of the control loops before the actual output signal can be measured. Compared to the standard amplifier measurements as presented in section 4.3 to 4.5 the duration of a measurement cycle increased quite much. Due to this reason no single-tone measurement over the power-frequency plane was performed.

The measurement program for the FFA is based on the feedforward controlling program. In addition to the problem of performing a correct measurement the program must decide, when the cancellation loops are balanced. This problem was solved by analyzing the power level of the residual pilot-tone at the output of the FFA. A measurement can be started when the power level of the residual pilot-tone is within a tolerance band for a given number of samples. The settings for the measurement of the adaptive controlled FFA are:

- the maximum power level of the pilot-tone has to be lower than +0.25 dB of the average power level
- this criteria must be achieved for 20 samples

It is not useful to check the lower limit of the tolerance band. Especially for the gradient controller problems can occur when it is operating near the optimum setting of a cancellation loop. Figure 5.17 presents the power level of the residual pilot-tone controlled by the gradient controller near the optimum point. The measurement circuit for the FFA is presented in figure 5.18.

The characterization of the bandwidth of the FFA was evaluated by the use of a single-tone frequency sweep measurement. During this process the vector attenuators were adjusted to have best signal suppression near the middle of the frequency band. Figure 5.19 presents the measured cancellation performance for the both loops. This measurement showed that a cancellation performance of more than 30 dB can be reached over a bandwidth of about 30 MHz.

The measurements of the complete FFA were performed with the following settings:

- A spectrum analyzer was used to measure the power of the carrier and the distortion cancellation signal. The advantage of this approach is the possibility to measure only a selected part of the spectra. Hence, the spectrum analyzer substituted the combination

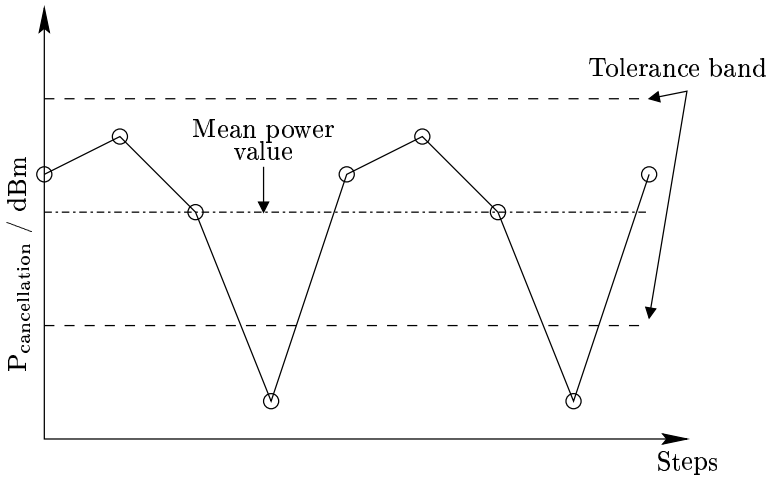

Figure 5.17: Behavior of the gradient controller near the optimum point

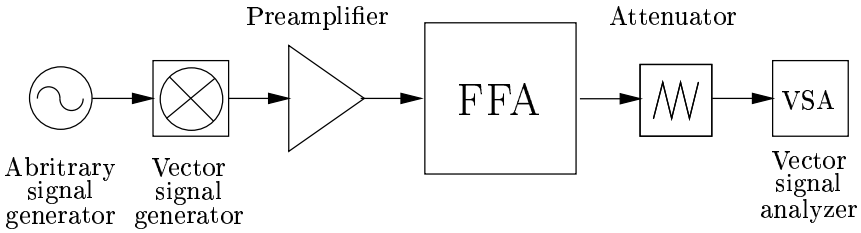

Figure 5.18: Measurement circuit of the FFA

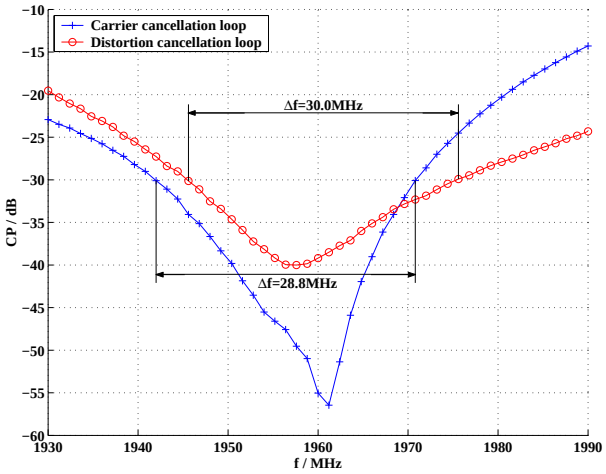

Figure 5.19: Cancellation performance measurement for the carrier and the distortion cancellation loop

of narrow-band filter and power detector. Both cancellation signals were passed to the

spectrum analyzer by the use of a RF-switch.

- The pilot-tone was located 410 kHz above the center frequency. The power level was set to be 30 dB below the main amplifier input signal. The residual pilot-tone at the output of the FFA was measured over a bandwidth of 20 kHz.
- Both loops were controlled by the gradient controller
- The input signals were generated by the use of the ROHDE&SCHWARZ signal generators AMIQ and SMIQ. A preamplifier was used to boost the power level to the desired value.
- The VSA produced by AGILENT TECHNOLOGIES was used to measure the output signal according to the GSM2+ specification.
- For all measurements of the FFA the following naming convention were used:
  - P_{in} named the input power to the complete feedforward structure.
  - $P_{in_{MA}}$ named the input power to the main amplifier of the FFA. It is convenient to use $P_{in_{MA}}$ because the measurement results of the main amplifier can be directly compared to the measurements of the FFA. For a given P_{in} the value of $P_{in_{MA}}$ can be calculated as (both power levels are measured in dBm):

$$P_{in_{MA}} = P_{in} - 6.7 \text{ dB} \tag{5.21}$$

Figure 5.20 illustrates the behavior of the FFA when a two-tone input signal is supplied. The first measurement was a power sweep at 1960 MHz. Afterwards a frequency sweep with a constant input power of $P_{in_{MA}}$ of 10 dBm was performed. By the use of the two-tone power sweep the

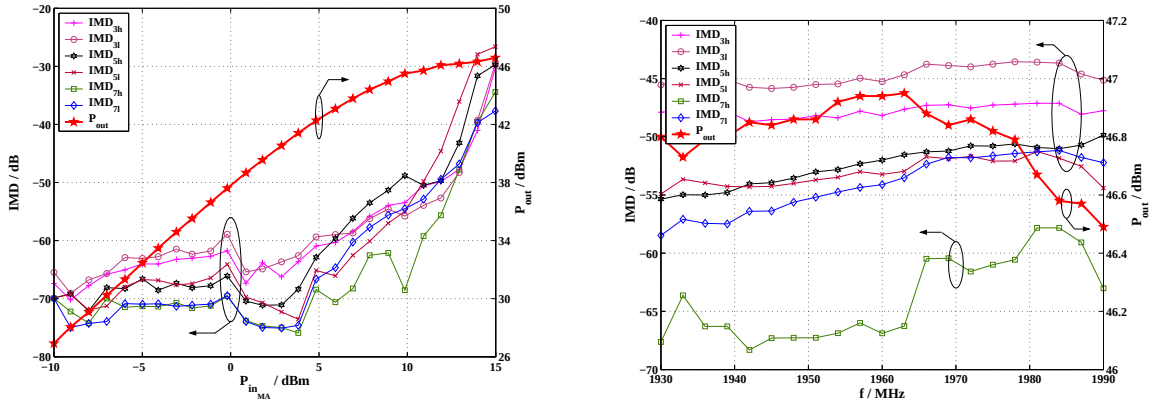

(a) (b)

Figure 5.20: Intermodulation distance of the FFA for a two-tone input signal at 1960 MHz (a) and for a constant $P_{in_{MA}}$ of 10 dBm (b)

third order intercept point was evaluated: $IP3_{output}$=56.4 dBm.

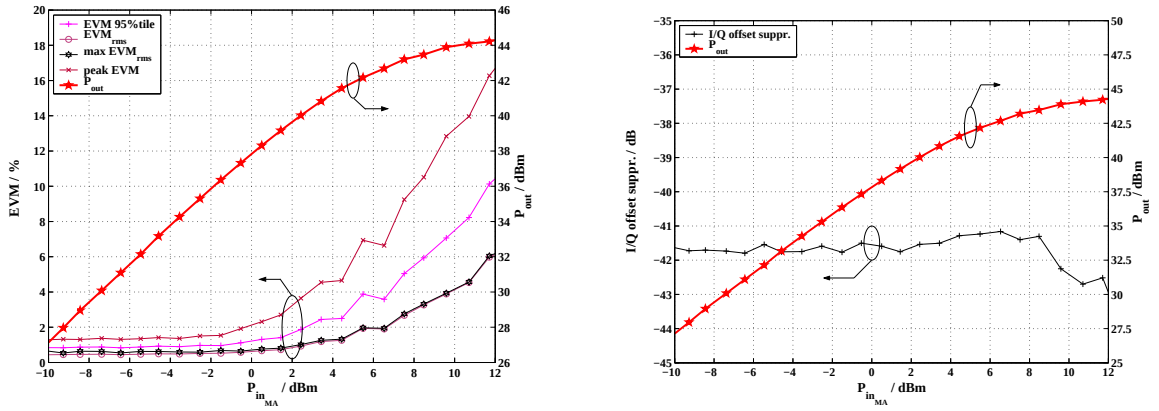

(a) (b)

Figure 5.21: Measurement of the EVM (a) and the I/Q offset suppression (b) at 1960 MHz

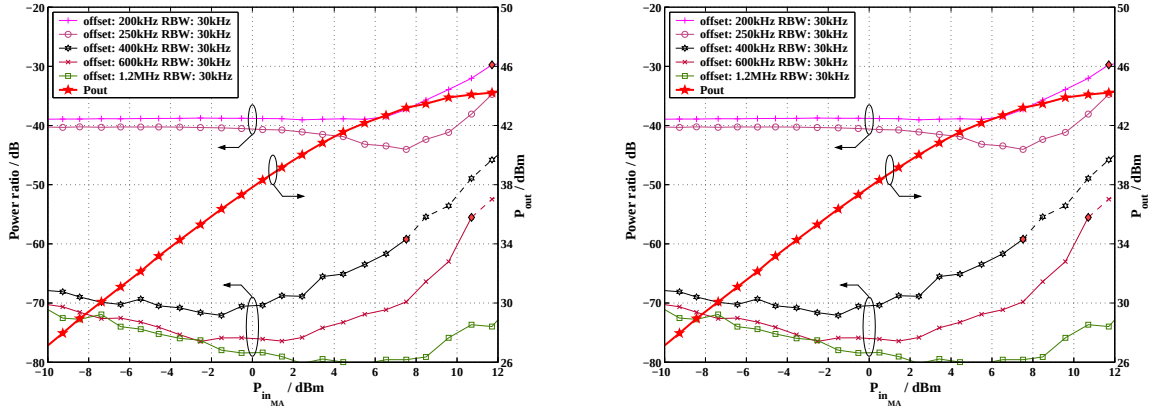

(a) (b)

Figure 5.22: Measurement of the lower (a) and upper (b) sideband of the spectrum mask at 1960 MHz

The GSM2+ compliance measurements were performed in the same way as for the main amplifier presented in section 4.4. Additionally to the power sweep measurement also a frequency sweep of the GSM2+ signal was performed. All GSM2+ input signals included power-ramping.

The dashed line-style in the EVM-measurement in figure 5.23 and 5.24 shows again the area where the FFA exceeds the limits given by the GSM2+ standard starting from the diamond shaped marker. The insufficient suppression of the pilot-tone cause the trouble with the measurement of the spectrum mask. To avoid this problems several possibilities can be found in the literature, like a frequency hopping or a spread spectrum pilot-tone.

The last measurements presented for the FFA are the frequency sweep measurements of a GSM2+ input signal with an input signal power $P_{in_{MA}}$ of 10 dBm.

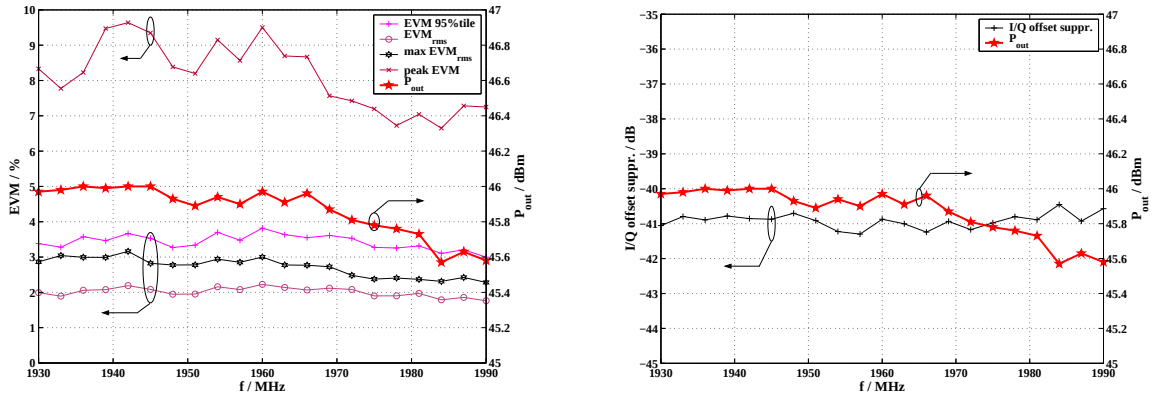

(a) (b)

Figure 5.23: Measurement of the EVM (a) and the I/Q offset suppression (b) at $P_{in_{MA}}$ of 10 dBm

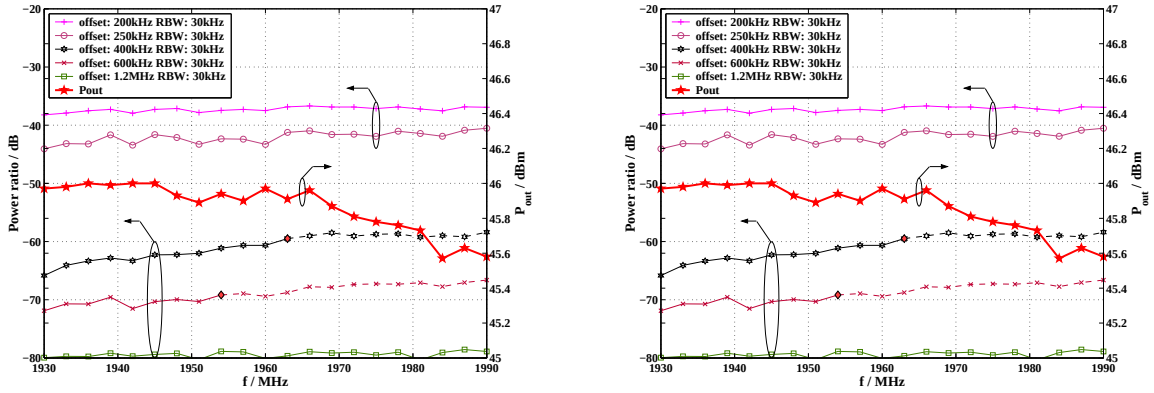

(a) (b)

Figure 5.24: Measurement of the lower (a) and upper (b) sideband of the spectrum mask at $P_{in_{MA}}$ of 10 dBm

5.5.1 Comparison between the main and the feedforward amplifier measurement results

After the measurement results for both amplifiers are known, the following figures of merit for the performance are compared:

- Gain
- Third order intercept point
- Intermodulation distance
- GSM2+ compliance measurement:
  - EVM

– spectrum mask

Gain

The gain of the FFA is 8.3 dB lower as the original amplifier. The reduction of the gain can be spilt into three parts:

- Input power splitter and directional coupler DC_3: 6.7 dB
- Delay line D_2 and directional coupler DC_2: 1.3 dB
- Higher compression of the output signal: 0.3 dB

The gain of the FFA could be easily increased by exchanging the input power splitter with a 10 dB directional coupler.

Third order intercept point

The IP_3 has been increased by 3.3 dB by the use of the adaptive feedforward structure. The quite low IP_3 of the FFA compared to the main amplifier can be ascribed to the lower gain of the FFA. If the $P_{in_{MA}}$ will be used for the evaluation of the IP_3 instead of the P_{in} the difference in the two figures of merit would be 11.3 dB.

Intermodulation distance

Figure 5.25 presents a comparison of the two-tone measurements for both amplifiers. If an intermodulation distance of 50 dB should be achieved, an improvement in the output power of about 18.8 dB can be reached by using the adaptive FFA.

GSM2+ EVM

Figure 5.26 presents a comparison of the EVM-measurements for both amplifiers. An improvement in the output power of about 2.3 dB can be reached if only the EVM-measurements are considered.

GSM2+ Spectrum mask

Figure 5.27 presents a comparison of the spectrum mask measurements for both amplifiers. In the case of the spectrum mask the chosen structure could not improve the performance of the original amplifier. Four reasons can be accounted for this result:

- Pilot tone:

  The location of the pilot-tone was 410 kHz above the center frequency. In the case of figure 5.27 only the lower, less critical part of the spectrum mask was compared. Still it seems that the location of the pilot-tone had a significant influence on the low performance results for the measurement of the spectrum mask.

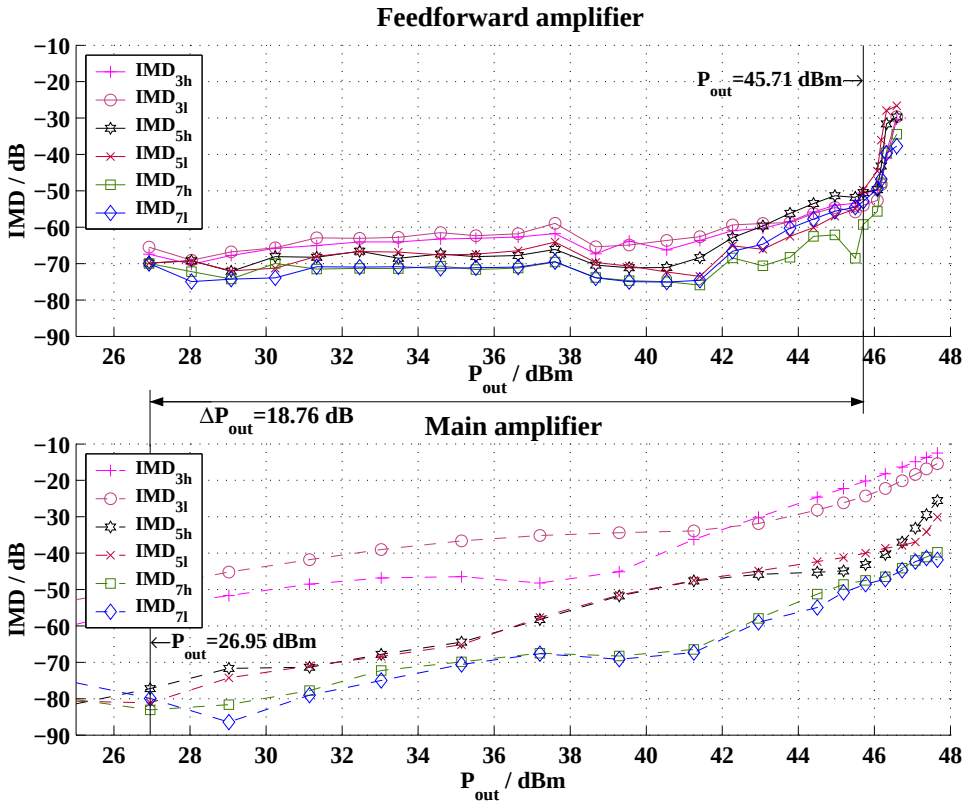

Figure 5.25: IMD measurement for the main and the feedforward amplifier at 1960MHz

Generally it would be interesting to compare this performance to a FFA operating with a completely passive distortion cancellation control.

- Error amplifier output spectrum:

  The distortion created by the error amplifier occupies much more bandwidth than the original input signal. Additionally this distortion is directly passed to the output of the FFA. Analyzing the achieved measurement results shows that the maximum output power of the error amplifier was too low, i.e. the distortion power created by the error amplifier was to high. Taking a closer look to the IMD measurement of the FFA presented in figure 5.20 it can be recognized, that the IMD was around -60 dB over the hole power sweep. The demand of the GSM2+ standard for a distortion level of more than 60 dB below the carrier starting from a frequency offset of 400 kHz from the center frequency is hard to achieve by the use of the realized FFA under this point of view.

- Realized structure:

  The worst case estimation for the cancellation performance of the carrier cancellation loop presented in section 5.2.1 shows that due to the insertion losses of the active devices a maximum cancellation performance of about 40 dB can be reached. Adding the inter-

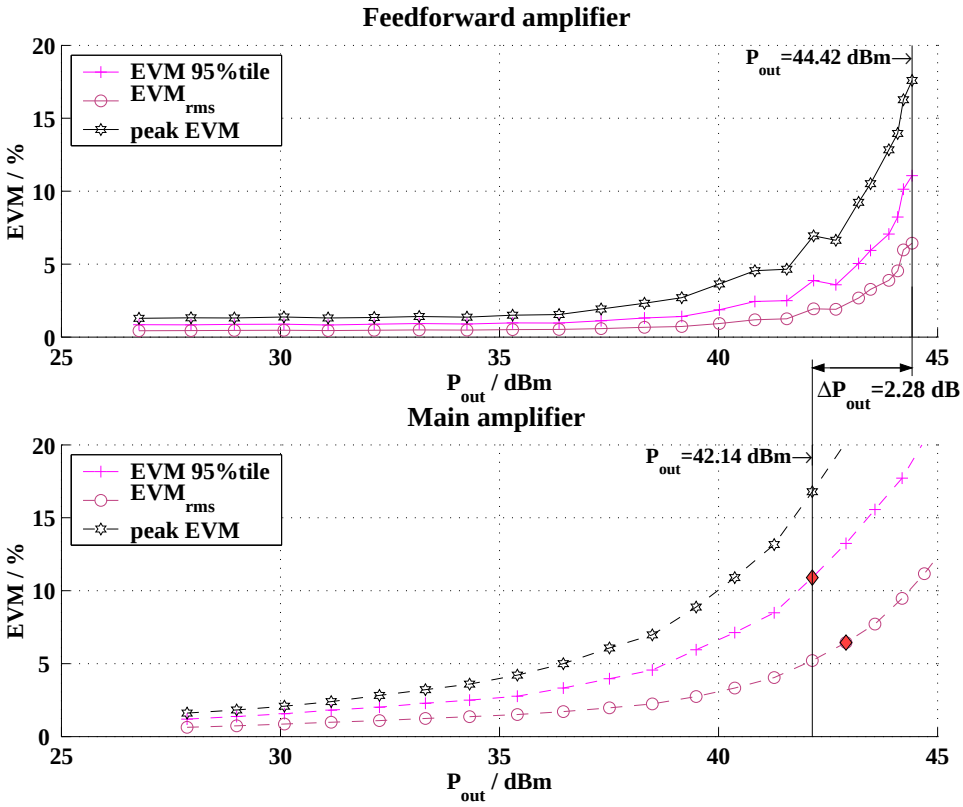

Figure 5.26: EVM measurement for the main and the feedforward amplifier at 1960MHz

modulation distance of the main amplifier of about 20 dB leads to a maximum IMD of about 60 dB at the output of the FFA, which was verified by the two-tone measurement in figure 5.20. Rearranging the feedforward structure could help to increase the maximum cancellation performance and hence should also improve the performance of the FFA for the GSM2+ compliance measurement.

- Insertion loss caused by the delay line and the directional coupler:

  The insertion loss of the delay line D_2 and the direction coupler DC_2 of about 1.7 dB is a big problem for the realized FFA. A reduction of the length of the delay line would limit the bandwidth of the FFA, but would lead to higher output power. For the case of a single-carrier FFA a cancellation bandwidth of about 2 MHz should be enough for the distortion cancellation loop. An additional measurement of the FFA operating with a minimum delay line length would be a interesting comparison.

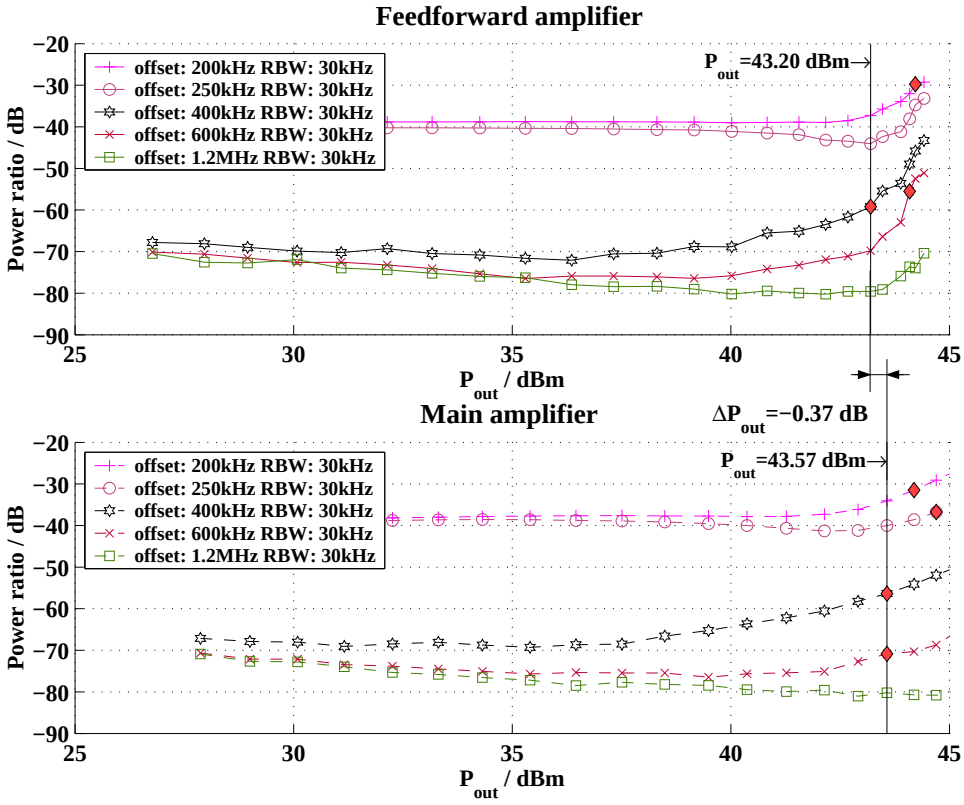

Figure 5.27: Lower spectrum mask of the main and the feedforward amplifier at 1960MHz

	Main amplifier	Feedforward amplifier
Gain	36.2 dB	27.7 dB
$IP3_{output}$	53.1 dBm	56.4 dBm
Amplifier output power		
IMD 50 dB	27.0 dBm	45.7 dBm
EVM (GSM2+)	42.1 dBm	44.4 dBm
Spectrum mask (GSM2+)	43.6 dBm	43.2 dBm

Table 5.4: Comparison summary

Chapter 6

Conclusion

The goal of this diploma thesis was to improve the performance of an existing amplifier by the use of the feedforward linearization technique. The feedforward amplifier was based on commercially available products. By the use of two adaptive controllers a stable operation of the FFA had been established. The measurement of the adaptive controlled FFA showed, that a significant performance improvement was achieved for a two-tone input signal. The measurement of the performance of the FFA according to the GSM2+ standard showed weaknesses in the range of the spectrum mask. The analysis of the causes of this weaknesses blazes the trail for further improvements of the realized FFA.

6.1 Improved feedforward structure

Figure 6.1 presents a structure which reduces the influence of the return loss of the active devices. The power splitters are exchanged by two directional couplers DC_6 and DC_7. The effects of the low return loss of the main amplifier input is avoided by the use of the directional coupler DC_6. Directional coupler DC_7 should keep the gain of the error amplifier at quite the same level.

6.2 Reduced delay matching

Accepting a delay mismatch for the distortion cancellation loop gives the possibility to shorten the length of the delay line at the output of the main amplifier. This will increase the output power of the main amplifier at a constant intermodulation distance or vice versa will reduce the distortion level for the same output power of the FFA. For a GSM2+ signal a distortion level of more than 60 dB below the carrier has to be achieved for a bandwidth of 1.2 MHz. Hence the cancellation performance of the distortion cancellation loop should be around 40 dB for the same bandwidth.

6.3 Feedforward and predistortion

Feedforward is perfectly suited to be used together with other linearization techniques. Any reduction of the distortion level of the main amplifier results directly in a reduction for the re-

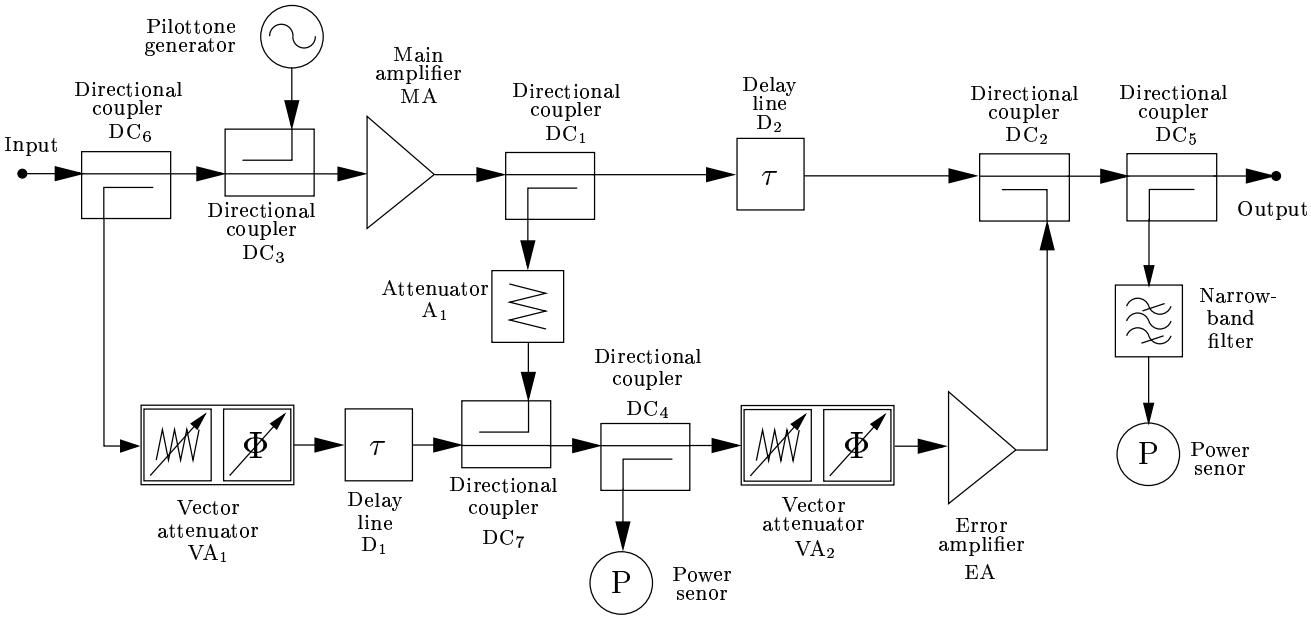

Figure 6.1: Improved feedforward structure

quirements of the error amplifier. Especially predistortion could be easily combined with the feedforward linearization technique. In *[HST+01, BWB98]* examples for the combination of analog predistortion and feedforward are shown. The combination of digital baseband predistortion and feedforward is another possibility to combine these techniques. Figure 6.2 illustrates a possibility to implement digital baseband predistortion into a feedforward structure.

6.4 Passive distortion cancellation loop control based on power detection

The problems caused by using a pilot-tone to evaluate the performance of the distortion cancellation loop were presented in section 5.5.1. The realization of the controlling system based on power detector is one of the cheapest possibilities to build a adaptive controlled FFA. To design an adaptive FFA which can control the distortion cancellation loop by the use of a power detector but without the disadvantages of a pilot-tone could be interesting for several practical applications. Based on a structure combining three cancellation loops and two power detectors this defaults can be fulfilled. A comprehensive evaluation of the performance of such a adaptive controlled FFA is still missing.

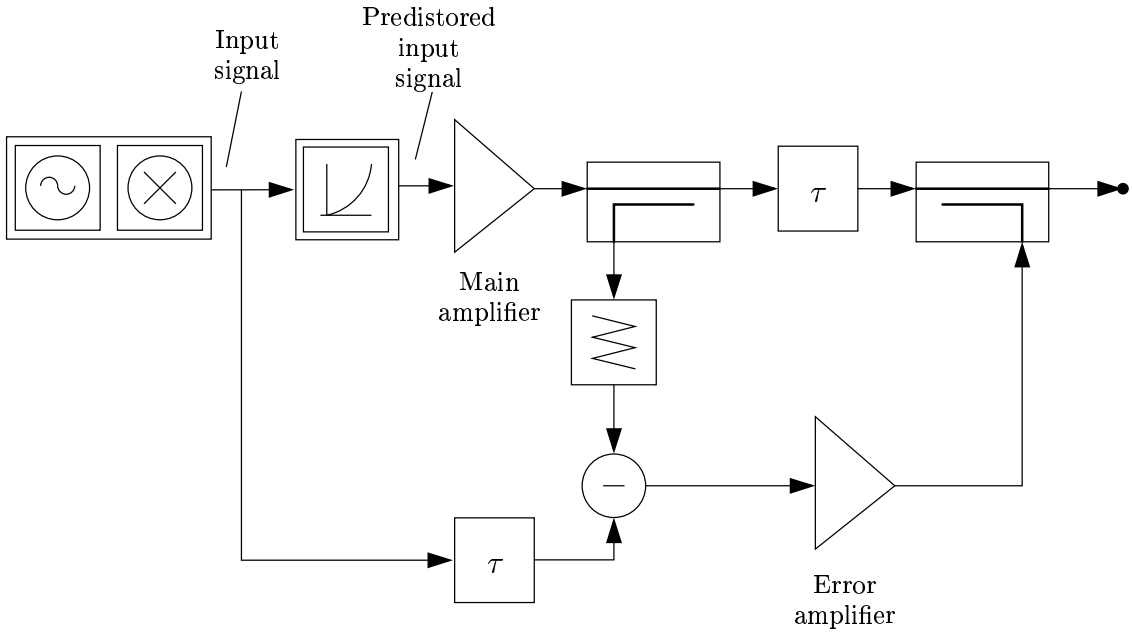

Figure 6.2: Digital predistortion and feedforward

Appendix A

Measurement programs

A main part of this diploma thesis was to measure and specify several RF-components. This was done by controlling the measure equipment over the GPIB-bus. The environment for managing the GPIB-interface, analyzing and displaying the measurement values was MATLAB® Version 6.1, Release 12.1 [Mat02]. By the use of the Instrument control-Toolbox [Mat01], an easy handable interface for the information exchange over the GPIB-bus was given. Additionally the powerful displaying commands were used to visualize the results. All of the program described afterwards are scripts, written in the MATLAB®-script language.

A.1 Vector attenuator measurement

A.1.1 Measuring the controlling function

The task for the script 'VAmeasure_V3' was to characterize the controlling function $S_{21}(I, Q)$ of the vector attenuator board in use. Two Keithley Model 2400 SourceMeters® were used to set the driving current. The HP8510C network analyzer measured the transfer characteristic for the operation point adjusted by the two driving currents. Figure A.1 shows the test circuit, which was used to measures the controlling function. The script 'VAmeasure_V3' is used to set the correct output currents and to measure the transfer characteristic. This script has no interactive user interface and no handover-parameters. All settings are directly written into the declaration of the main data structure. The parameters are:

`freq` Hz; Frequency at which the vector attenuator is measured.

`load_through_cal` (0,1); Specifies if the through-calibration is already performed and can be loaded into the memory.

`calset` (1-8); Select the correct calset from which the calibration should be loaded. If a new calibration is to be performed, it will be saved at the specified calset number. In this chase the calset saved at this entry will be overwritten.

`P_measure` dBm, This values defines the output power of the sweeper during the measurement.

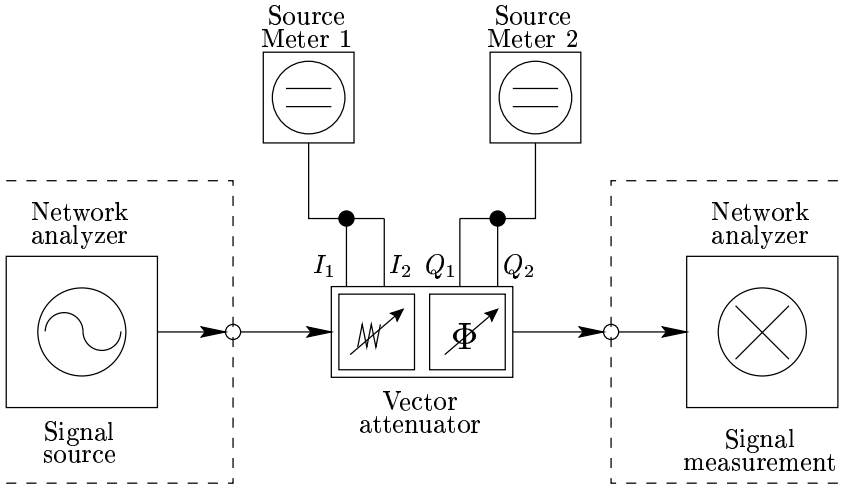

Figure A.1: Vector attenuator test circuit

`P_AverageFact` (1,2,4,8,16,...); The averaging factor specifies the number of measurements which are done for each operation point. The mean of all measurement for this operation point is used as the result.

`I_VA_list` A; This list of current values will be applied to both, the inphase and the quadrature current. The entries are set at the output of the SourceMeter® one after the other.

`U_VA` V; Sets the level for the maximum output voltage to drive the control current.

`VA_OutputFilename` Shows the name for the file in which the measured data are saved.

`VA_User_Preset` (0,1); If this value is active, the USER PRESET at the network analyzer will be performed before the measurement is started.

`GPIB_8510` (0-32); GPIB-address of the network analyzer

`GPIB_8510_Systembus` (0-32); GPIB-address from the systembus of the network analyzer. (Not used)

`GPIB_Source1` (0-32);The GPIB-address of the SourceMeter® is used to supply the inphase current

`GPIB_Source2` (0-32);The GPIB-address of the SourceMeter® is used to supply the quadrature current

`GPIB_InputBufferSize` Bytes; The size of the GPIB-inputbuffer is important, when a complete measurement is read from the network analyzer. In this case the buffer size can be estimated by: buffersize $\geq$ frequency points $\cdot$ 8.

`GPIB_Timeout` s; Sets the time in which the GPIB-device has to react.

The script works according to the structure chart illustrated in figure A.2.

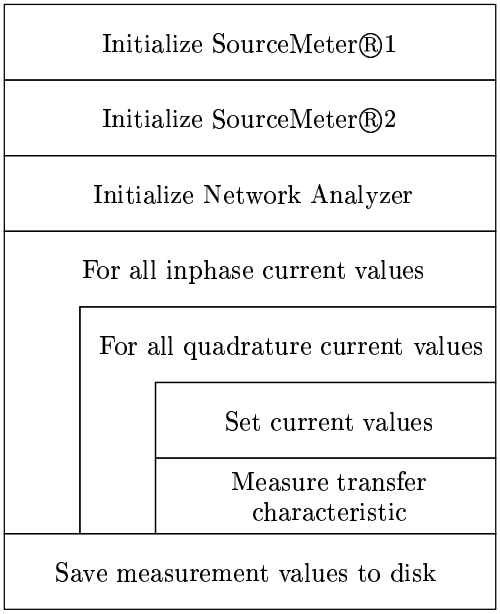

Figure A.2: Flowchart of the 'VAmeasure_V3' script

A.2 Amplifier gain measurement

The MATLAB® script 'gainmeasurement' is an interactive program for the measurement of the complex instantaneous gain of an amplifier. The network analyzer HP8510C provides the possibility to calibrate one port to a constant output power over the selected frequency sweep. This feature is used to measure the characteristic of nonlinear amplifiers in magnitude and phase-shift. The graphical user interface should help to enter all parameters for the measurement correctly and should inform about the progress of the measurement.

A.2.1 Measurement principle

The structure of the program is designed to simplify the setting of the parameter at the network analyzer for a correct measurement. For a typical measurement the following steps have to be taken:

1. Flatness calibration:

   A reference measurement determines the actual output power at port 1 of the network analyzer over the whole frequency range. The recorded output power values are afterwards used to correct the power settings for the sweeper, so that a constant output power at port 1 is achieved for each frequency point.

2. Calibration:

   After acquiring constant output power at port 1, a through-calibration is performed to eliminate the effects of cable, attenuators, preamplifier, etc. Hence the calibration mea-

surement specifies the whole test circuit but without the DUT (**D**evice **U**nder **T**est). This measurement should be performed at the highest possible output power to reduce the noise-effects. Figure A.3 shows possible configurations for the calibration measurement.

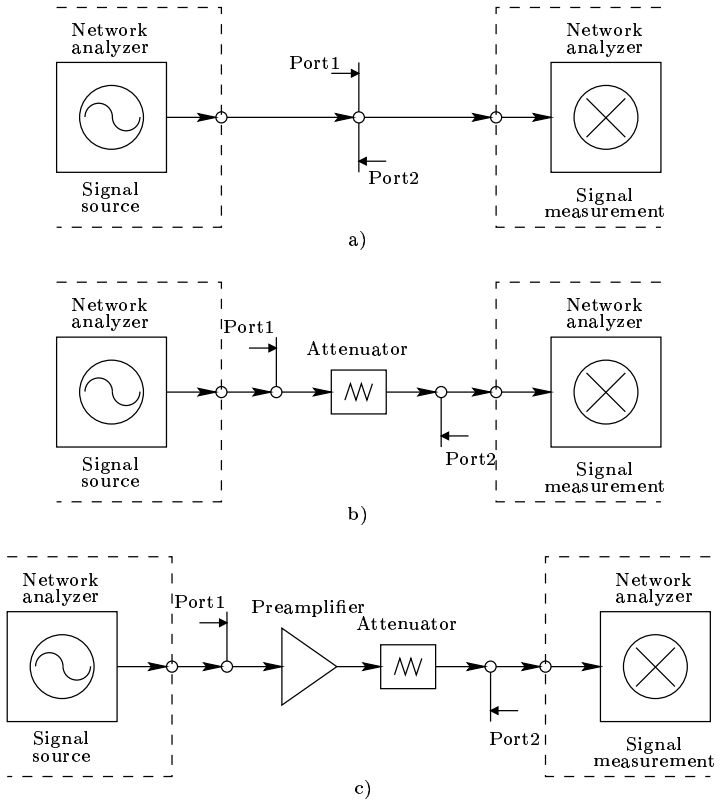

Figure A.3: Three calibration possibilities

3. Measurement:

   After the network analyzer is calibrated, the measurement of the DUT can be performed. A frequency sweep will be done for each chosen power value. The result of the measurement is a surface over a power-frequency plane, which can be used to documents the AM-AM and AM-PM conversion of the DUT.

A.2.2 User interface

Figure A.4 shows the applet which appears after starting the script. The main components are:

1. Menu bar:

   Including file, settings, option and help menu

2. Selected structure:

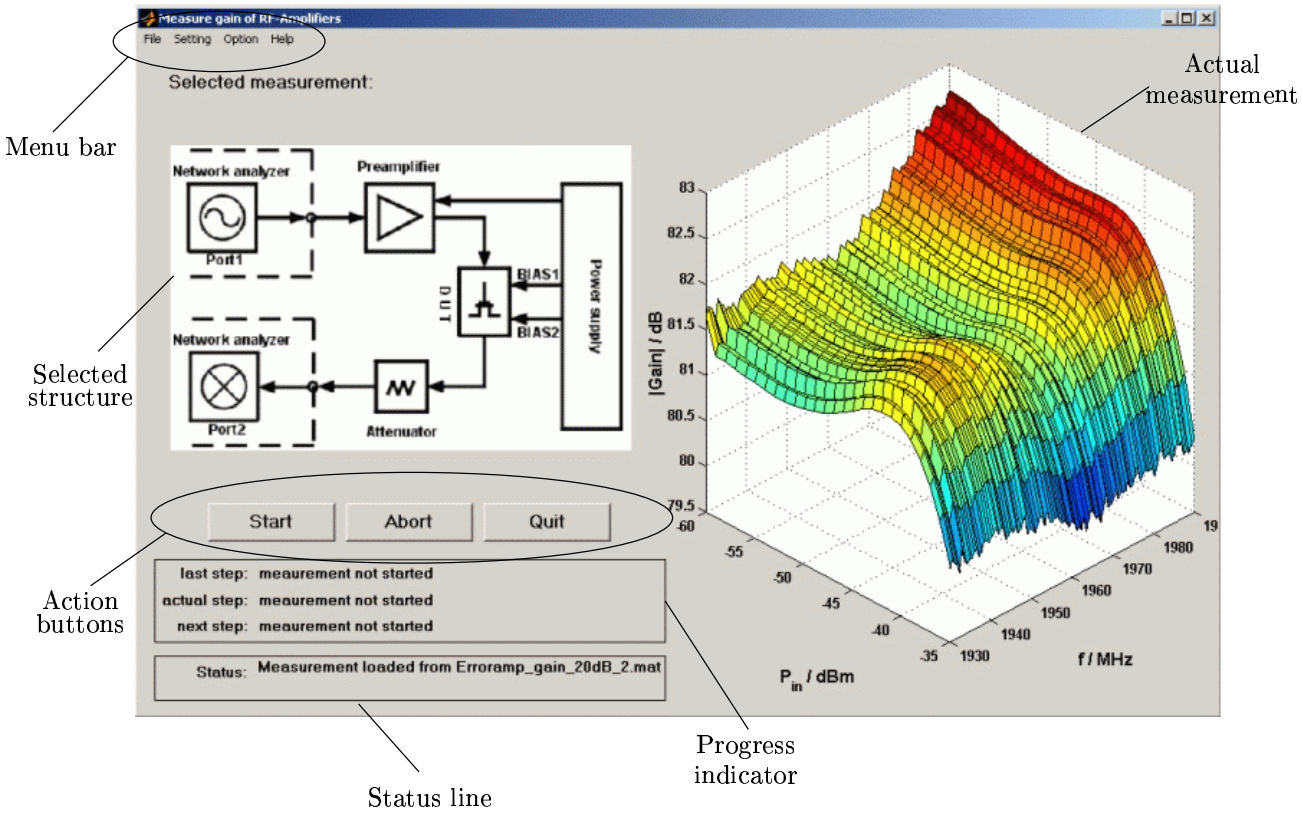

Figure A.4: Startup screen of gainmeasurement applet

Shows a block diagram of the selected measurement structure according to the actual measurement settings

3. Progress indicator:

   The progress indicator informs about the actual state of the measurement after the process is started, including the previous, the actual and the next action. This indication should help to interrupt the program before an unwanted action is carried out. Together with the Abort-button this tool can prevent a damage of the DUT.

4. Status line:

   In the status line comments to the actual executed action are written, like a confirmation that the actual settings have been changed after accessing the settings menu.

5. Action buttons:

   The three buttons 'Start', 'Abort' and 'Quit' are the main program control buttons. The start-button start a measurement based on the actual settings. Pressing the abort-button interrupts the measurement without loosing the measurement-values. The quit-button immediately aborts the execution of the program and closes the applet.

6. Actual measurement figure:

   The actual measurement-values are visualized within this figure. A switch between the presentation of the magnitude or the phase of the measured gain can be done in the option menu. This figure can also be used to display previous measured data, if they are loaded into the program by the use of the load-command.

File menu

The commandos located in the file pull-down menu can be used before and after a measurement process. The pull-down menu includes the following commands:

- Load:

  The load-command is used to load an old measurement into the program. The measurement-values are then displayed within the measurement figure.

- Save:

  After a measurement process is finished the measurement data can be saved to a MATLAB® '*.mat'-workspace-file.

- Print:

  The print entry to the file-menu includes two sub-menu points:

  - Amplitude
  - Phase

  These commands can be used to print the actual available measurement data in the chosen presentation.

- Quit:

  Similar to the quit-button, this command will close the applet. If some measurement data are available in the memory which are not saved to a file, a message window will ask you if you want to proceed without saving.

Settings menu

Similar like the measurement-values, also the complete settings for a measurement can be loaded into the program and saved to a file. A saved settings-file is a independent MATLAB® '*.mat'-workspace-file, which can be kept together or separated from the measurement-file. All entries to the settings pull-down menu are used to manage the measurement process:

- Frequency:

  Pressing this command will activate the frequency-settings applet. All information about the frequency range and the through-calibration for the measurement are adjusted within this applet.

- Power:

  Activating this entry shows the power-settings applet. Here you can enter a set of power values at which the device should be measured. Additionally all settings for the power flatness calibration are entered here.

- Bias:

  The program is designed to handle two biasing points and a preamplifier. By the use of this applet these possibilities can be set according to the demand of the DUT.

- GPIB:

  The program is designed to interact with the HP8510C network analyzer and a HP6626 4-channel DC-power supply. Activating this applet provides the possibility to change the settings for the GPIB-interface.

- Transfer characteristic:

  The program is able to measure the instantaneous complex gain of a device. For simulations the envelope transfer characteristic is needed. After activating the flag 'transfer characteristic' in the option menu, a power series fit of the instantaneous gain is performed. Than the coefficients are converted according to equation 3.30, shown in chapter 3.3.2, to get the envelope transfer characteristic. It has to be mentioned that the convergence of the power series fit is only given, if the number of power values is about 7-10 times the order for the power-series fit.

- Load settings:

  This menu entry provides the possibility to load a settings-file into the program. All previous settings are overwritten.

- Save settings:

  The actual measurement settings are saved to a file when accessing this menu point.

Frequency settings applet

Figure A.5 shows the frequency settings applet. The following adjustments can be taken:

- Measurement mode:

  The two measurement modi 'step' and 'ramp' are important for the behavior of the network analyzer at large frequency range and high number of averages. In the step-mode each frequency point is set one after the other. First all averages are done for the actual frequency point before the next one is set. This is an advantage for measurements with a high level of averages (more than 16 average set). When the network analyzer is set to ramp-mode it makes a number of complete frequency sweeps equal to the average value. If the time for a measurement is not critical, it is for sure better to use the step mode.

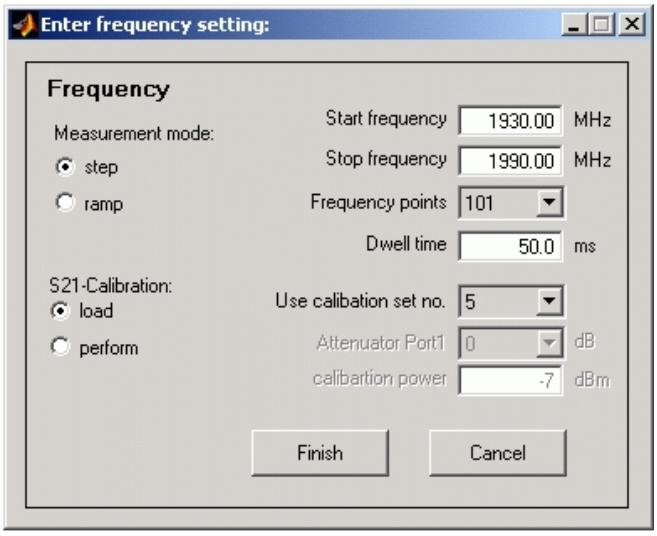

Figure A.5: Frequency settings applet

- Frequency range settings:

  The frequency range is specified by the two values 'Start frequency' and 'Stop frequency'. The frequency step size is given by the use of the value 'Frequency points'. The 'Dwell time' setting is only used in the step-mode. It specifies the settling time which is needed to stabilize the measurement for each frequency point.

- S21-calibration:

  The S21-through-calibration can be either performed or a saved calibration can be activated. In both cases a calset number must be selected. If a calibration has to be performed, it is important to choose a free calset, because the selected calset entry will be overwritten. Additionally the output power of the sweeper and the value of the port attenuator has to be selected for the calibration measurement. The output power at the port should be chosen as high as possible to avoid the noise-effects during the calibration measurement. Also it is important to mention, that the calibration is only valid as long as the same attenuator-value is used. Changing the port attenuator during the measurement will cause a discontinuity in the phase-shift of the device under test!

Power settings applet

Figure A.6 shows the power settings applet. This applet includes the settings for the sweeper output power, power flatness calibration and some parameter for the control of the sweeper:

- Automatic power setting:

  The output power at port 1 is a combination of the sweeper output power and the port attenuator value. The values for the sweeper and the port attenuator can be selected according to a list or set automatically by the program. When the flag 'enter power list'

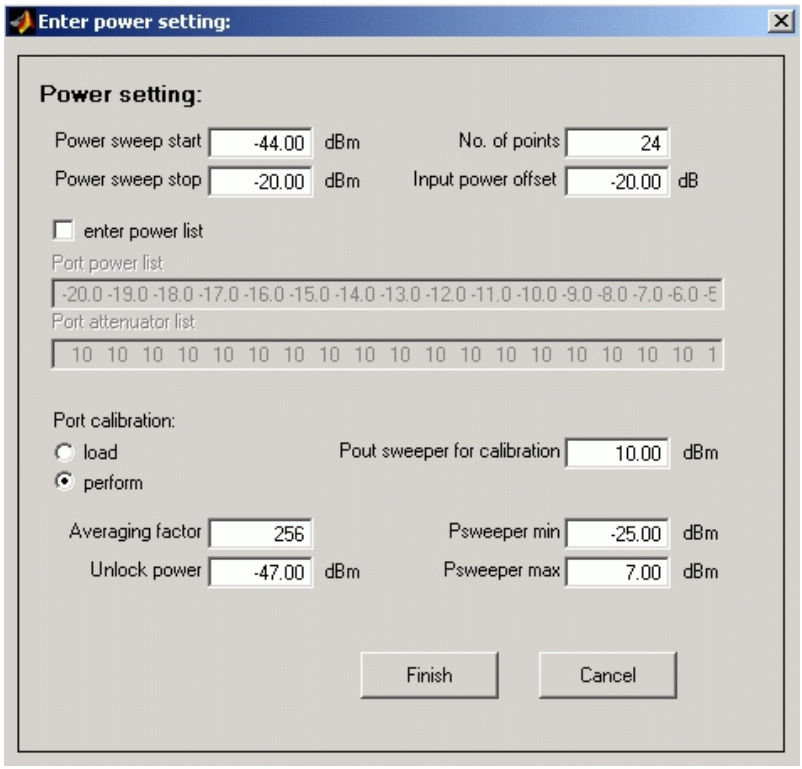

Figure A.6: Power settings applet

is disabled, the program tries to find the optimal combination for the sweeper output power and the port attenuator value. A change to the next higher attenuator value (the attenuator is set in 10 dB steps) is done, when the actual sweeper output power would exceed the value of 'Psweep max'. This could cause some trouble with the calibration as mentioned before. Similar to the frequency range the power step size is calculated as $\frac{\text{Psweep stop}-\text{Psweep start}}{\text{No of points}}$. Another important limitation to the automatic selection of the power values is the 'Unlock power'. Any combination of sweeper output power and port attenuator which results to an output power below the unlock level will be avoided, because the tracking generator will unlock in such a case and the measurement will be corrupted.

- Manual power setting:

  The values for the sweeper and the attenuator can be chosen by hand if the flag 'enter power list' is activated. In this case the number of entries to the 'Port power list' and the number of entries to the 'Port attenuator list' will be kept at the same value. If the length of both lists is unequal, the 'Port attenuator list' will be automatically set to the same length as the 'Port power list'. If such a modification is performed, a message-box will be shown. The values in the list could be entered one after the other separated by spaces or by the use of the MATLAB® list-function. For example, the following list can be entered:

```
-20 : 2:-10  -9.5 : 0.5 : -8
```

This list will be expanded to:

```
-20.0 -18.0 -16.0 -14.0 -12.0 -10.0 -9.5 -9.0 -8.5 -8.0
```

If one of the values exceeds the limits given by 'Psweep max' and 'Psweep min' the whole entry will be ignored.

- Input power offset :

  When using a preamplifier, the effects of this amplifier are measured during the calibration measurement and hence are compensated. Unfortunately this will lead to a wrong indication of the input power for the DUT in the measurement figure. A work around to this problem was done by the use of the 'Input power offset' value. This value is added to the actual input power to correct the indicator in the measurement figure. Positive 'Input power offset'-values will increase the power indication.

- Port calibration:

  In this part of the applet all settings for the flatness calibration are entered. For a successful port calibration a power meter set on GPIB-address 13 is needed, which should be able to measure the input power between -10 dBm to 10 dBm. Activating the radio-button 'perform' will allow the program to perform the complete flatness calibration. This process can take up to half an hour depending on the number of frequency points set and on the measurement speed of the power meter. The sweeper output power should be set to 10 dBm for the flatness calibration.

- Averaging factor:

  The 'Averaging factor' specified how often the measurement for a frequency point (in step-mode) or for a frequency sweep (in ramp-mode) is repeated. The mean of this set of measurements is than taken as the actual measurement value. The chosen average-factor must be a power of 2 to be accepted.

- Sweeper parameter:

  Three important parameters have to be set for the sweeper. The 'Unlock power' sets the lower limit for a correct phase measurement. The values 'Psweep max' and 'Psweep min' set the operation range for the sweeper, in which the absolute accuracy is within the chosen limits. These values are important for the correct measurement of a DUT and have to be acquired before the measurement is started.

Bias settings applet

Figure A.7 shows the bias settings applet. This applet includes the settings for the preamplifier and the two bias-points:

- Preamplifier:

  If a preamplifier is used the following changes in the measurement process are taken:

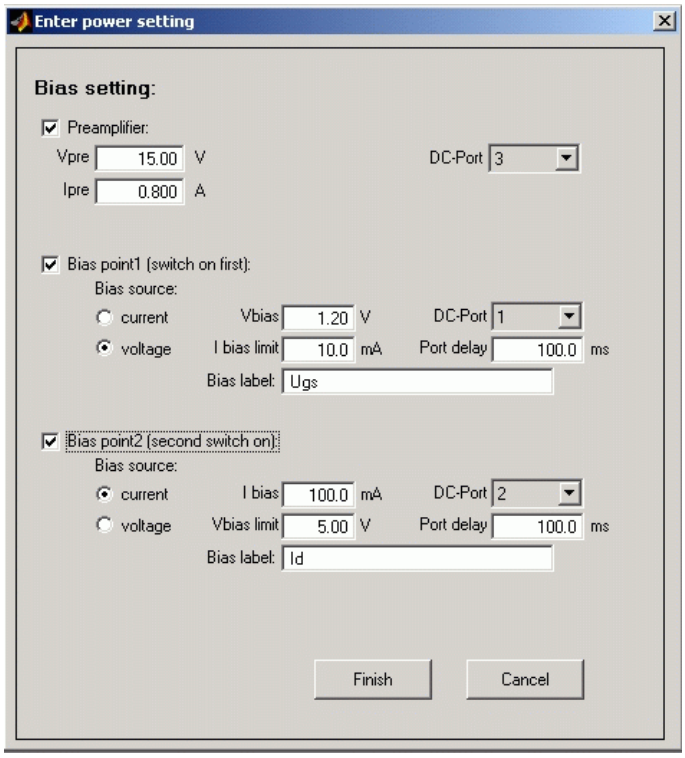

Figure A.7: Bias settings applet

- Activate the preamplifier before the calibration measurement is started.
- Deactivate the preamplifier before the main amplifier is connected to the test circuit.
- After the main amplifier is switched on, activated the preamplifier again.
- Switch the preamplifier off before the main amplifier is disconnected.

If a preamplifier is used, the gain of this amplifier should be set into the 'Input power offset'-field located in the power settings applet. The informations needed to drive the preamplifier are:

- Nominal supply voltage
- Maximum input current
- Port of the DC-power supply where the preamplifier is connected to

- Bias points:

  The idea behind the bias-point is to enable the possibility to measure prototype transistor amplifiers. Due to this reason both bias point can be configured to a voltage or a current source. Additionally an order in activating the bias points is set. Bias point 2 is the last one to be activated and the first one to be deactivated. Generally the bias points are activated

after the confirmation for the connection of the main amplifier was given. The following parameters can be set for each bias point:

- Current source selected:
  - Nominal output current
  - Maximum output voltage
- Voltage source selected:
  - Nominal output voltage
  - Maximum output current
- Bias point label
- Port of the DC-power supply where the bias point is connected to.
- A 'Port delay' defining the settling time which should be waited after the bias point was activated

The settings of the bias-points are saved to the measurement file for documentation.

GPIB settings applet

Figure A.8 shows the GPIB settings applet. The parameters available in this applet are:

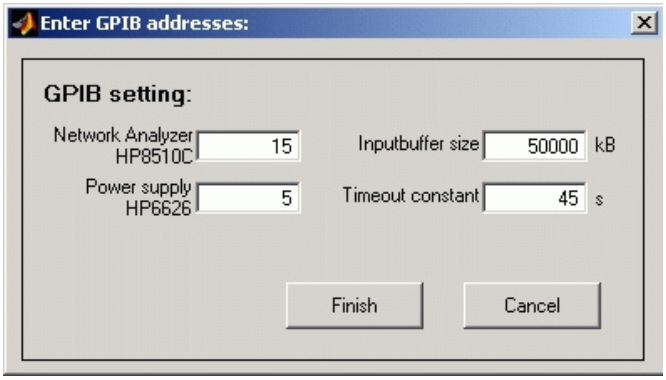

Figure A.8: GPIB settings applet

- network analyzer GPIB address
- DC power supply GPIB address
- Inputbuffer size:

  This value determines the size of the input buffer when reading from the network analyzer. The size can be estimated by: buffersize $\geq$ Frequency points $\cdot$ 8.
- Timeout constant:

  Limits the time duration within a GPIB-device has to react without creating a timeout exception

Transfer characteristic applet

Figure A.9 shows the transfer characteristic settings applet. Three parameters are used to

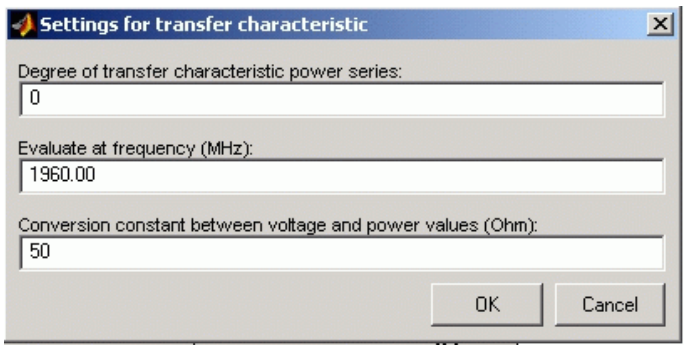

Figure A.9: Transfer characteristic settings applet

configure the transfer characteristic calculation:

- Degree of the power series

  Sets the order of the power-series which will be used to fit the instantaneous gain at the chosen frequency.

- Evaluation frequency:

  Selects the frequency point at which the fit will be done.

- Conversion constant:

  The fit will be done for the voltage gain. The specified resistance will be used to convert the power values into voltage values.

Option menu

In this menu the options to the program can be selected:

- Display:

  – Amplitude
  – Phase

  This option allows to select the kind of presentation for the complex gain.

- Transfer characteristic:

  The calculation of the power series coefficients for the envelope characteristic is done after measuring the DUT when this flag is activated.

A.2.3 Measurement file structure

Saving a measurement will create the following variables:

```
GAIN
f
p
bias1
bias2
```

where GAIN keeps all measurement points as linear complex values, f names all measured frequency points in Hz and p includes all measured power values in dBm. The struct-variables bias1 and bias2 are only saved when they where used. To show the magnitude of the gain over the frequency-power-plain in logarithmic units use the following command:

```
surf(p,f,20*log10(abs(GAIN)));
```

A similar command can be used to present the phase of the gain:

```
surf(p,f,unwarp(angle(GAIN)));
```

A.3 Measuring the amplifier response on a two-tone input signal

The MATLAB®-script 'TwoTone' was written to measure the response of an amplifier on a two-tone input signal. The input signal was generated by the use of an arbitrary signal generator and a vector signal generator. Compared to the classical two-tone signal generation by the use of two signal generators combined with a 6 dB power-combiner this approach has two major advantages:

- The level of the two input-tones is equal without any calibration measurement
- An appreciable reduction of RF-components which are needed to build the test circuit can be achieved

The major disadvantage of this system is the mixer-passage of the vector signal generator. In the case of the Rhode&Schwarz vector signal generator SMIQ the mixer-passage signal is about 50 dB lower than the desired output signal. Hence the contribution to the output signal power and to the intermodulation created by the device under test is quite low. In the case of a two-tone output signal of the generator, the mixer-passage signal lies exactly between the two main tones. Such a frequency component cannot be created by an intermodulation distortion. Figure A.10 shows the test circuit for the two-tone measurement. For the correct determination of the input and the output signal power the two optional power meter can be used. A preamplifier may be used to boost the output signal of the vector signal generator.

The script 'TwoTone' has no interactive user interface and no handover-parameters. All settings are directly written into the declaration of the main data structure. The parameters are:

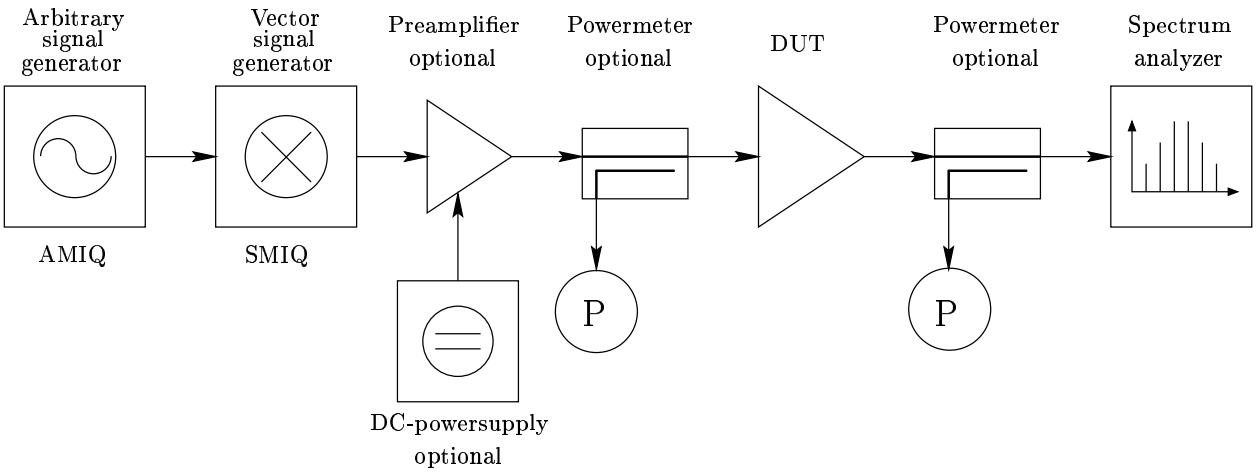

Figure A.10: two-tone measurement test circuit

`tone_spacing` Hz; Frequency spacing between the two main tones.

`NoOfPoints` (1,2,...); Specifies the number of points used for the creation of the baseband two-tone signal.

`SA_center` Hz; Sets the center frequency for the spectrum analyzer.

`SA_span` Hz; The frequency span of the spectrum analyzer should be chosen to display all interesting components of the output signal.

`SA_Reflevel_list` dBm; This list allocates a reference level for each measured power value. The selection of the correct reference levels assures a constant measurement accuracy.

`SA_RBW` Hz; Specifies the value of the resolution bandwidth.

`SA_Sweeptime` s; A large sweep time of the spectrum analyzer results in a slow measurement, but increases the number of averages performed at the detector for each frequency point.

`SMIQ_center` Hz; The center frequency of the vector signal generator and the spectrum analyzer may differ!

`SMIQ_power_list` dBm; This list includes all SMIQ output power values at which the device under test should be measured. If the SMIQ_power_list and the SA_Reflevel_list have a different number of elements, the measurement will be interrupted.

`Pin_Offset_SMIQ` dB; This offset will be added to the power-level set at the SMIQ. It can be used to compensate the effects of cables, directional couplers preamplifiers, etc. which will alter the signal between the output of the SMIQ and the input of the device under test. For a reduction of the signal the offset must be: Pin_offset_SMIQ < 0!

`Pin_Offset_PM` dB; This offset names the difference between the power measured by the input power meter and the real input power. If the measured power is lower than the real input power, this offset must be a negative number.

`Pout_Offset_SA` dB; This offset specifies the difference between the power measured by the spectrum analyzer and the real output power. If the measured power is lower than the output power provided by the DUT this offset must be a negative number.

`Pout_Offset_PM` dB; This offset names the difference between the power measured by the output power meter and the real output power. If the measured power is lower than the output power of the DUT, this offset must be a negative number.

`measure_main_tones` (0,1); If this flag is activated, the power of each main-tone is measured separately.

`use_powermeter_output` (0,1); This flag indicates, if the output powermeter is used.

`use_powermeter_input` (0,1); This flag indicates, if the input powermeter is used.

`V_PreAmp` V; The HP6626 DC-powersupply is used to drive the preamplifier. This variable is used to specify the level of the supply voltage. If no preamplifier is used V_PreAmp has to be zero.

`I_PreAmp` A; Specifies the maximum current for the preamplifier DC-supply.

`PreAmp_Output` (1-4); The HP6626 DC-powersupply make for port available.

`OutputFilename` Shows the name for the file in which the measured data are saved.

`GPIB_SA` (0-32); GPIB-address of the spectrum analyzer FSEK.

`GPIB_HP6626` (0-32); GPIB-address of the HP6626 powersupply.

`GPIB_SMIQ` (0-32); GPIB-address of the SMIQ vector signal generator.

`GPIB_AMIQ` (0-32); GPIB-address of the AMIQ arbitrary signal generator.

`GPIB_PM_in` (0-32); GPIB-address of the input power meter.

`GPIB_PM_out` (0-32); GPIB-address of the output power meter.

`GPIB_InputBufferSize` Bytes; The size of the GPIB-inputbuffer is important, when a complete measurement is read from the spectrum analyzer.

`GPIB_Timeout` s; Sets the time in which the GPIB-device has to react.

The script works according to the structure chart illustrated in figure A.11.

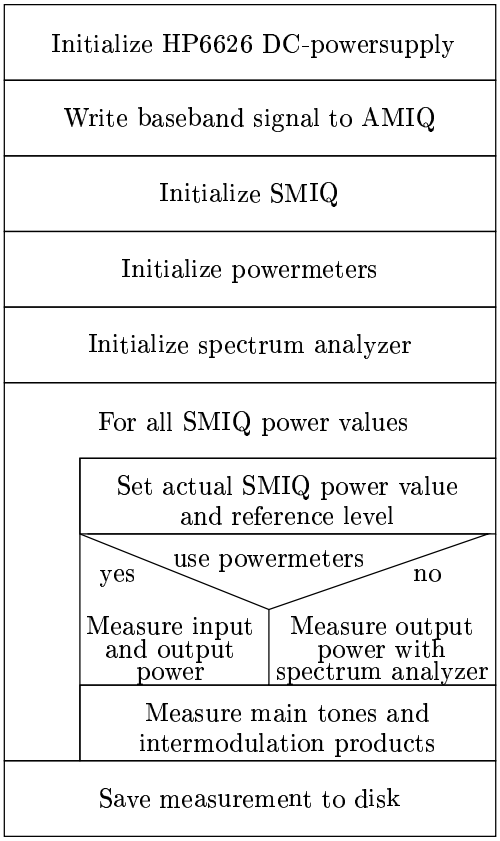

Figure A.11: Flowchart of the 'TwoTone' script

A.4 Measuring the delay mismatch in a cancellation loop

According to section 5.3.1 the network analyzer can be a helpful tool if a cancellation loop suffers from a time delay mismatch. By the use of a network analyzer different time delays can be compared to each other. Hence the usage of a variable delay-line and a network analyzer could iteratively find the correct time delay for a cancellation loop.

The task for the 'HPcancellation' script is to find the correct settings for the vector attenuator to minimize the amplitude and phase mismatch at a given center frequency. After this process is finished the length of the cancellation signal display at the network analyzer is evaluated. This value can then be used to compare the different delay-line settings. Figure A.1 shows the two measurement circuits, for the carrier and the distortion cancellation loop. Before the network analyzer can accomplish a correct measurement, a calibration measurement has to be performed. In the case of a cancellation loop this mean to completely disable the cancellation process. The easiest solution for this problem is to remove the delay line from the cancellation loop and terminate the two open ends in the loop by the use of two terminating impedances.

The script 'HPcancellation' sets the output currents at the two current sources and measure the cancellation signal at the given frequencies. This script has no interactive user interface and

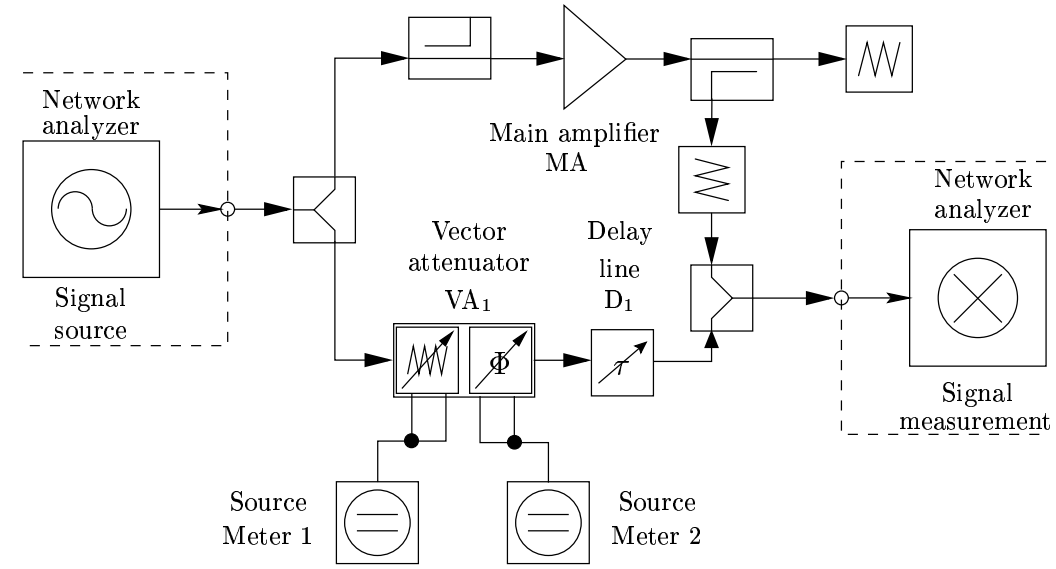

(a)

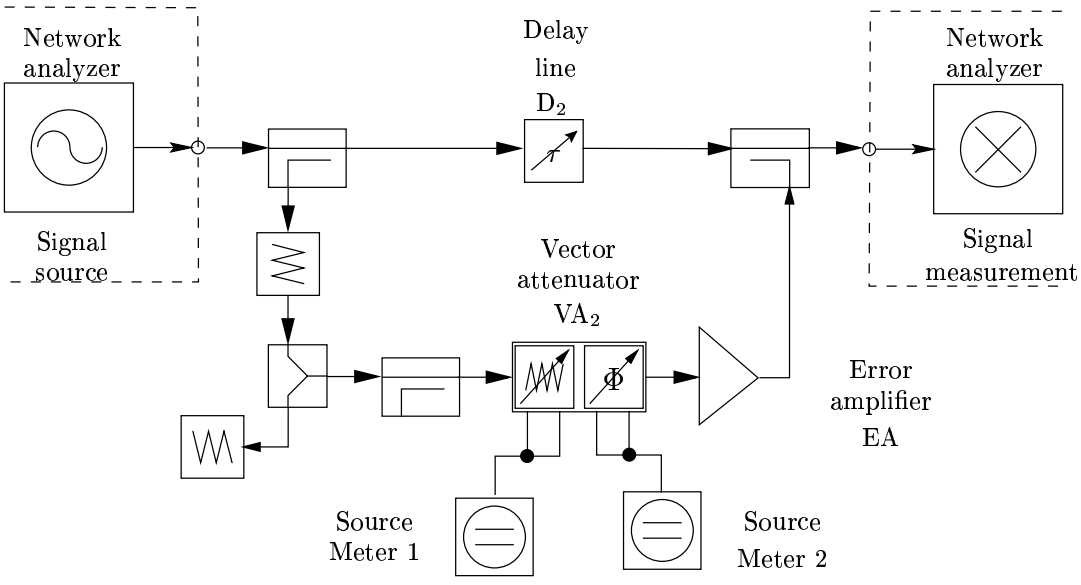

(b)

Figure A.12: Measurement circuits for the carrier (a) and for the distortion cancellation loop (b)

no handover-parameters. All settings are directly written into the declaration of the main data structure. The parameters are:

`freq_start` Hz; Start frequency for the measurement.

`freq_stop` Hz; Stop frequency for the measurement.

`freq_NoOfPoints` (3,5,7,...); Specifies the number of frequency points within the measurement interval (must be an odd number).

`freq_setSeg` (0,1); If this flag is activated, a frequency segment consisting of `freq_stop`, `freq_start` and `freq_NoOfPoints` will be set.

`fcal_exists` (0,1); This flag indicates, if the flatness calibration of output port 1 is already performed.

`cal_through` (0,1); Activating this flag will force the program to perform a through-calibration.

`P_cal_through` dBm; Specifies the output power which will be set during the through-calibration.

`Att_cal_through` (0=0dB, 1=10dB, 2=20dB, ...); Sets an additional internal attenuator at port 1 for the calibration measurement.

`load_trough_cal` (0,1); This flag will cause the loading of an existing calibration.

`calset` (0,...,8); Specifies the number of the calset at which the performed calibration will be saved, or from which an existing calibration will be loaded.

`Pcal` dBm; Specifies the output power at port 1 during the flatness calibration.

`Psweep_max` dBm; Sets the upper limit for the output-power of the sweeper after the flatness calibration is activated.

`Psweep_min` dBm; Sets the lower limit for the output-power of the sweeper after the flatness calibration is activated.

`P_measure` dBm; Specifies the output-power during the measurement process.

`P_Att_measure` dB; Activates an additional internal attenuator during the measurement. The value can be set in steps of 10 dB.

`P_AverageFact` (2,4,8,16,...); Specifies the number of measurement which are taken for each frequency point. This factor must be a multiple of 2. If the value is set to zero the averaging will be disabled.

`V_PreAmp` V; Sets the output voltage for the preamplifier (continuous running amplifier). If the preamplifier should be disabled `V_PreAmp` should be set to zero.

`I_PreAmp` A; This value limits the current for the preamplifier.

`PreAmp_Output` (1,...,4); Specifies the output channel at the DC-power source HP6626 at which the preamplifier is connected to.

`I_max` A; Specifies the upper limit for the output current of the current sources.

`I_min` A; Specifies the lower limit for the output current of the current sources.

`Sourcemeter` (0,1); This flag decides if the GPIB-commandos for the SourceMeter® or for the KEITHLEY 224 current source should be used.

`I_low_limit` A; For the minimum search a step-algorithm with variable step size is used. This value will provide a lower limit for the step size of the controller.

`GPIB_HP8510` (0,...,32); GPIB Address of network analyzer 8510C.

`GPIB_HP8510_Systembus` (0,...,32); GPIB Address of the Systembus call (not used).

`GPIB_HP6626` (0,...,32); GPIB Address of the HP6626 Powersupply.

`GPIB_KEITHLEY224_1` (0,...,32); GPIB Address of the current source 1 supplying the inphase current.

`GPIB_KEITHLEY224_2` (0,...,32); GPIB Address of the current source 2 supplying the quadrature current.

`GPIB_InputBufferSize` Bytes; The size of the GPIB-inputbuffer is important, when a complete measurement is read from the network analyzer. In this case the buffer size can be estimated by: buffersize $\geq$ frequency points $\cdot$ 8.

`GPIB_Timeout` s; Sets the time in which the GPIB-device has to react.

Before the program terminates it will show the achieved signal cancellation at the center frequency and the length of the cancellation signal in the MATLAB® command window. The script works according to the structure chart illustrated in figure A.13. If the vector attenuation is manually set, the length of the cancellation signal can be achieved by the use of the MATLAB® function `getcancel` which is described in the next subsection.

A.4.1 Evaluating the length of a cancellation signal: 'getcancel'

The getcancel-function assumes that the network analyzer is connected to a cancellation loop as shown in figure A.12. It tries to access the network analyzer at GPIB-address 15 and evaluates the length of the cancellation signal in the linear-polar display. The function returns the length of the cancellation signal. A typical function-call would be

```
mylength=getcancel;
```

The function takes no handover variables. If any parameter has to be changed, it must be done in the source-code.

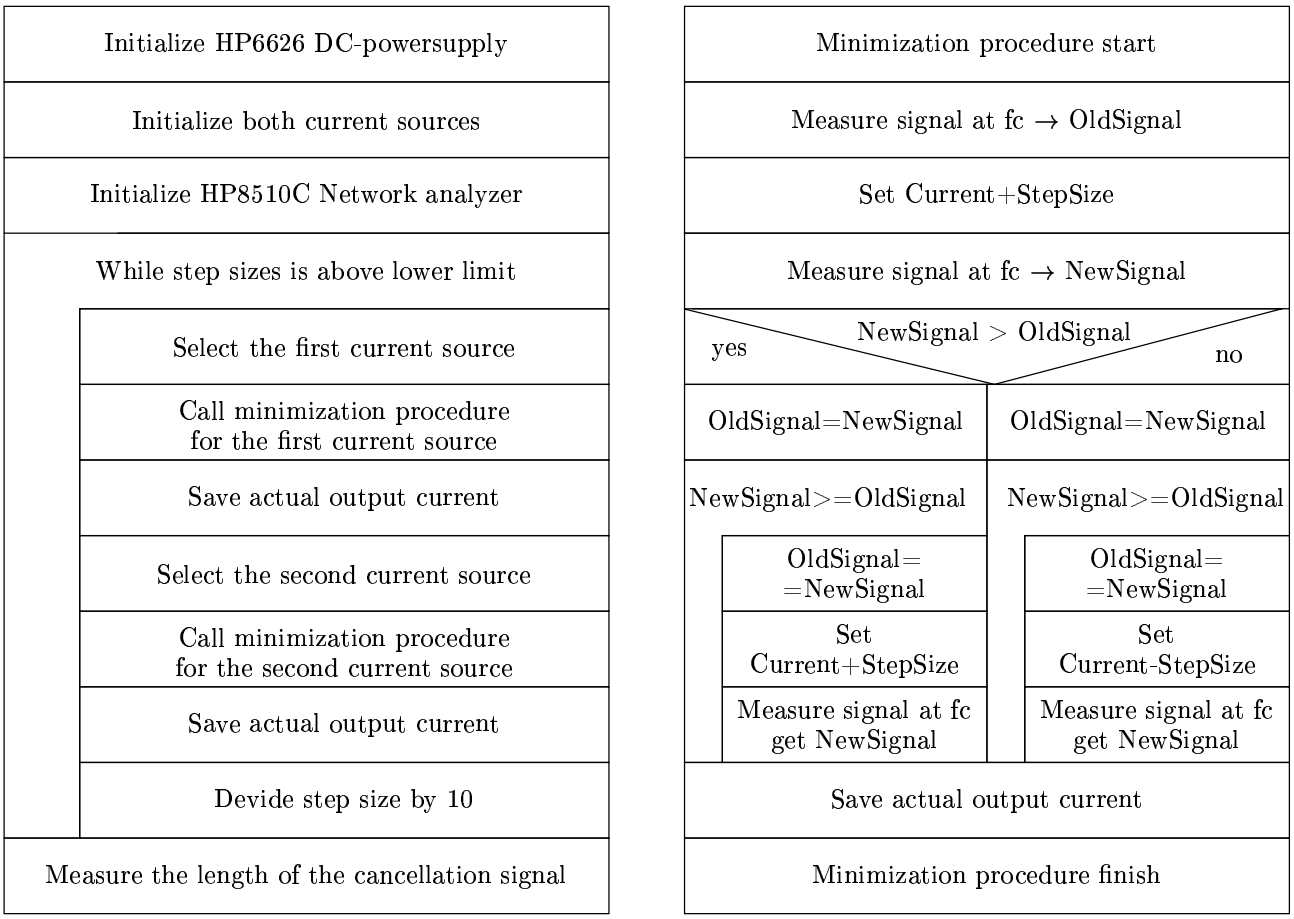

Figure A.13: Flowchart of the 'HPcancellation' script

Bibliography

[Bar00] Arntz Barney. Second oder effects in feedforward amplifiers. *Applied Microwaves and Wireless*, pages 66–75, January 2000.

[BG64] J. Brown and E.V.D. Glazier. *Telecommunications*, volume One. Chapman and Hall LTD, 11 New Fetter Lane, London EC4, 1964.

[Bla28] Harold S. Black. Translating system, U.S. Patent 1,686,792, October 1928.

[Bla37] Harold S. Black. Negative feedback amplifier, U.S. Patent 2,102,671, December 1937.

[BWB98] Donald B. Blecher, Michael A. Wohl, and Kent B. Bagwell. Feed-forward correction loop with adaptive predistortion injection for linearization of RF power amplifier, U.S. Patent 5,760,646, June 1998.

[Cav95] James K. Cavers. Adaptation behavior of a feedforward amplifier linearizer. *IEEE Transactions on vehicular technology*, 44(1):31–40, February 1995.

[CP99] Nuno Borges de Carvalho and Jose Carlos Pedro. Compact formulas to relate ACPR and NPR to two-tone IMR and IP3. *Microwave journal*, pages 76–86, December 1999.

[CTC99] Jiunn-Tsair Chen, Huan-Shang Tsai, and Young-Kai Chen. The optimal RLS Parameter tracking algorithm for a power amplifier feedforward linearizer. *IEEE Transactions on ciruits and systems—II*, 46(4), April 1999.

[ETS00] ETSI. Digital celluar telecommunication system (Phase 2+); Radio transmission and reception. *ETSI-Standards*, ETSI TS 100 910 V8.6.0, September 2000. Technical specification.

[ETS01a] ETSI. Digital celluar telecommunication system (Phase 2+); Enhanced data rates for GSM evolution (EDGE); Project scheduling and open issues. *ETSI-Standards*, ETSI TR 150 059 V4.0.0, April 2001. Technical specification.

[ETS01b] ETSI. Digital celluar telecommunication system (Phase 2+); Modulation. *ETSI-Standards*, ETSI TS 100 959 V8.3.0, June 2001. Technical specification.

[HST+01] K. Horihuchi, Y. Sakai, K. Totani, H. Senda, Masatoshi Nakayama, Yukio Ikeda, and Osami Ishida. A high efficiency feedforward amplifier with a series diode linearizer for cellular base stations. *Microwave Symposium Digest, MTT-S International*, 2, May 2001.

[JBS92] Michael C. Jeruchim, Philip Balaban, and Sam K. Shanmugan. *Simulation of Communication Systems*, volume Application of Communication Theory. Plenum Press, New York, 233 Spring Street, New York, N.Y. 10013, 1992.

[KB96] Peter B. Kenington and David W. Bennett. Linear distortion correction using a feedforward system. *IEEE Transactions on vehicular technology*, 45(1), February 1996.

[Ken00] Peter B. Kenington. *High-linear RF amplifier design*, volume Artech House microwave library. Artech House, INC., 685 Canton Street, Norwood, MA 02062, 2000.

[KLY97] Sang-Gee Kang, Il-Kyoo Lee, and Ki-Suk Yoo. Analysis and design of feedforward power amplifier. *IEEE*, June 1997.

[KPD01] Dimitrios Karampatsis, Joao L. Pinto, and Izzat Darwazeh. Transmitter modeling and EVM estimation for the GSM Evolution - EDGE. *ICT International Conference on Telecommunication, Posters*, June 2001.

[KWW97] Peter B. Kenington, P. A. Warr, and R. J. Winkinson. Analysis of instability in feedforward loop. *ELECTRONICS LETTERS*, 33(20):1669–1671, September 1997.

[Lau86] Pierre A. Laurent. Exact and approximate construction of digital phase modulations by superposition of amplitude modulated pulses (amp). *IEEE Transcations on Communications*, 34(2), February 1986.

[Mag98] Gottfried Magerl. Hochfrequenztechnik 1. The Institute of Communications and Radio-Frequency Engineering, Technical University of Vienna, Gußhausstr. 35-37, 1040 Wien, Juni 1998.

[Mat01] MathWorks, Inc. *Instrumentation Control Toolbox for use with Matlab®*. The MathWorks, Inc., 3 Apple Hill drive, Natick, MA 01760-2098, Juni 2001.

[Mat02] MathWorks, Inc. *Using Matlab®*. The MathWorks, Inc., 3 Apple Hill drive, Natick, MA 01760-2098, July 2002.

[MPT97] MPT. A vector attenuator for feedforward amplifier and RF predistortion use. *Microwave jornal*, October 1997.

[MPT00] MPT. *MPT 1820VA Vector Attenuator*. Micro Precision Technologies, Inc., Manor Parkway 12-B, Salem, NH 03079, December 2000.

[Pot99] Nick Pothecary. *Feedforward linear power amplifiers*, volume Artech House microwave library. Artech House, INC., 685 Canton Street, Norwood, MA 02062, 1999.

[SSL90] James K. Steel, D. Scott, and S. Ludvik. A 6-18GHz high dynamic range MMIC amplifier using a feedforward technique. *Microwave Symposium Digest, MTT-S International*, 2:911–914, 1990.

[Tec99] Powerwave Technologie. Improved performance of MCPAs using adaptive linearization technology. Powerwave Technologie, INC., Corporate Headquaters, 2026 McGaw Ave., Irvine, CA 92614, 1999.

[ZCBK96] G. Zhao, F. M. Channouchi, F. Beauregard, and A. B. Kouki. Digital implementations of adaptive feedforward amplifier linearization technique. *Microwave Symposium Digest, MTT-S International*, 2:543–546, 1996.